9-14-2008

The Production of Designed Potential Protein Contrast Agents and their Encapsulation in Albumin Microspheres

Julian A. Johnson

Recommended Citation

THE PRODUCTION OF DESIGNED POTENTIAL PROTEIN CONTRAST AGENTS

AND THEIR ENCAPSULATION IN ALBUMIN MICROSPHERES

by

JULIAN A. JOHNSON

Under the Direction of Drs. Jenny J. Yang and Zhi-ren Liu

ABSTRACT

Using protein design, a series of metal binding proteins have been designed, allowing the local factors that contribute to metal affinity and thermostability to be studied. Those proteins with the highest metal binding affinities had the lowest apo-form T_m and the largest ΔT_m upon metal binding. In this thesis, major steps have been taken toward applying the engineered protein to MR imaging. The progress of magnetic resonance imaging is hindered by low specificity and rapid elimination of FDA-approved MRI contrast agents. The engineered protein contrast agent has been conjugated to a cancer-specific targeting peptide and encapsulated in albumin microspheres to provide tandem passive and active tumor targeting. Also, a simple, high-yield purification method has been developed.

INDEX WORDS: Microspheres, CD2, Protein design, Contrast agent

THE PRODUCTION OF DESIGNED POTENTIAL PROTEIN CONTRAST AGENTS

AND THEIR ENCAPSULATION IN ALBUMIN MICROSPHERE

By

JULIAN A. JOHNSON

Thesis Submitted in Partial Fulfillment of the Requirements for the Degree of

Master of Science

In the College of Arts and Sciences

Georgia State University

2007

THE PRODUCTION OF DESIGNED POTENTIAL PROTEIN CONTRAST AGENTS

AND THEIR ENCAPSULATION IN ALBUMIN MICROSPHERES

By

JULIAN A. JOHNSON

Major Professors:	Zhi-Ren Liu
	Jenny J Yang
Committee:	Giovanni Gadda

Electronic Version Approved:

Office of Graduate Studies
College of Arts and Sciences
Georgia State University

August 2007

ACKNOWLEDGEMENTS

TABLE OF CONTENTS

List of Tables

List of Figures

List of Abbreviations

Bom   bombesin

BSA   bovine serum albumin

B2m   beta-2-microglobulin

CD2.D1   Domain 1 of wild-type cluster of differentiation 2 (PDB ID 1HNG)

FRET   fluorescence resonance energy transfer

HER-2   Human epidermal growth factor receptor isoform 2

IB   inclusion bodies

NMR   Nuclear magnetic resonance

MRI   Magnetic resonance imaging

ScFv   Single chain antibody

SDS-PAGE   sodium dodecyl sulfate polyacrylamide gel electrophoresis

UVCD   ultraviolet circular dichroism

1   Introduction: Motivation and Hypotheses

1.1   Design of Ca(II)/La(III) binding Protein with Different Charged Ligand Residues

CD2.7E15 is a designed metal binding protein based on the N-terminal domain of the cell adhesion protein cluster of differentiation 2 (CD2.d1) (*1*). Site directed mutagenesis was used to create a metal binding site on the surface of the protein. Initially the intention was to utilize this designed metal binding protein to understand the local factors associated with Calcium binding (*2, 3*). Calcium signaling is an essential part of life, but the actual process of calcium binding is poorly understood. Factors that are suspected to play a role in calcium binding affinity include the ligand type, the electrostatic environment, the net charge of the protein and the metal-binding geometry. Some of the problems that complicate the study of calcium binding in nature include metal-to-metal interactions and multiple binding sites (e.g.: calmodulin with its four binding loops). Lanthanide ions share coordination properties that are similar to those required by Ca (II); therefore, lanthanides are often used to probe calcium binding sites in proteins.

In our lab, we have taken two approaches to studying calcium and lanthanide binding in single site systems. The first approach is to insert the binding loops of a calcium binding protein that occurs in nature (such as calmodulin) into proteins that do not naturally bind calcium ions. We call this the grafting approach. Our lab has

successfully studied the calcium binding affinity of all four calcium binding loops present in calmodulin using this approach. Our lab is also looking to use this approach to design GFP-based calcium sensors.

The second approach is called the design approach. The design approach utilizes computer algorithms to locate potential sites for binding ligands within a stable host protein that does not have a metal binding site.

The first objective of this thesis is to generate single site systems that will eliminate cooperativity and global conformational change so that the local factors can be studied. In the future it may be possible to design proteins that fold or unfold in response to changes in local calcium concentration. Also, designing calcium binding proteins has given our lab significant insight into the features of calcium binding sites. Our lab recently located the calcium binding site of the newly discovered calcium sensing receptor (CaSR). In addition to studying the effects of net charge and ligand type on calcium/lanthanide binding affinity, we would like to relate the trends observed in net charge, ligand type, and metal binding affinity to any possible trends in calcium conferred stability. In nature, calcium often plays a role in stabilization. In the case of the bacterial protease thermolysin, there is a very significant T_m difference between the apo and the calcium loaded enzyme. The objective of the research discussed in chapter 2 is to carry out conformational analysis of 7E15 and its charged variants in the presence and absence of bound metal and to determine the thermal stability of these variants with and without metal.

1.2   Use of Designed Protein as a MRI Contrast Agent

Due to calcium's spectroscopically silent nature and the similarities between lanthanide and calcium coordination geometry, lanthanide metals (e.g. Gadolinium, Terbium and Lanthanum) are used to probe the metal binding site using fluorescent resonance energy transfer from tryptophan residues (*4*). Our designed protein, which is referred to as CD2.7E15 or simply 7E15, has a high affinity for gadolinium (*2, 3, 5*) and our lab later discovered the need for high affinity Gadolinium chelators in magnetic resonance imaging (MRI).

Magnetic resonance imaging is growing in popularity in the clinical and research arenas due to its non-invasive nature and its potential to produce high clarity images (*6-8*). MRI boasts numerous advantages over other imaging techniques such as fluorescence, X-ray, and positron emission tomography: MRI provides a true volume rendering, is unhindered by tissue depth, produces no toxic by-products, uses no harmful radiation, and is not affected by light scattering or photobleaching (*9, 10*). MRI provides a three dimensional representation, the clarity of which is a function of the difference in relaxation time between water molecule protons in adjacent, physiologically distinct tissues. There is considerable research directed toward the development of molecules capable of enhancing the difference in relaxation time of nearby water protons. Members of this diverse class of molecules are called MRI contrast agents and their potency is measured by their relaxivity (R_1 or R_2 with units of $M^{-1}s^{-1}$). To date, the relaxivity of contrast agents has failed to reach levels that are theoretically possible. The relaxivity of current FDA approved contrast agents is 20 to 50 times lower than the theoretically

possible value, the most popular of which is Gd-DTPA. Since relaxivity is positively correlated with molecular radius, the designed metal binding protein CD2.7E15 possesses a relaxivity that is 10 to 20 times higher than that of Gd-DTPA, the most widely used MRI contrast agent.

Because of its high relaxivity, use of CD2.7E15 rather than Gd-DTPA is favorable because less contrast agent (in mg per kg of bodyweight) would be required to produce a sufficient image. Additionally, Gd-DTPA is considered a blood pool agent, meaning it does not have a specific partitioning to any particular organ or tissue. The construct CD2.7E15 can be engineered to include on or more specific peptide tags. In this thesis, a CD2.7E15 construct conjugated to bombesin, is studied (referred to throughout this thesis as CD2.7E15.bom or 7E15-bom). The bombesin tag is an analog of gastrin releasing peptide, which possesses a high affinity for the gastrin releasing peptide receptor (*11-13*). The gastrin releasing peptide receptor is overexpressed on 20-40 % of colon cancer cells and 30-60% prostate cancer cells (*14-16*). The receptor may also be overexpressed in some lung carcinomas (*12, 17*) and some ovarian carcinomas (*18*). The receptor number can reach 1×10^6 per cell (*19*). Current methods of MR imaging cannot discern anatomical differences that are less than 1-2 mm in diameter. If the specific tag can enrich the contrast agent in surrounding tissues, the intensity and clarity of MRI can be improved to detect tumor metastases <2 mm. Several problems with this research venture will be discussed in this thesis, including the potential pharmacokinetic manipulation of the contrast agent, and the production (expression and purification) of the protein contrast agents.

1.3   Production of Engineered Proteins

The copious research necessary to move this project from theoretical prospect to the clinic will require rapid, reliable, high throughput production of CD2.7E15. Since the early stages of CD2.7E15 studies, CD2.7E15 was expressed in the pGEX-2T vector, which confers an N-terminal glutathione-S-transferase (GST) tag, facilitating affinity column purification using a column containing sepharose beads covalently conjugated to glutathione (the GST substrate). GST is a 27 kDa protein known as glutathione-S-transferase. 7E15 is approximately 11 kDa and proteins of this size can have difficulty becoming soluble in the bacterial cytoplasm. The size (27 kDa) and N-terminal conjugation of GST probably facilitates the solubilization of the entire fusion protein (*20*).

There are several disadvantages to the current purification method. GST does not always fold properly, which prevents GST from binding to the glutathione-sepharose beads during affinity column purification (the initial step of purification in this procedure). In fact, during the purification procedure a considerable amount of protein remains in the cell pellet after sonication and centrifugation, presumably this is denatured and/or aggregated insoluble fusion protein. Also, fusion protein is detected in the waste after affinity column purification, which may be soluble fusion protein that has been rendered nonfunctional during expression or the purification procedure. The size and disulfide bonds of GST result in a protein that does not refold well, so recovering the entire fusion protein would be tedious. The caveat is that CD2.d1 is a small protein with a very stable IgG fold, which generally refolds very well (*21*). Presumably, 7E15 will

refold well, since it shares a nearly identical secondary and tertiary structural arrangement with CD2.d1 and differs by only three amino acid substitutions (*5*). Finally, the GST fusion system requires that 7E15 be cleaved from GST using thrombin, an expensive enzyme, which, although highly active on a defined amino acid sequence, retains some measurable activity on virtually all Arg-Gly and Gly-Arg bonds (*22, 23*). Deliberate exposure to thrombin may result in further loss of valuable product and an unforgiving purification procedure. The average yield of CD2.7E15 purified using the GST fusion system is 6 mg/L cell culture and the average yield of CD2.7E15-bombesin purified using this method is approximately 3 mg/L cell culture (Fig 2.1).

Bacterial expression has the potential to produce enormous amounts of protein when overexpression is induced. Because of the relative size of GST to 7E15—27 kDa and <12 kDa, respectively—the GST-fusion expression system devoted most of the expression resources to GST rather than 7E15. Also, as aforementioned, GST does not refold well. A study by Lichty et al surveyed the cost of protein purification and found that, GST-fusion proteins were inferior to histidine tagged proteins (*24*). The most popular form of the histidine tag (histag) consists of six histidine residues in sequence. These residues bind to nickel immobilized by a chelator bound to sepharose or agarose beads. The histag's small size allows most of the expression effort to be devoted to the target protein. In the event of aggregation, it is hypothesized the histag probably will not interfere in the refolding process to the extent that GST does; the histag has been shown to have no significant effect on crystal structures (*25*) and several purification procedures have been developed to refold histidine tagged proteins (*26*). Therefore, the second

objective of this study is to develop a rapid, efficient protein purification method to produce a large quantity of engineered proteins.

1.4 Encapsulation of Engineered Proteins in Albumin Microspheres

In addition to the problems encountered in our current protein production system, the formulation of our contrast agent has yet to be optimized for tumor-specific delivery of sufficient amounts of our contrast agent. Typically, injected drugs are found in their highest concentrations in the liver, spleen, and kidney. Protein drugs are no exception (see the appendix of this thesis for a detailed review of the biodistribution of protein drugs) (27-31). Since MRI contrast enhancement is highly dependent on local concentration of the contrast agent, nonspecific accumulations in the kidney, liver and spleen are highly undesirable and may possibly hinder the detection of small tumors near these organs. To alter the pharmacokinetics, albumin microspheres and targeting peptides will be used. Albumin microspheres were first described in 1974 by PA Kramer as a means for achieving specificity in drug delivery (32, 33). Microspheres shift the Biodistribution to the following: the vasculature, by increasing the circulation time; the lungs, via selective phagocytosis by lung associated macrophages; and inflamed tissues or tumors, due to enhanced capillary permeability in these regions (34-37). Albumin microspheres are immunologically inert, nontoxic, and degrade into nontoxic amino acids (38-41). There are several means to prepare microspheres, but the most homogenous is spray-drying. Spray-drying requires exposure to >100 °C to rapidly evaporate moisture from the drug-albumin preparation. Spray drying has been used on several proteins with disturbances in structure and function ranging from negligible (42-44) to greater than

50% inactivation (*45-47*). The effect of spray drying on the folding, metal binding properties, and, perhaps most importantly, the relaxivity of the protein contrast agent 7E15 is examined in this thesis.

The third objective of this project is to develop high throughput purification methods for the designed protein Gd-chelating MRI contrast agents and to test the effect of albumin encapsulation on the Biodistribution and relaxivity of these molecules. Each topic will be explored in detail throughout Part I of this thesis.

1.5   Overview of the organization of this thesis

Chapter 2 discusses the effect of net charge and ligand type on calcium binding affinity and calcium conferred thermal stability. The research directed towards determining the metal binding affinities was largely done by Dr. Anna Wilkins Maniccia for her PhD dissertation (Georgia State University Department of Chemistry, summer 2005), and Dr. Wei Yang (post-doctoral associate in Dr. Jenny J Yang's lab, 1998-2007).

Chapter 3 describes the development of a novel purification procedure for the designed protein based MRI contrast agents, while Chapter 4 describes the procedures necessary to encapsulate them in spray dried albumin microparticles. Chapter 5 focuses on the biophysical characterization of the purified histidine tagged CD2.7E15 before and after spray drying.

Chapter 6 Summarizes the major findings from part one of the thesis (chapters 2-5)

Chapter 7 introduces the protein beta-2-microglobulin and its importance in prostate cancer metastases. Chapter 8 entails the procedures directed towards beta-2-

microglobulin expression and purification. Chapter 9 describes the efforts towards

inserting a histidine tag in the C-terminal of this protein.

Appendix I: Chapter 10 describes the efforts to express a single-chain anti-HER-2

antibody in E.coli and the purification steps necessary to purify the protein.

Appendix II: Chapter 11 is a review entitled Biodistribution of Protein Drugs.

The review describes the general trends in metabolism, elimination, and distribution

observed when protein drugs are administered to mammals. The review mostly focuses

on intravenous administration.

2   The Effect of Net Charge and Ligand Type on the Thermal Stability of Calcium Binding Proteins

Calcium binding sites are generated using site directed mutagenesis to change wild type residues according to the necessary parameters. In the case of CD2.7E15, the desired coordination geometry is a pentagonal bipyramidal arrangement with an oxygen atom at each vertex (Fig 2.1). All work presented in this work was done on designed calcium binding proteins.

Domain one of CD2 (CD2.D1) was chosen as the host protein for our engineered calcium binding sites. The topology of domain CD2 is similar to the calcium-dependent cell adhesion protein Cadherin. The size of CD2-D1 (99 amino acid residues) allows for easy expression and purification. CD2 has been shown to withstand mutations at forty different residues without significant deviations from the native fold. CD2 maintains its native fold through a wide pH range (pH 1 – 10) and salt concentrations (0 - 4 M). Finally, NMR and X-ray structures are available for CD2 so that biophysical analysis results can be compared to wild type data. These characteristics make CD2 an excellent scaffold for our designed and grafted calcium binding sites (Fig 2.1).

Previous studies done by Dr. Anna Wilkins-Maniccia (ICPMS, Tb (III) competition, ITC) have shown that 7E15 has a calcium binding affinity in the sub-micromolar range. The binding site of 7E15 has a net charge of negative five. According to the acid pair hypothesis outlined by Reed and Hodges (1980), EF-hand (class one) calcium binding sites with a net charge of negative four are stronger than calcium binding sites of other net charges (-2, -3, or -5) provided that the negatively charged ligands are at

opposite vertices in the coordination sphere (eg:-x, x and –y, y). CD2.7E15 is a class two calcium binding protein.   We would like to explore the effects of net charge on our class of binding site (class two). Our lab has designed variants of CD2.7E15 with binding ligands mutated from negatively charged ligands (Glu or Asp) to similar neutral binding ligands (Gln or Asn). These mutants are called EEDDN, EENDN, and NENDN after the single-letter code for the binding ligands.

Table 2.1
The residues composing the metal binding sites in 7E15 and its variants. The original residues of wild type cd2.d1 are shown in the first row.

protein	15	56	58	62	64	Net charge
Wt CD2.d1	N	E	L	D	K	-1
7E15	E	E	D	D	D	-5
EEDDE	E	E	D	D	E	-5
EEDDQ	E	E	D	D	Q	-4
EEDDN	E	E	D	D	N	-4
EENDN	E	E	N	D	N	-3
NENDN	N	E	N	D	N	-2

Green= positive   Blue= neutral   Red= negative

The variants of 7E15 could also allow the study of the effects of different binding ligands in calcium binding affinity. Variant EEDDQ was designed so that its binding affinity could be compared to variant EEDDN. These variants have net charges of negative four and differ only in the residue at the 64th position. Variant EEDDE was designed so that its binding affinity could be compared to 7E15. Both of these proteins

have a net charge of negative five and they differ only in the residue at the 64th position.

7E15 has an aspartate while EEDDE has a glutamate.

The table below shows the position of the original residues in CD2, the potential

binding ligands of CD2.7E15, and the corresponding residues in the five variants.

Variants of 7E15 were thermally denatured in the presence and absence of calcium

(1mM EGTA or 10mM $CaCl_2$) to determine the T_m in various conditions. Several

variants were analyzed in the presence of 50 uM Terbium Chloride ($TbCl_3$). We will

ultimately use these trends to generalize the effects of net charge and ligand type on

metal binding affinity and calcium-conferred thermal stability.

2.1   Materials & Methods

2.1.1   Cloning and Molecular Biology

All variants were mutated by Dr. Anna Wilkins Maniccia. The details are found

in her PhD Dissertation (Summer 2005, Georgia State University Department of

Chemistry). The 7E15 sequence was inserted between the BamH1 and the EcoR1

restriction sites of the pGEX-2T vector (GE Healthcare/Pharmacia Biotech).

2.1.2   Transformation

To begin the procedure, a 1.5ml eppendorf tube containing approximately 100 uL

desired competent cells (BL21 (DE3) for expression, DH5α for DNA purification) was

obtained from a stock of competent kept at -80° C. The cells were placed on ice to thaw

and aliquotted into two 50 µL samples. One sample receives 0.5-1.0 µl of desired

plasmid DNA while the other did not receive DNA (this is the negative control). The thawed cells and DNA were mixed by pipetting up and down or gently flicking the bottom of the tube. The cells were left on ice for at least thirty minutes after the addition of DNA. The heat shock was done by placing the cells in a 42 °C water bath for ninety seconds and then putting the cells back on ice for two minutes. Then, 50 μL LB media was added and the media was mixed with the cells by pipetting up and down or by gently flicking the bottom of the eppendorf tube. The tubes were then incubated at 37 °C for 30 minutes. 50 μL of the solution was added to desired agar plates (LB-Amp plates for expression) and streaked onto the plates with a sterile triangle. The plates were then incubated at 37° C overnight. The following morning, the plates were wrapped in parafilm and placed upside-down in the refrigerator to retard drying of the agar gel. No plates were kept longer than one month.

2.1.3   Protein Expression of CD2.7E15 and its Variants

A single successfully transformed colony was inoculated into 500 mL LB media containing 100 mg/L ampicillin. The colony was allowed to grow overnight at 37 °C and 180 to 220 rpm agitation. 50 to 100 mL overnight culture was inoculated into 1 L fresh LB medium (100 mg/L ampicillin). Expression at 30 or 37 °C was monitored by measuring the light scattering of the media (O.D.$_{600nm}$). When the O.D.$_{600nm}$=0.8 to 1.0, 1 mL of 1 M IPTG solution was added to the growth to induce protein expression. After three (37 °C expression) to five hours (30 °C expression), the cells were harvested by in 500 ml bottles at 7 krpm for 15-20 minutes using a GS3 rotor. The cell pellets were

collected using a spatula and less than 5 ml PBS buffer and placed in a 50 ml falcon tube

and stored at -20 °C for purification at a later date. The supernatant was discarded.

2.1.4 Protein Purification

2.1.4.1 Affinity Column Purification of GST-fusion protein-

The desired cell pellet was thawed out on ice or in cold water. 20-50 ml lysate

buffer per 2L culture pellet was added to re-suspend the cell pellet. Also, DTT was added

to this mixture to a final concentration of 5μM. This solution was sonicated 4-5 times for

~60 seconds using a Branson 450 Sonifier with the duty cycle set on 90 with 1-5 minutes

between sonications. The solutions were kept on ice during sonications. The solutions

were centrifuged in 50 ml tubes at 17 krpm for 20 minutes using the S34 rotor after

sonications. The supernatant is then filtered with a 0.45 μm filter. At this point a sample

was collected for analysis using SDS-PAGE. The supernatant was placed on ice before

gravity binding to the Glutathione agarose bead affinity columns. At this point a 20 μl

sample of the flow through is taken for analysis using SDS-PAGE. The flow through

was then passed over the columns a second time for further binding. Then the columns

were washed with 10-20 ml 1X PBS buffer. A 20 μl sample of the beads was taken at

this point for analysis using SDS-PAGE. Usually a 1:5 BioRad protein assay is used to

determine whether or not any fusion protein was bound to the beads. If the fusion protein

has bound (indicated by a color change from copper to deep blue), cleavage of the fusion

protein was done using thrombin protease (20 μl per column thrombin and 3-4 ml 1X

PBS buffer per column). The cleavage was done for 3-12 hours at room temperature.

The columns were then washed with 20-50 ml 1X PBS buffer per column and allowed to elute fusion protein. At this point the elution was checked with 1:5 BioRad protein assay to determine if protein is being eluted. Also, a 20 µl sample was taken from the beads as well as the elution for analysis using SDS-PAGE. The elution was then concentrated using an Amicon brand concentrating apparatus (180 ml) with a 3 kDa molecular weight cutoff membrane. Solutions are concentrated to 7-10 ml. Further purification was using size exclusion and/or ion exchange chromatography.

2.1.4.2 Size Exclusion Chromatography

6-10 ml of elution from affinity column purification was injected into FPLC system. When the elution volume was greater than 20 ml the elution was concentrated using an Amicon high pressure concentrating apparatus and an Amicon membrane filter before injection. Samples are filtered with a 0.45 uM filter before injection. Proteins were purified using a size exclusion column and the concentration of each fraction was measured using the UV absorbance (280 nm) and the molar extinction coefficient of WT CD2 (11700 M^{-1} cm^{-1}).

2.1.4.3 Purification using HiTrap SP HP column-

CD2 variants are purified according to isoelectric point after being purified in our G75 size exclusion columns. First, the fractions containing protein are treated with acetic acid to lower the pH to the 3-4 range. The proteins are bound to the column in 50 mM sodium acetate/acetic acid buffer solution (pH 4.5) referred to as buffer A. Our FPLC machine is programmed to allow multiple 10 ml sample injections. Proteins are eluted

with 50 mM Tris-HCl (pH 8) referred to as buffer B. The concentration is determined using the UV absorbance (280 nm) and the molar extinction coefficient of WT CD2 ($11700 \; M^{-1} \; cm^{-1}$).

2.1.5   Secondary Structure analysis: Far UV Circular Dichroism-

Samples of the protein solution were prepared in 10 mM TRIS buffer with a pH of 7.4. Trials were done in the presence of 10 mM $CaCl_2$ to observe the effect of bound calcium to conformation. Trials were also done in the presence of 10 mM EGTA to observe the conformation of the variants in the absence of calcium. All samples were approximately 20 μM protein. Samples were allowed to mix at 4°C for thirty minutes after being prepared. All scans were done in a quartz 200 mm UV cell. The samples were scanned from 260 nm to 200 nm. Four to six scans were taken and averaged to get one spectra. Scans were done at 50 to 100 nm per minute. After the scans were taken, a scan of the buffer used was subtracted from the protein spectra.

2.1.6   Determining T_m using Far UV Circular Dichroism -

Scans were taken at each the desired temperature interval. The scans were done in six accumulations and a 100 nm/min scanning speed. Thermal denaturation was done in the presence and absence of Ca (II) (10 mM $CaCl_2$ vs. 1 mM EGTA). Thermal denaturation scans were also taken in a 50 uM Tb(III) solution in order to compare terbium-conferred thermal stability to calcium-conferred thermal stability. The fractional change wass plotted against the temperature to obtain a T_m (using *Kaleidagraph* ™ software).

2.1.7 Tryptophan Fluorescence

The tertiary structure of CD2.7E15 and its charged variants was investigated using tryptophan fluorescence. 2 μM protein samples in 10 mM PIPES, pH 6.8 or 20 mM PIPES, 10 mM KCl, pH 6.8 were excited at 282 nm and the emission spectra of tryptophan residues was observed from 300 to 400 nm. All measurements were taken at room temperature (approximately 27 °C)

2.1.8 Surface Potential Calculations

Surface potential calculations were done by Dr. Wei Yang. The protein surface potential and energy of CD2.7E15 variants were calculated using the DelPhi program based on model structures. The model structures of CD2.7E15 with the Ca^{2+} coordinations were generated by the design program and the structures of the other variants were generated by the program SYBYL (Tripos Co.) from CD2.7E15. The protons were first added in the pdb files using SYBYL. The apo-form structures simply removed the coordination of Ca^{2+} and the Ln^{3+}-loaded form structures simply replaced the Ca^{2+} with a Tb^{3+} at the same coordination. In DelPhi calculation (*48-50*), the interior and exterior dielectric constants were set to be 4 and 80, respectively. A salt concentration of 10 mM in solution was used. To compare the energy output from the DelPhi program, only the energy of the protein part was used. That is, the energy on the Ca^{2+} or Tb^{3+} was subtracted for the metal-binding forms of the proteins.

2.2   Results & Discussion

As shown in Figure 2.1, CD2.7E15 is a rational designed Ca^{2+}-binding protein with an engineered Ca^{2+}-binding site at the B, E, and D β-strands of the host protein CD2. CD2.7E15 is also called EEDDD after the designed ligand residues at the sequential positions 15, 56, 58, 62, and 64 (the same nomenclature was used for its variants). CD2.7E15 has been chosen as an excellent template to investigate the effects of charge and ligand type on the Ca^{2+} binding based on following considerations. First, this metal binding site is well embedded on the protein frame, allowing for the study of the interrelationship of calcium binding affinity, protein stability, and local factors. We have previously shown that the cluster of five negatively charged residues at this location has not disrupted the folding of the protein and that the metal binding has not altered the global conformation of the protein (5). Second, the conformational sensitive locations at wild type residues E56 and D62 are remain unchanged and the mutations were made on the other three ligand residues. Third, a series of variants that have net charges from -5 to -2 at the site were then generated by replacing Asp or Glu by Asn or Gln with its derivative without a sidechain charge (Table 1). Variants with net charges of -1 or 0 have not been generated since they are not expected to exhibit significant Ca^{2+} binding. Fourth, the variants EEDDD and EEDDE as well as EEDDN and EEDDQ have the same number of charges in their binding pockets with only one methylene group size difference at the last ligand position (64) to allow us to reveal the contribution of ligand types.

2.2.1 Conformational analysis of the 7E15 variants

At 25 °C the s.4 and 2.5far-UV CD spectra for all of the variants show a single negative maximum at ~216 nm nearly identical to the wild type CD2, which is an indicator of β-sheet proteins. Moreover, the Trp fluorescence emission spectra of the variants have a single maximum at 327 nm, which is the same as CD2 (Figure 2.4) . This suggests that the mutations have not altered the native folding arrangement. The metal ions alter neither the CD nor the Trp fluorescence spectra, suggesting the absence of global conformational changes upon the metal binding (Figs 2.4 and 2.5). 7E15 and the 7E15 variants all have a mostly beta sheet structure nearly identical to that of CD2.D1. The secondary structural differences with and without metal are minimal, resulting in overlapping far UVCD spectra for the metal free (1 mM EGTA) and calcium loaded forms (10 mM CaCl$_2$). According to Trp fluorescence spectra, the protein 7E15 and its variants do exhibit tertiary packing that is significantly different from wild-type CD2.D1 with or without metal.

2.2.2 FRET Metal Binding Studies of CD2.7E15 and its Variants

The metal binding studies were done by Anna Wilkins Maniccia for her PhD dissertation (Georgia State University, Department of Chemistry, summer 2005). . Taking advantage of the closely located aromatic residues in the host frame,Trp32 and Tyr76, metal binding of the 7E15 variants was investigated using aromatic sensitized fluorescent resonance energy transfer (FRET). The addition of the wild type CD2 into a Tb^{3+} solution caused a mildly 2-3 fold increase of the Tb^{3+} fluorescence emission at 545

nm due to the nonspecific interactions. On the contrary, the addition of EEDDD (7E15), EEDDE, EEDDN, and EEDDQ into the Tb^{3+} resulted in more than 30-fold increases in Tb^{3+} fluorescence emission. The addition of EENDN resulted in a smaller signal enhancement at the same protein concentration. The addition of NENDN only resulted in a slight enhancement that is comparable to the CD2, suggesting that the protein does not bind to Tb^{3+} or the binding affinity is very weak, which agrees with the prediction by the surface potential. The cited at 280 nmTb^{3+}-binding affinities were obtained by directly titrating Tb^{3+} into protein (Table 1). The variants with -5 charges have the strongest Tb^{3+}-binding affinities of < 1 μM. The variants with -4 charges have Tb^{3+}-binding affinities at μM level. The weaker binding of EENDN was not accurately measured due to the limitation of solubility that prohibits the usage of high Tb^{3+} concentration for this series of proteins. La^{3+} binding affinities were obtained by competitive titrating of La^{3+} into Tb^{3+}-protein mixtures and monitoring the decrease in Tb^{3+} fluorescence intensity at 545 nm. The trend of La^{3+}-binding affinities for the 7E15 variants is the same as that for Tb^{3+}, that is, the variants with a net charge of -5 show the strongest binding followed by the variants with a net charge of -4, -3 and -2. The addition of Ca^{2+} into Tb^{3+}-protein mixture led to only small decrease in the Tb^{3+} fluorescence, suggesting the competition between Ca^{2+} and Tb^{3+} is inefficient and Ca^{2+}-binding affinities are weak. Therefore, alternative method is required for the measurement of Ca^{2+}-binding affinities.

2.2.3   Metal Titrations using NMR

All metal titrations using NMR were done by Dr. Wei Yang. The Ca^{2+}-binding

affinity of EEDDD has been determined to be 100 ± 50 μM from the chemical shift

changes of the residues proximate to the metal binding position using ^{1}H-^{15}N HSQC

spectra. Similar Ca^{2+} titrations have been performed on the other variants. Ca^{2+}

specifically induced the movements of several resonances while the other resonances

maintain the same positions through the whole titration process for the variants with -4

and -5 charges. As an example, Fig. 5a shows the ^{1}H-^{15}N HSQC spectra of EEDDQ.

Based on the original assignment of EEDDD, part of the resonances in the spectra of

other variants has been identified. Several moved resonances are from the ligand residues

or neighbouring residues including G61, L63, Q64, E58, E56, and K66 as well as Q22.

The Ca^{2+}-binding affinities of EEDDE, EEDDQ, and EEDDN were obtained by

following the change of these residues. Unlike the Tb^{3+} and La^{3+} binding, EEDDQ with -

4 charges has a stronger Ca^{2+}-binding affinity than EEDDE with -5 charges. In addition,

the net chemical shift changes induced by Ca^{2+} binding for EEDDQ are greater than that

for EEDDE. On the contrary, EENDN possesses minor but evident resonance movement

at high Ca^{2+} concentration while NENDN does not undergo any significant changes with

the addition of up to 13 mM Ca^{2+}. This suggests that EENDN has a weak Ca^{2+} binding

ability while NENDN does not have observed Ca^{2+} binding. Furthermore, the results

confirmed that the chemical shift changes of the variants with higher negative charges are

from the Ca^{2+} binding but not from other processes such as salt effects.

2.2.4 Charge effects on Ca^{2+} and Ln^{3+} binding affinities.

The 7E15 variants with a net charge of -5 at the designed site have the strongest binding affinities for Tb^{3+} and La^{3+} followed by the variants with -4, -3, and -2 charges. However, for Ca^{2+} binding, a net charge of -5 is not always preferred compared to that of -4. The results correlate well with the previous experimental and theoretical studies that indicate that Ln^{3+} binding prefers a higher number of charged ligands compared to Ca^{2+} binding. Theoretical calculations from Lim and colleagues have shown that Ln^{3+} prefers -5 charges while Ca^{2+} prefers -4 when the ligands have freedom to adjust the binding geometry. In addition, denser negative charges and buried environment favor Ca^{2+} displacement by La^{3+}. Falke el al. have experimentally shown that mutating a Gln residue in the Ca^{2+}-binding site of galactose binding protein to an acidic residues (D and E) or to a structurally similar residue (N) almost completely abolished Ca^{2+} binding while the Ln^{3+} show a slightly higher binding affinity. This is due to that trivalent Ln^{3+} binding is more efficient in compensating the increased repulsion of the charged side chains than divalent Ca^{2+} binding. The galactose binding protein has optimized size and charge in the coordination sphere for Ca^{2+}.

The metal binding sites in the 7E15 variants are on the surface of the proteins. Their binding geometry is not completely restricted and also not completely free to be adjusted. For Ln^{3+} binding, the effects of charge interaction are dominant. Thus, the La^{3+} and Tb^{3+} binding affinity decrease follows the trends of net negative charge decrease. However, for Ca^{2+} binding, contradicted results were obtained. The variant EEDDQ with -4 charges has higher Ca^{2+} affinity than EEDDE. It seems that a compromise between the

charge interaction and geometric arrangement is achieved. One more methylene group in the sidechains of EEDDE or EEDDQ provides additional freedom for the sites, making them more similar to the theoretical calculation that a net charge of -4 is preferred. On the other hand, the Ca^{2+}-binding geometry of EEDDD and EEDDN is relatively restricted. As a result, the repulsion of the negative charges has less difference between the Ca^{2+}-loaded and Ca^{2+}-free forms. Since the apparent binding affinity is dependent upon the energy difference between the Ca^{2+}-loaded and Ca^{2+}-free forms of the protein, the attraction introduced by the bound Ca^{2+} becomes the dominant factor and the higher charged sites possess stronger binding affinities. Therefore, the determinant for such higher Ca^{2+}-binding affinity is the decreased stability at the Ca^{2+}-free form of the protein instead of the increased stability at the Ca^{2+}-bound form. The lowered thermal transition point of EEDDD supports this hypothesis. Overall, when the binding geometry or the charge distribution during the binding process is not restricted, Ca^{2+} prefers -4 charges. If the charge distribution is limited in a narrow region, denser charges might attract Ca^{2+} more strongly. It is noteworthy that in natural proteins a cluster of 4 or 5 negative charges often makes the protein in a different conformation or unfolding.

2.2.5   Effects of Steric Size on Metal Binding binding

The generally used ligand types to generate a Ca^{2+}-binding site are D, E, N, and Q. A statistic study has shown that Asp is the most preferred ligand in naturally-evolved Ca^{2+} binding sites followed by Glu, Asn, and Gln. That is, charged ligands are preferred over non-charged ligands (D and E over N and Q) due to the charged nature of Ca^{2+} and shorter sidechains are preferred over longer ones (D and N over E and Q) due to

unknown reasons. However, in 7E15 variants, a short sidechain does not show advantage over a longer one. While EEDDD possesses a higher Ca^{2+} affinity than EEDDE, EEDDN possesses a lower affinity than EEDDQ. As mentioned previously, substitution of Gln with Asn in the galactose binding protein results in the Ca^{2+} binding affinity decrease. It looks like that as long as the Ca^{2+}-binding pocket formed properly, the steric size of the ligand residues is less important for the Ca^{2+} binding. Thus, the less frequency for E and Q in naturally-evolved Ca^{2+}-binding sites might be determined by factors other than the Ca^{2+} binding, such as the requirement of conformational changes or proper stability. In 7E15 variants, the additional sidechain methylene group increases the thermal transition points both in the absence and presence of cations.

2.2.6   Thermal Stability of CD2.7E15 and its Variants in the Apo-form

The thermal transition points (T_m) of all variants were obtained using far-UV CD (Fig 2.6). 7E15 and its variants lose their native conformations at 90 ºC and the unfolded state resembles that of wild type CD2. CD2 has a melting temperature of 61 ± 1 ºC (*51*). The clustered negative charges at the β-strands decrease the thermal stability of EEDDD (41 ± 1 ºC) and EEDDE (45 ± 3 ºC) in the absence of metal. The -4 charged variants have higher T_m values of 53 ± 2 ºC for EEDDN and 56 ± ºC for EEDDQ under the same conditions. The EENDN (61 ± 1 ºC) and NENDN (62 ± 1 ºC) have similar Tm values with CD2 in the absence of metal (Fig 2.7).   Upon binding Ca^{2+} or Tb^{3+}, the T_m values of -4 and −5 charged variants of 7E15 increase. A ~10 ºC Tm increase was observed for EEDDD and EEDDE. A ~5 ºC increase of T_m was observed for EEDDN and EEDDQ.

For EENDN and NENDN with less charge at the binding site, the presence of Ca^{2+} or Tb^{3+} has not caused significant differences in the T_m values. As a result, although the trend of thermal transition points all following CD2 ~ NENDN ~ EENDN > EEDDQ > EEDDN > EEDDE > EEDDD both in the presence and absence of Ca^{2+} or Tb^{3+}, the net difference is smaller in the presence of the cations.

2.2.7   The Effect of Ligand Type and Net Charge on Thermal Stability

Surface charge-charge relationships have been shown to play a major role in protein stability and may potentially be manipulated to increase protein thermal stability (*52*). The effects of charged ligand residues on the stability of the proteins Table 2.2 the absence of Ca^{2+} with gradually increased T_m values (Figure 2.7) versus the decreased net charges -5 to -2. The protein surface potential calculation also indicated a similar trend. The repulsion between the negative charges is obviously the determinant for such charge-related thermal transition differences. In addition, it has been noticed that T_m values for EEDDD and EEDDN in the presence and absence of Ca^{2+} are lower than the corresponding T_m values for EEDDE and EEDDQ with the same net charges. It is likely that the additional methylene of Glu or Gln allows the sidechain oxygen atoms to rotate away from the others such that any charge interaction is reduced. The longer ligand may also allow increase in van der Waals interactions with nearby residues. This is different from the DelPhi calculation that shows EEDDE and EEDDQ have higher energy levels in the absence of cations. This difference is likely arisen from the fixed local conformations in the calculation, which assumes that the ligand sidechains retain similar positions among different variants as well as in the absence and presence of cations. Indeed, in

solution, the freedom provided by the additional sidechain length allows the protein to adopt a local conformation with a less charge density.

Binding of Ln^{3+} or Ca^{2+} neutralizes the charge repulsions, resulting in the thermal transition point increase. More the charge clustered at the location, greater the effect of the cation binding. EEDDD and EEDDE underwent a T_m enhancement of ~10 °C and EEDDN and EEDDQ underwent a T_m enhancement of ~5 °C while the effect of Ca^{2+} or Tb^{3+} binding on the T_m of EENDN and NENDN is insignificant. Many proteins require Ca^{2+} for structural stabilization. For example, Ca^{2+} binding increased the thermal transition points of equine lysozyme or α-lactalbumin more than 45 °C (*53*). The thermal transition point of Ca^{2+}-loaded E-cadherin domains 1 and 2 is 25 °C higher than that of the apo-form (*54*). The role of Ca^{2+} in stabilizing secondary and tertiary structures is not always reflected by dramatic conformational change (*55*). Similarly, 7E15 variants do not have significant secondary structural differences in the presence or absence of Ca^{2+} Ca^{2+} conferred thermostability (Table 2.2).

2.2.8   Protein surface electrostatic potential.

The electrostatic energy levels of proteins provide clues on the cation binding and stability of the proteins. For 7E15 variants, the relative Ln3+ and Ca2+ binding as well as the thermal stability from the electrostatic calculation and the experimental measurement agree each other at most cases. For example, the variants with more negative charges possess stronger Ln3+ affinities and lower thermal transition temperatures. The variants EENDN and NENDN do not bind to Ln^{3+} and Ca^{2+} or have very weak binding affinities. In the presence of divalent or trivalent cations, the thermal transition points increases and

the increasing level is related to the clustered charge numbers. However, the prediction is not completely consistent with the experiments, mainly for EEDDE and EEDDQ. The electrostatic potential is calculated based on the model structures and the residue atoms are assumed to be unmoved upon the cation binding. This is not true since at least local conformation rearrangement will occur upon the binding. Therefore, the energy difference between the cation-free and –loaded forms reflects more the relative strength of pure cation binding process but not including the energy cost for the conformational change. The higher Tm values for EEDDE and EEDDQ compared to EEDDD and EEDDN indicate that EEDDE and EEDDQ maintain relatively lower energy levels both with and without the cation binding. The results suggest that without the global conformational changes, longer sidechains facilitate the local geometric adjustment to stabilize the protein. In addition, the apparent Ca^{2+} binding affinity depends on the energy difference of the two forms of the protein. Thus, the effect of the longer sidechains on the affinity depends on the different effects on the apo- and loaded forms (56-59).

2.3   Conclusions

In summary, in a relatively restricted Ca^{2+}-binding site, more negative charges facilitate the Ca^{2+} and Ln^{3+} binding accompanying with a tradeoff of protein stability due to the high energy level of the apo-forms. When the apo-form of the protein is capable of maintaining a relatively lower energy due to the global or local conformational change, a charge number of -4 is preferred for Ca^{2+} over -5 because at the Ca^{2+}-loaded form the attraction between the Ca^{2+} and the fifth negative charge cannot compensate the repulsion of multiple negative charges. It looks like that the steric size of the ligand residues is not

crucial as long as the Ca^{2+}-binding pocket is properly formed but the additional freedom of E/Q over D/N facilitates lowering the energy level of the protein. Ca^{2+} or Ln^{3+} binding increases the thermal transition temperatures relating to the clustered charge numbers at the site. The development of steadfast trends in Ca^{2+}-conferred thermal stability and Ca^{2+} binding affinity in relation to net charge and ligand type would be beneficial. Using these trends, it may be feasible to develop mutant Ca^{2+}-dependent thermozymes with enhanced stability. More importantly, a better understanding of the key factors involved in Ca^{2+} binding affinity and Ca^{2+}-conferred thermal stability will aid in dissecting the role of aberrant Ca^{2+} binding proteins in diseases.
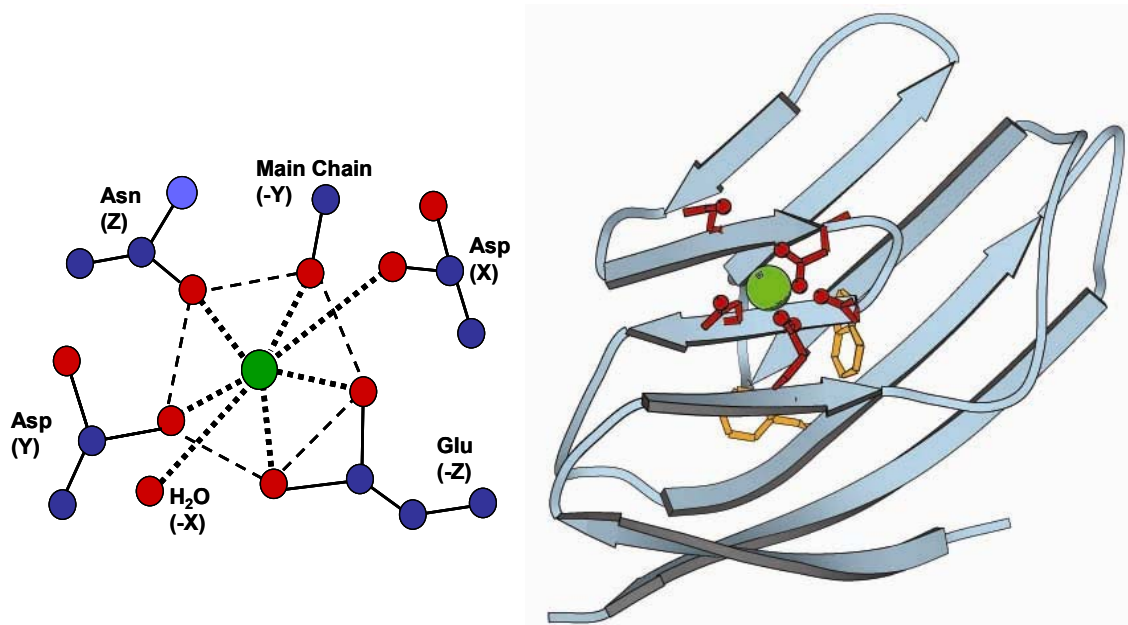
Figure 2.1 Design of Calcium binding protein CD2.7E15
Left: pentagonal bipyramidal arrangement of the metal binding site. Right:
Molscript of CD2.7E15 based on the solution structure of CD2.D1 (PDB ID 1HNG)
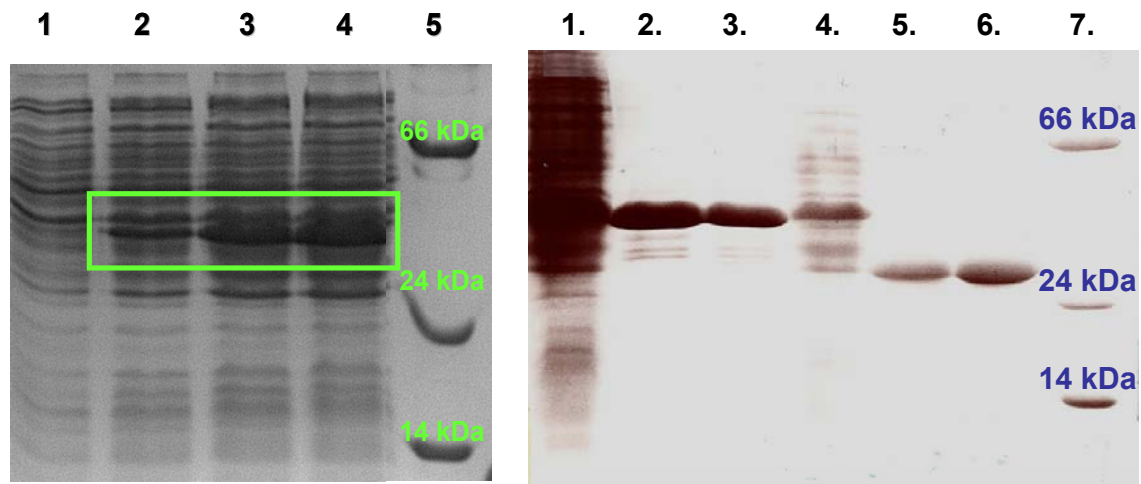
Figure 2.2 pGEX-2T Expression and Purification SDS-PAGE
SDS-PAGE of a CD2.7E15 variant expressed using a GST-fusion system (pGEX-2T
vector). Left: expression of a CD2.7E15 variant. Lane 1 is before induction, lanes 2,
3, and 4 are taken at one hour increments after induction with 0.4 mM IPTG.
Right: Affinity column purification. Lane 1 is the supernatant after sonication,
lanes 2 and 3 are the Glutathione sepaharose beads after binding to the supernatant,
lane 4 is the waste after binding, lanes 5 and 6 are the glutathione sepharose beads
after cleavage with thrombin protease, and lane 7 contains the molecular weight
standards.
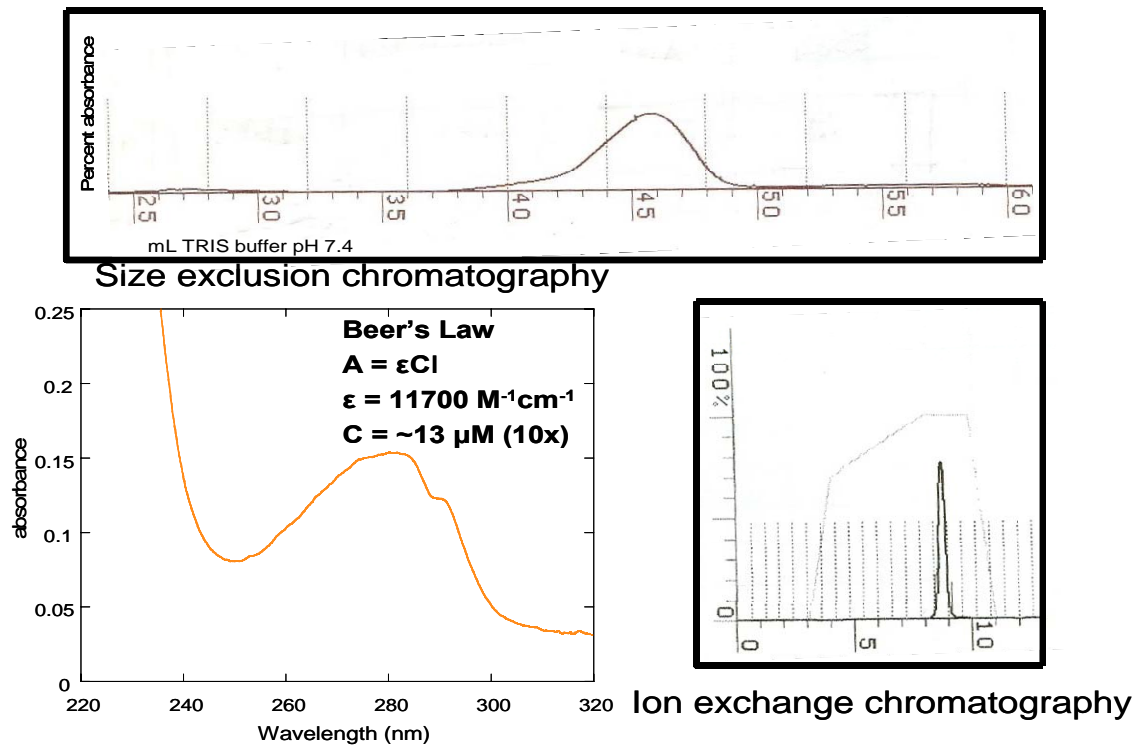
Figure 2.3 pGEX-2T purification
Top: size exclusion chromatograph. Lower left: example of UV absorbance
spectrum of purified protein. Lower right: cation exchange chromatograph
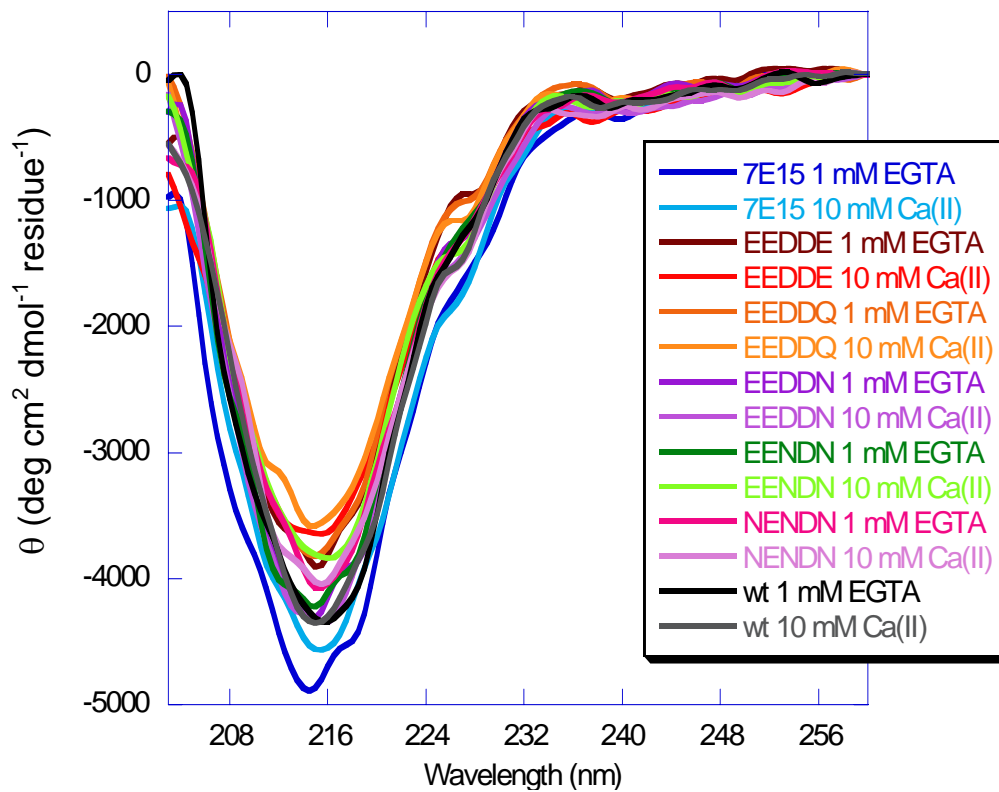
Figure 2.4 Far UVCD analysis of CD2.7E15 and its variants
Far ultraviolet circular dichroism spectra of CD2.D1, and the CD2.7E15 variants
with and without calcium. .
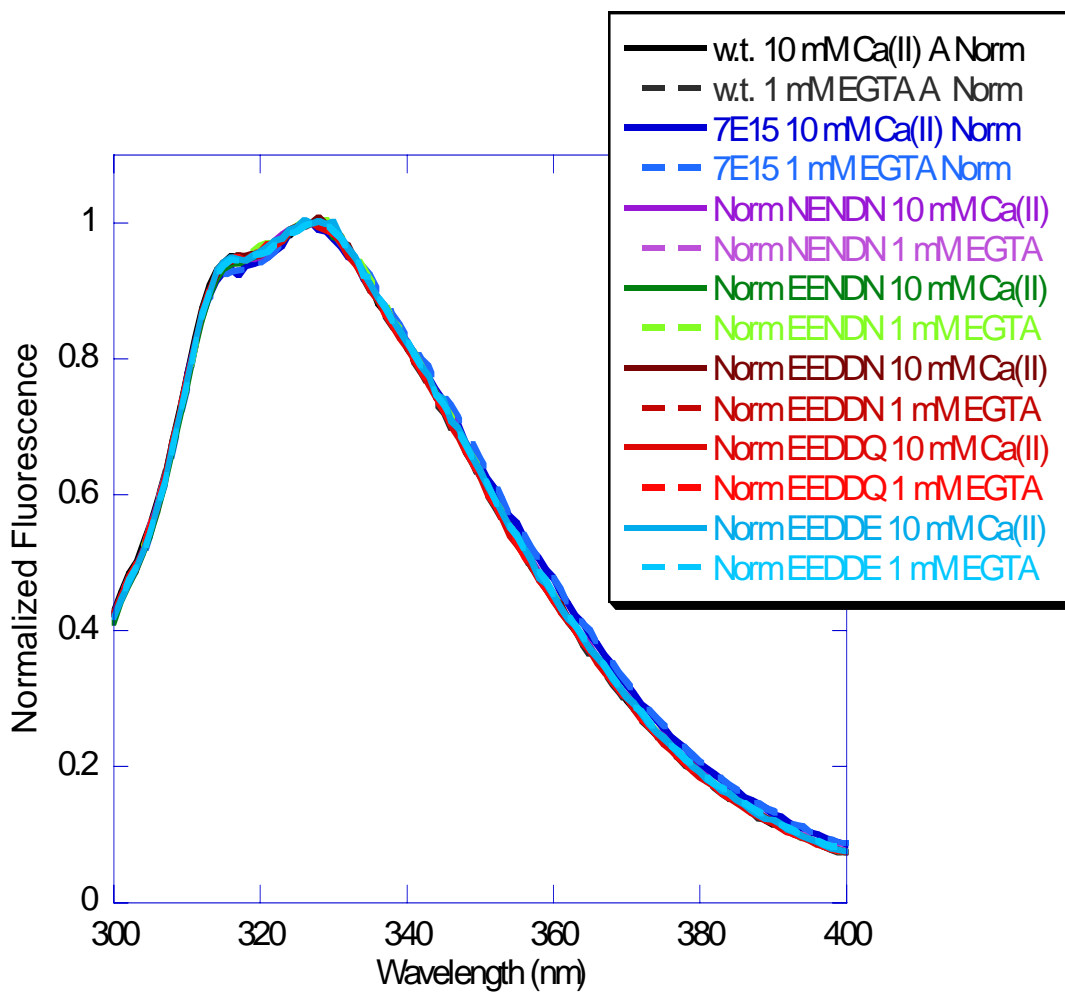
Figure 2.5 Trp Fluorescence Spectra of CD2.7E15 and its Variants
Tryptophan fluorescence emission specra of CD2.D1, and the CD2.7E15 variants
with and without calcium
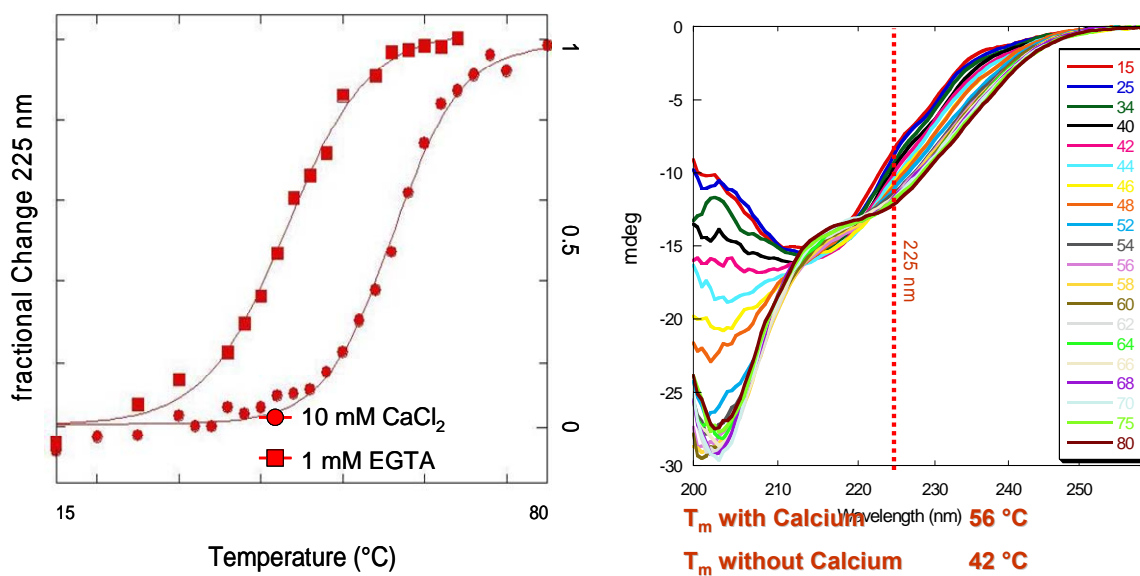
Figure 2.6 Temperature Dependence of CD2.7E15 monitored by Far UVCD
Left: Fractional change of far UVCD signal (in mdeg) at 225 nm with increasing temperature from 15 to 80 °C. Right: far UVCD spectra of CD2.7E15.EEDDE in increasing temperature.

Table 2.2 Summary of T_m Values Observed using Far UVCD
Melting temperatures (T_m) of CD2, CD2.7E15, and CD2.7E15 variants determined
by fractional change of CD signal at 225 nm. All experiments were done in 10 mM
TRIS, 10 mM KCl plus 10 mM CaC$_2$, 1 mM EGTA, or 50 uM Tb(III).

Protein	T_m Ca(II)	T_m EGTA	T_m Tb(III)
CD2	64.3 ±2.5	68.2 ±1.3	---
7E15/EEDDD	51.1	40.9	---
EEDDE (-5)	56.1	44.2 ±1.5	63.5±1.6
EEDDQ (-4)	61.0 ±1.3	55.9 ±0.6	59.5±0.5
EEDDN (-4)	56.7	51.9 ±1.5	53.7±0.5
EENDN (-3)	59 ±1.1	61.3 ±1.5	58.7±1.8
NENDN (-2)	57.7 ±1.2	60.2 ±2.8	58.2±3.6

3   Increasing the Yield of 7E15 and 7E15-bom

The second objective of this work is to develop a simple, rapid, high-yield protein purification procedure for the engineered protein contrast agents (see detailed introduction in section 1.2). This section describes the expression and purification experiments directed towards increasing the yield of purified CD2.7E15 and CD2.7E15-bom beyond the levels previously attained using pGEX-2T vector and BL21 E. coli expression system (described in Chapter 2).

3.1   Materials and Methods

3.1.1   Cloning

All cloning experiments were done by Lixia Wei (PhD candidate at the time of this thesis, Georgia State University Department of Biology). The CD2.7E15 or CD2.7E15-bom sequence was removed from a pGEX-2T vector using BamH1 and EcoR1. The 7E15 sequence was then ligated into the modified pET30a vector. The pET30a vector was modified by removal of the S Tag and the 7E15 and 7E15-bombesin sequences were ligated into the modified pET30a vector using BamH1 and EcoR1.

3.1.2   Transformation of E.Coli

pGEX-2T vectors with ampicillin resistance (T7 promoter) were used for the cloning and site-directed mutagenesis. Protein sequences were between BamH1 and

EcoR1 restriction sites. The pGEX-2T vector allows for the expression of a Glutathione S-Transferase (GST) fusion protein with a thrombin protease cleavage site so that affinity column purification using agarose/glutathione beads can be used to capture the protein of interest and then remove the protein from the GST using thrombin. The designed proteins can be cleaved from the GST in the column or in solution.   Transcription of the fusion protein sequence was controlled by the lac promoter so that expression could be induced at a desired time.

The heat shock technique was used to transform all E. coli. To begin the procedure, a 1.5ml eppendorf tube containing approximately 100 uL desired competent cells (BL21 (DE3) for expression, DH5α for DNA purification) was obtained from a stock of competent kept at -80° C. The cells were placed on ice to thaw and aliquotted into two 50 µL samples. One sample receives 0.5-1.0 µl of desired plasmid DNA while the other did not receive DNA (this is the negative control). The thawed cells and DNA were mixed by pipetting up and down or gently flicking the bottom of the tube. The cells were left on ice for at least thirty minutes after the addition of DNA. The heat shock was done by placing the cells in a 42 °C water bath for ninety seconds and then putting the cells back on ice for two minutes. Then, 50 µL LB media was added and the media was mixed with the cells by pipetting up and down or by gently flicking the bottom of the eppendorf tube. The tubes were then incubated at 37 °C for 30 minutes. 50 µL of the solution was added to desired agar plates (LB-Amp plates for expression) and streaked onto the plates with a sterile triangle. The plates were then incubated at 37° C overnight.

The plates were wrapped in parafilm and placed upside-down in the refrigerator the subsequent morning. No plates were kept longer than one month.

3.1.3 Expression of Histidine Tagged CD2.7E15 and CD2.7E15-bomesin

Lauria-Bertani broth was prepared according the recipe in the appendix. A single colony from a transformed plate with the plasmid of the desired protein was inoculated into at least 100-500 ml of LB broth with an ampicillin concentration of 100 μg/ml for overnight growth at 37° C and 200-220rpm agitation. The following morning, 30-100 ml of the overnight growth was transferred to 1L of fresh LB broth with a kanamycin concentration of 30 mg/L. The flask was then incubated at the desired temperature and 200-220 rpm agitation. The growth of the cells was monitored by measuring the optical density (light scattering) at 600 nm and comparing to the optical density of LB before the addition of cells. When the desired optical density was reached (0.8-1.0), the cells were induced with 0.2-1.0 mM IPTG. Samples were taken during expression for analysis using SDS-PAGE. The first sample was always taken immediately before induction with IPTG and subsequent samples were taken at various times during expression. The cells were allowed to grow 2-4 hours after induction according to the progress of cell growth as indicated by optical density readings. The cells were harvested by centrifugation in 500 ml bottles at 7 krpm for 15-20 minutes using a GS3 rotor. The cell pellets were collected using a spatula and less than 5 ml PBS buffer and placed in a 50 ml falcon tube and stored at -20 °C for purification at a later date. The supernatant was discarded.

3.1.4 Isolation of Inclusion Bodies Enriched with Insoluble Protein

The desired cell pellet was thawed out on ice or in cold water. 20-50 ml 200 mM NaCl, 50 mM Tris, 1 mM EDTA, pH 8.0 per 2L culture pellet was added to re-suspend the cell pellet from expression. First, the suspended cell pellet was homogenized in a commercial blender by blending 2-3 times for 30 seconds. This solution was sonicated 6 times for 90 seconds using a Branson 450 Sonifier with the duty cycle set on 90 with 5-10 minutes between sonications. The solutions were kept on ice during sonications. The solutions were centrifuged in 50 ml tubes at 17 krpm for 20 minutes using the S34 rotor after sonications.

After cell lysis and centrifugation, inclusion bodies were found in the cell pellet. The cell pellet also contains other insoluble impurities. To remove the lipid-soluble impurities, cell pellets were resuspended in 1% Triton X-100 and re-centrifuged. This procedure was repeated for 3-4 cycles before nondenaturing or denaturing solubilization.

3.1.4.1 Solubilization in Arg

To solubilize inclusion bodies, 300 mg washed inclusion bodies was dissolved in 10 mL 1 M Arg, 200 mM NaCl, 50 mM TRIS, 1 mM EDTA, pH 8.0 for 16 to 20 hours at 4 degrees Celsius with agitation. This protocol is modified from Umetsu et al, who used listed their arginine concentration as 2M (*60*). Since arginine is not soluble at lower temperatures at 2 M, the concentration of arginine was reduced to 1 M for this study.

3.1.4.2   Solubilization in Urea for refolding

To solubilize inclusion bodies under denaturing conditions, washed inclusion

bodies were dissolved in 8 M Urea overnight at 4 °C with agitation. Refolding was done

by diluting the solubilized cell pellet in half with 50 mM TRIS, pH 8.0, or 20 % Sucrose,

50 mM TRIS, pH 8.0. Refolding volumes <1 mL were done using a microdialyzer kit

and 3 kDa cellulose membranes. First, the solubilzed protein was placed in the

microdialyzer well and the well was covered with parafilm. Next, the buffer

compartment was filled with the desired buffer and placed at 4 °C on a magnetic stirring

plate. The buffer was changed after 1 hour, and again after 4 hours, then allowed to

equilibrate overnight. The proteins refolded at volumes >1 mL had to be placed in

cellulose dialysis bags. The bags were placed in 2 L desired buffer and placed at 4 °C on

a magnetic stirring plate. The buffer was changed after 1 hour, and again after 4 hours,

then allowed to equilibrate overnight.

3.1.5   Ni-sepharose affinity column chromatography

Gravity-flow Ni-sepharose affinity chromatography was done by decanting

solubilized protein in the denatured or refolded form into a Ni-Sepharose column

provided by GE Healthcare. Protein was eluted from the column using 0.5 M Imidazole.

The column was provided by GE Healthcare.

3.1.6   Size exclusion chromatography

6-10 ml of crude protein was injected into a Pharmacia Biotech FPLC system.

When the elution volume was greater than 20 ml the elution was concentrated using an

Amicon high pressure concentrating apparatus and an Amicon membrane filter before injection. Samples are filtered with a 0.45 μm filter before injection. Proteins were purified using a size exclusion column and the concentration of each fraction was measured using the UV absorbance (280 nm). The experimentally determined molar extinction coefficient for domain one of wild type CD2 was used for CD2.7E15 (11700 $M^{-1}cm^{-1}$). To determine the concentration of CD2.7E15.bom, the theoretical extinction coefficient (19630 $M^{-1}cm^{-1}$) calculated based on the primary sequence (available at *http://www.basic.northwestern.edu/biotools/proteincalc.html*) was multiplied ratio obtained by taking the experimentally-determined extinction coefficient of CD2.d1 divided by the theoretical value for CD2 ((11700 $M^{-1}cm^{-1}$)/ (13940 $M^{-1}cm^{-1}$)). Fractions with a A_{280}/A_{260} ratio less than 1.0 were rejected, since this would indicate significant nucleic acid contamination.

3.1.7   Cation exchange chromatography

A 5 mL cation exchange column provided by Pharmacia Biotech was used for IEC. Proteins were bound to the cation exchange column at pH 3.0-4.0 and eluted with a buffer gradient beginning at pH 4.5 and ending at pH 8.0. The protein in the resulting fractions was collected according to the quantification procedure in section 1.1.6. Fractions with a A_{280}/A_{260} ration less than 1.0 were rejected or subjected to further purification. Addition of benzonase nuclease during the sonication procedure mad the incidence of a A_{280}/A_{260} ration less than 1.0 a rare occurrence.

3.1.8 MALDI Linear Positive Mass Spectrometry

The purity of the protein was assessed using MALDI mass spectrometry. The samples were scanned in a sinapinic matrix on an ABI Voyager-DE™ Pro Workstation (MALDI) in the linear positive mode. All mass spectrometry samples were done in 50 mM Tris, pH 8.0. The samples were given to the Georgia State University's Biotechnology Core Facility. The samples were stored at 4 °C until analysis.

3.1.9 Calculation of Protein Concentrations

Protein concentrations were determined by measuring UV absorbance from 350 nm to 220 nm. A minimum volume of 800 μL was used in a 1 cm quartz cell. First, the Shimadzu spectropolarimeter was baselined from 350 nm to 220 nm using nanopure water. Then, a blank was kept in the standard slot while the samples were measured in the sample slot.

Because large particles scatter light, a high absorbance at 350 nm relative to absorbance at 280 nm (>about 10 % maximum absorbance at 280 nm) was taken to indicate precipitation. When precipitation was detected or anticipated, samples were 10x diluted with buffer or scanned after the addition of 100 mM Arginine, pH 8.0.

To obtain the protein concentration, the absorbance at 350 nm was subtracted from the absorbance at 280 nm (which should be the absolute highest peak in the spectrum). Then, Beer's law was applied to calculate protein concentration using the relevant extinction coefficient ($A=\varepsilon cl$). The experimentally determined extinction coefficient for wild-type CD2.D1 is 11700 M^{-1} cm^{-1}. The extinction coefficient for 7E15 and histidine-tagged 7E15 (pET30a vector) is taken to be identical to that of CD2.D1

because no aromatic residues have been added or replaced, and the tertiary structures are not significantly different (see Chapter's 3 and 5). The theoretical extinction coefficient for 7E15 based on the primary amino acid sequence is 13940 M^{-1} cm^{-1} and that of 7E15-bombesin is 19630 M^{-1} cm^{-1}.

The theoretical extinction coefficient of 7E15-bom was corrected by dividing the experimentally determined extinction coefficient of 7E15 by the theoretical extinction coefficient to give 16500 M^{-1} cm^{-1}.

Thus the extinction coefficients used throughout this thesis are as follows:

7E15, CD2, and his-7E15:   11700 M^{-1} cm^{-1}

7E15-bom: 16500 M^{-1} cm^{-1}

3.2   Results & Discussion

3.2.1   Expression

To optimize expression of histidine tagged CD2.7E15, we have varied temperature of expression and concentration of IPTG. The expression of the contrast agent in the pET30a vector was found to require relatively high concentrations of IPTG to induce expression (1mM). 0.1 mM, 0.3 mM and 0.5 mM were unsuccessful at inducing any appreciable expression. The protein could be detected using Western blot using an anti-CD2 antibody, but not on SDS-PAGE stained by coomasie blue (Fig 2.3.2). The expression at 1 mM IPTG was able to produce large amounts of protein, as evidenced by the sizeable expression band visible on SDS-PAGE (Fig 2.3.3).

To determine whether or not the high expression level of 1 mM IPTG induction could be utilized to yield soluble protein, the temperature of expression was changed to 30 °C for 5 hours and 22 °C overnight (data not shown). Both procedures resulted in inclusion body formation with CD2.7E15 absent from the supernatant after sonication, indicating that the variation in temperature had not affected the solubility of expressed protein.

Overall, when 1 mM IPTG is used to induce expression at 37 °C, a very large expression band can be seen on coomasie blue stained SDS-PAGE at the appropriate molecular weight (see Fig 3.3). The protein at this band reacts with anti-CD2 antibody in Western blot, confirming that it is the desired protein. CD2.7E15-bom was also successfully expressed at 37 °C for four hours (expression data not shown). The final expression band seen is very thick on SDS-PAGE, often thicker than that seen for pGEX-2T expressed CD2.7E15, which is remarkable since the pET30a construct is much smaller than the GST-fusion protein produced by the pGEX2T vector.

3.2.2   Purification

The purification of his- CD2.7E15-bom was initially attempted under denaturing conditions. The inclusion bodies were solubilized in 8M urea and dialyzed against 10 mM Tris, 10 mM KCl. The dialysis produced a large mass of white precipitate. After centrifuging the precipitate, soluble protein remained suspended. This protein could be purified using cation exchange (Fig 3.5) for a yield of 6 mg/L cell culture, which already exceeds the yield provided by the GST fusion system (2mg/L cell culture of 7E15-bom).

The refolding of CD2.7E15-bom was attempted against 20% sucrose at low volumes (400-500 uL) and various concentrations. The sucrose causes preferential hydration of proteins, which would thermodynamically favor the most compact structure (*61*). In the case of globular proteins such as CD2 and its mutants, this is probably the native state. The protein remained soluble in the 20 % sucrose and seemed to have a secondary structure similar to CD2.7E15 purified using the GST-fusion system, as evidenced by the mostly beta-sheet secondary structure (Fig 3.4). However, this method was not suitable when the purification was scaled up to 1, 4, and 10 mL. This may be due to the difference in dialysis procedure. The lower volumes used a microdialysis system, where a single permeable membrane below the sample allows solvent exchange. The larger volumes required the protein sample to be placed in a dialysis bag, which allows solvent exchange from all directions. This rapid removal of sugar may have destabilized the protein.

Nondenaturing solubilization as described by Umetsu et al (*60*) was found to be the best solubilization procedure; yielding an average of 20 ± 5 mg/ 300mg wet solubilized inclusion bodies for his- CD2.7E15. Histidine-tagged CD2.7E15-bom did not solubilize well in the high arginine buffer (data not shown), which could be due to a lack of secondary or tertiary structure in the insoluble form. Cell lysis using sonication results in a cell pellet that contains most of the desired protein for CD2.7E15 and CD2.7E15-bom (Fig 3.7). Washing in 1 % Triton X-100 probably removes lipid-soluble contaminants, which seems to relieve some of the smudging of SDS-PAGE (Fig 3.7).

The protein solubilized using 1 M arginine solution was exceptionally pure after size exclusion chromatography as visualized by SDS-PAGE (Fig 3.7). The SDS-PAGE shows no impurities and the linear positive mode MALDI mass spectrum contains two major impurities at 10648, 15771 Da/ charge (Fig 3.8). The arginine solubilization provides an initial enriching procedure because the CD2.7E15 is the main constituent of solubilized protein. The protein of interest is sufficiently different in molecular mass from most of the other solubilized proteins to be purified using a G75 sepharose size-exclusion chromatography column.

CD2.7E15-bom could not be solubilized in 1 M arginine, which may suggest that it is unfolded in inclusion bodies. The protein was successfully solubilized in 8 M Urea and refolded using 20 % Sucrose (Fig 3.4). The protein was unfolded in 8 M Urea as shown by the random coil far UVCD spectrum and became mostly beta sheet after dialysis against 20 % Sucrose, 50 mM Tris, 50 mM KCl, pH 8.0. The protein did not acquire a secondary structure identical to 7E15 purified using the GST-fusion system because of the additional random coil character conferred by the histidine tag and the fourteen residue bombesin tag. This refolding procedure was successful at volumes less than 1 mL, but did not scale up very well. The proteins refolded using this protocol were subsequently purified using size exclusion chromatography before the far UVCD spectrum was taken (Fig 3.4).

A simple solubilization using 8 M Urea and dialysis against 50 mM Tris, 50 mM KCl was attempted. The solubilized inclusion bodies precipitated after dialysis. The insoluble fraction was removed by centrifugation and the supernatant was purified using

cation exchange chromatography (Fig 3.5). The yield of CD2.7E15 bom using this procedure was 6 mg/ L cell culture, which already exceeds the yield of CD2.7E15-bom using the GST-fusion system.

The solubilized protein was also purified in denaturing conditions using a Ni-sepharose column. The resulting elution was pure, but it precipitated (Fig 3.5).

Nondenaturing solubilization is superior to the refolding techniques explored in this chapter because it takes advantage of proteins that are already fully or partially folded rather than exposing the protein to denaturing conditions, from which it could potentially fail to recover. The insoluble aggregates after arginine solubilization could be subjected to a refolding procedure in the future to develop a more efficient purification method. The majority of the insoluble pellet is the desired protein and the majority of the protein solubilized by 1M Arginine is the desired protein.

Solubilization at 4 ℃ does not solubilize as much DNA: the ratio of 280 nm/260 nm absorbance for 4 ℃ solubilization was 1.25 compared to 1.13 for 27 °C and 1.02 for 37 ℃ (Fig 3.6). Solubilized DNA can interfere with further purification using FPLC, as the peak monitor only detects absorbance at 280 nm which can come from the tail of a strong absorbance at 260 nm. This may be a result of arginine's reduction in protein thermal stability (*62*).

3.2.3   MALDI Mass Spectrometry

The protein his- CD2.7E15 was analyzed using linear positive MALDI masss spectrometry. The major m/z peak was found at 12356.4 Da. The molecular weight of his-7E15 is 12356 Da by mass spectrometry, which is 1067 Da larger than CD2.7E15

purified using the GST fusion system, a result of eight residues at the N-terminal of CD2.7E15 (HHHHHHSSG) conferred by the pET30a vector (Fig 3.8). This has to be considered when comparing the yields of his- CD2.7E15 and CD2.7E15 purified using the GST fusion system. The addition of the histidine tag and its accompanying residues constitute a 10 % increase in molecular weight, which is insignificant given the massive increase in purification yield.

3.3 Conclusions and Future Work

Induction with 0.3 mM IPTG can produce expression levels detectable by Western blot with an Anti-CD2 antibody, but western blotting techniques are considerably more sensitive than coomassie blue stain (Fig 3.2). For these studies, and, more importantly, the proposed application of CD2.7E15, a much higher expression level is needed. The pET30a vector requires induction with IPTG concentrations in excess of 0.5 mM, but the resulting expression level is high (Fig 3.3).

The histidine-tagged CD2.7E15 protein can be purified using either refolding or nondenaturing solubilization. Nondenaturing solubilization in 1 M Arg probably works by causing preferential hydration of the individual molecules that are fully folded, which would favor the most compact solution structure (*63, 64*). The most compact structure of a globular protein like CD2 or CD2.7E15 is probably the native structure. It is possible that this high concentration of arginine could cause partially folded intermediates that have been sequestered into inclusion bodies to adopt the compact native structure. According to the data presented here it is most likely that the arginine is releasing proteins from inclusion bodies that are already folded or sufficiently close to the compact

globular structure. The solubilization buffer contains 200 mM NaCl, which may act to increase hydrophobic interactions such that unfolded proteins that have aggregated at hydrophobic contacts remain insoluble, while the arginine keeps the proteins that are folded in a compact state. The selective solubilization of the overexpressed CD2.7E15 can be seen in the SDS-PAGE (Fig 3.6). The 8 M Urea solubilizes all constituents of the inclusion bodies, folded and unfolded, while the 1 M Arg buffer solubilizes only the proteins that were folded, which is predominantly the overexpressed protein of interest. 8 M urea preferentially binds to proteins, causing indiscriminate solubilization and unfolding (*65*).

Looking at solubilization in 4 °C, 27 °C, and 37 °C, There seems to be a temperature dependence of arginine solubilization with 4 °C providing the most protein solubilized. This can be seen on SDS-PAGE and is in good agreement with the absorbance ratio between 280 nm and 260 nm—4 °C has the most protein solubilized and the highest ratio of protein to DNA solubilized (Fig 3.6).

The overlapping Trp fluorescence spectra of CD2 and CD2.7E15 purified using 1 M Arg solubilization is the strongest piece of evidence for a fully compact tertiary structural arrangement (Fig 4.1). This is an important piece of information, as it goes against the classical method of purification from inclusion bodies. This is also a shining example of the stability of CD2; it has managed to maintain its tertiary structure after three mutations have been made to produce a surface metal binding site, a 6 x histidine tag has been added to the N-terminal, and it has been sequestered in inclusion bodies.

In summary, the non-denaturing solubilization purification procedure developed in this section has exceeded the yield of CD2.7E15 purified using the GST-fusion system by taking advantage of inclusion body purification, selective nondenaturing solubilization of overexpressed protein, and subsequent purification using size exclusion chromatography.

In the future, an additional or alternative purification step should be explored because the protein contains some impurities detected by linear positive MALDI mass spectrometry. The first alternative purification method should be FPLC Ni-chelating column chromatography or gravity-flow Ni-Sepharose chromatography after arginine solubilization. Also, perhaps solubilization in various concentrations of arginine, urea, and GdHCl can be compared to determine the optimal conditions of nondenaturing solubilization.

Because a histidine tagged protein cannot be used *in vivo,* a thrombin cleavage site is included between the histidine tag and the protein. This is also important because the histidine tag is probably affecting the solubility of CD2.7E15, which can normally be concentrated to 200 to 400 uM concentrations without excipients, while the histiding-tagged protein purified in this thesis was found to require 0.1% polysorbate 20 to achieve approximately 200 uM concentration.
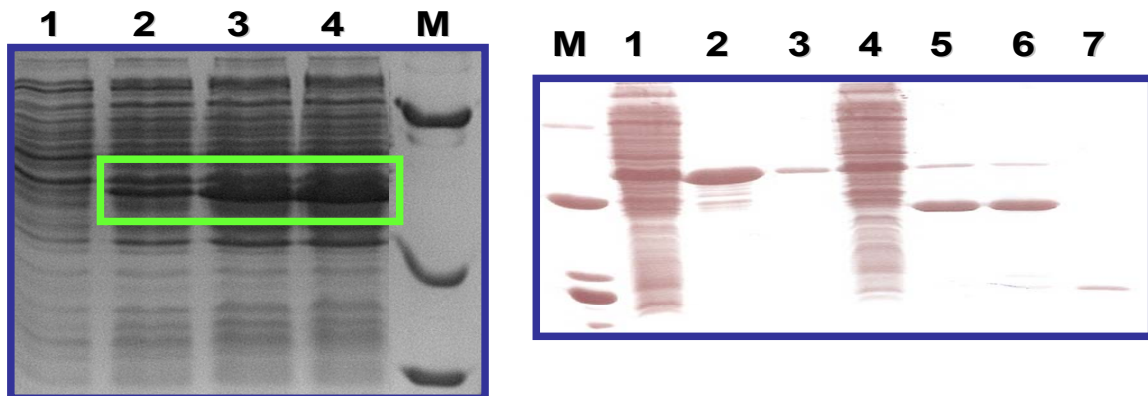
Figure 3.1 pGEX-2T Expresion and Purification SDS-PAGE
SDS-PAGE analysis of expression and purification of CD2.7E15. Lanes marked M are the protein standards of 66, 24, and 14 kDa. Left: CD2.7E15 expression using pGEX-2T. Lane 1 is the cells before induction with 0.3 mM IPTG and lanes 2, 3, and 4 are taken at 1 hour increments after induction. Right: Glutathione-sepharose affinity column purification of CD2.7E15. Lane 1 is the supernatant after sonication, 2 & 3: beads after binding, 4: waste after binding, 5 & 6: beads after thrombin cleavage, 7: elution after cleavage.
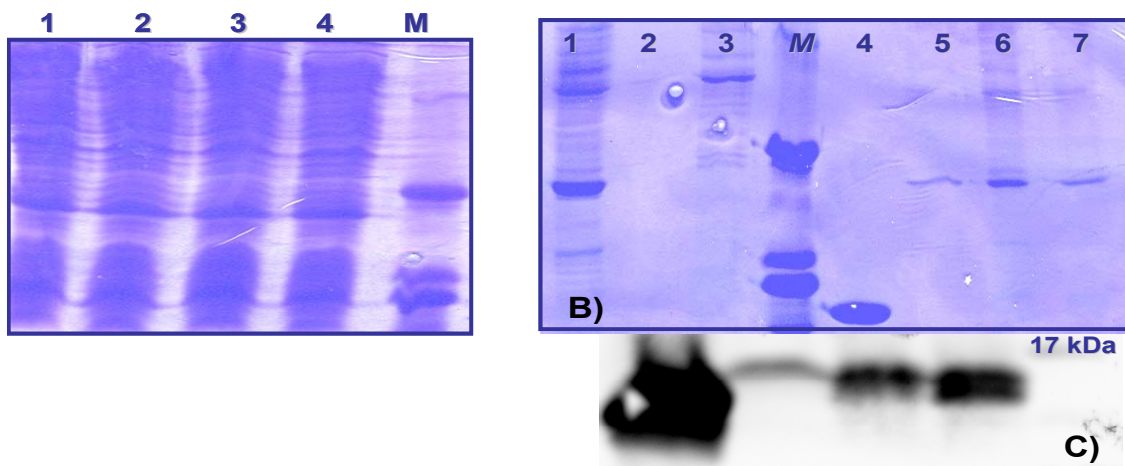
Figure 3.2 Failed his-7E15 Expression and Purification SDS-PAGE
A) SDS-PAGE of expression of his-7E15-bombesin in pET30a. Lane 1 is 1 hour after induction with 0.4 mM IPTG, Lane 2 is 2 hours after and so on. M contains the MW standards, which, from top to bottom, are 66, 24 and 14 kDa. B) Lane 1 is Ni-NTA fraction 5, Lane 2 is a dilution of Ni-NTA fraction 6, Lane 3 is fraction 6 from the Ni-NTA column, Lane 4 is 7E15 purified using a GST-tag, lane 5 is SEC fraction 9, lane 6 is SEC fraction 10, and lane 7 is all other SEC fractions. The protein marker is in the lane marked "M." C) Western blot using an anti-CD2 monoclonal antibody. The lanes are, from left to right: 7E15 purified using the GST-system (lane 4 in figure 2B); 7E15-bom-his (lane 5 in figure 2B); 7E15-bom-his (lane 6 in figure 2B); and 7E15-bom-his (lane 7 in figure 2B).
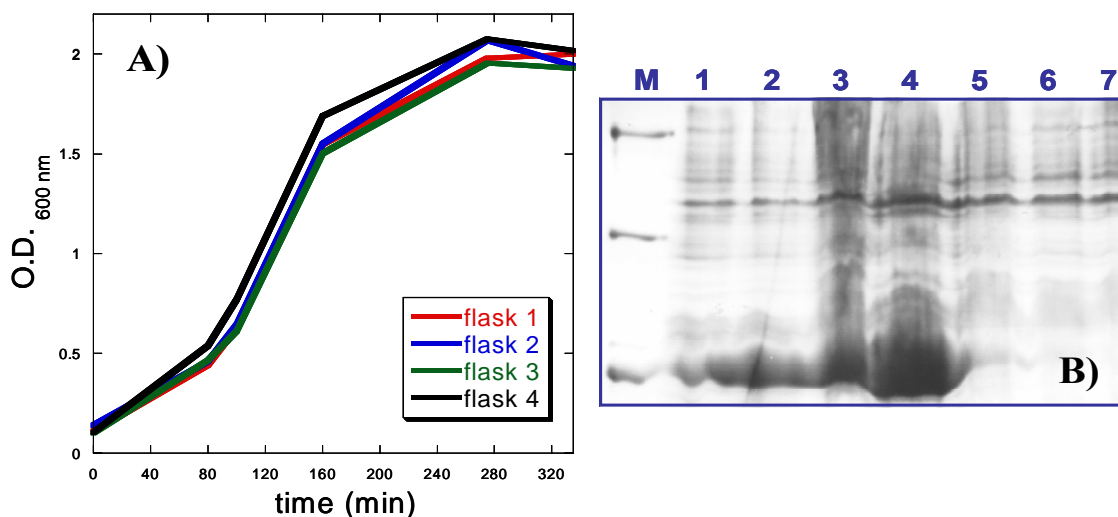
Figure 3.3 Successful pET30a Expression Growth Curve and SDS-PAGE
Left: Expression of CD2.7E15 using a pET30a vector in BL21 cells monitored by
optical density at 600 nm. Right: SDS-PAGE analysis of CD2.7E15 expression. M:
protein standards 66, 24, and 14 kDa, 1-4: 1 hour increments after induction with
1.0 mM IPTG, 5-7: before induction.
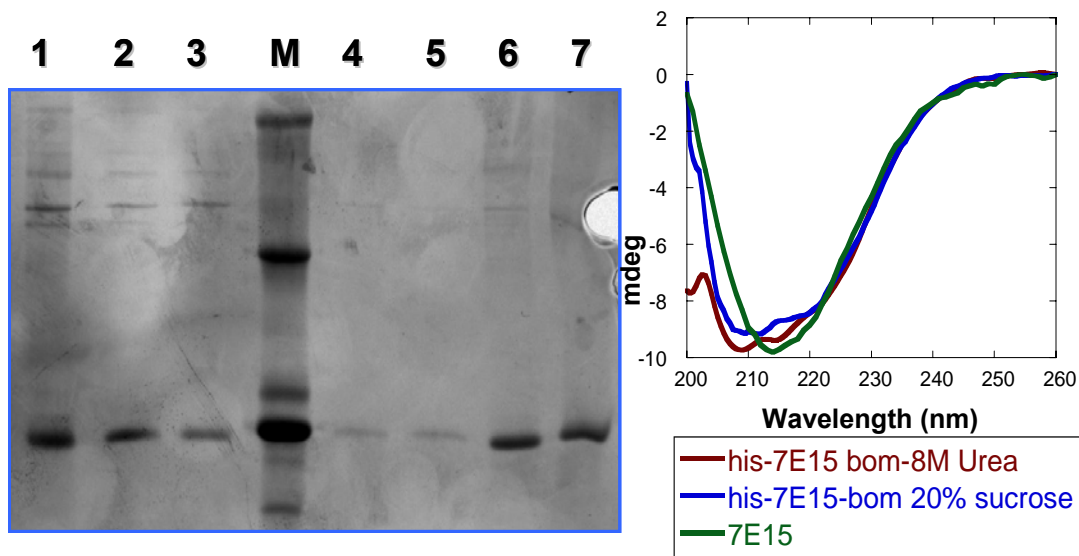
Figure 3.4 Refolding of his-7E15-bom in Sucrose
Left: SDS-PAGE analysis of CD2.7E15 (lanes 1-3) and CD2.7E15.bom (lanes 4-7)
refolded against 20% sucrose solution and then purified using size exclusion
chromatography. M is the protein molecular weight standards of 66, 24, and 14
kDa. Right: Far ultraviolet circular dichroism spectra of CD2.7E15.bom unfolded
and refolded in 20 % sucrose compared to 7E15 purified using the GST-fusion
system (10 mM TRIS, pH 8.0).

Figure 3.5 Purification SDS-PAGE
SDS-PAGE analysis of CD2.7E15 each gel contains MW standards of 66, 24, and 14
kDa. Left: IB's solubilized in 8 M and the SN after dialysis. Center: Fractions after
CEC purification. Right: the left lane is the waste after Ni-Sepharose purification
and the right lane is the elution.

T (°C)	Abs ratio 280/260 nm
4	1.25
27	1.13
37	1.02

Figure 3.6 Arg Solubilization Temperature Dependence
Left: SDS-PAGE analysis of CD2.7E15 solubilized in 1 M arginine and 8 M Urea.
Center: Ratio between UV absorbance of IBs solubilized at different temperatures.
Right: CD2.7E15 solubilized at 4, 27, and 37 degrees Celsius. The markers for each
SDS-PAGE gels are 66, 24, and 14 kDa.

Figure 3.7 Arginine Solubilization and SEC Purification
SDS-PAGE analysis of CD2.7E15 purified using Arginine solubilization and size exclusion chromatography. Left: Solubilization procedure. 1: supernatant after sonication, 2: supernatant after washing with 1% Triton X-100, 3: cell pellet after sonication, 4: supernatant after solubilization with 1 M Arginine, 5: cell pellet after washing, 6: cell pellet after solubilization and centrifugation.

$$6178 = \text{his-7E15} + 2H^+$$
$$12356 = \text{his-7E15} + H^+$$
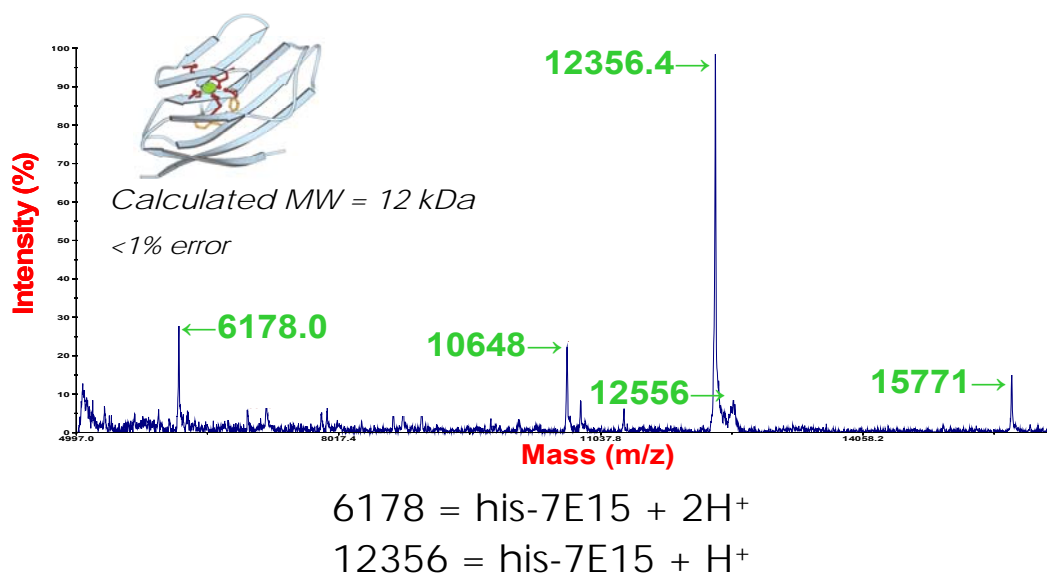
Figure 3.8 Linear positive mode MALDI mass spectrometry analysis of CD2.7E15 purified using 1 M Arginine solubilization and size exclusion chromatography.

4   Preparation and Physical Properties of Microspheres Consisting of Albumin Encapsulated Contrast Agents

Albumin microspheres are micrometer-sized capsules consisting of an albumin scaffold in which drug molecules may be immobilized. The albumin molecules are crosslinked with glutaraldehyde, with the degree of crosslinking determining the time required for the albumin matrix to disperse and release the loaded drug (see figure 4.1). Albumin encapsulation has the following applications in optimal drug delivery: sustained or timed release, prolonged circulation time, targeted delivery, high-capacity drug delivery, non-immunogenicity, and protection from proteases.

Due to the selective portioning of micrometer-sized particles, albumin encapsulation will provide our contrast agent with a prolonged circulation time and targeted delivery (*43*). Microspheres shift the Biodistribution to the vasculature by increasing circulation time and selective phagocytosis by endothelial cells (*32, 66-68*). Haswani, et al found that 46% of free gentamicin accumulated in endothelial cells, while 86% of encapsulated gentamicin was found in endothelial cells. Also, selective phagocytosis of albumin microspheres by lung-associated lymphatic tissues has been observed. Finally, and perhaps most relevant to this thesis project, the interstitium of tumors and inflamed tissues receive large amounts of injected microspheres due to enhanced capillary permeability (*34-37*).

The high capacity of albumin microspheres (up to 10 to 20 % drug by weight) is a major advantage due to the concentration dependence of contrast-enhanced MR imaging.

The scaffold molecule, bovine serum albumin (BSA), is nonimmunogenic and protects encapsulated products from proteases (*38-40, 69*).

The glutaraldehyde crosslinking process creates a covalent linkage between free amino groups (either lysine or N-terminal) in the BSA so that BSA polymers are created. The degree of BSA crosslinking can be manipulated to cause microspheres to release their contents slower (sustained release) or after a certain period of suspension (timed release). In the future, microspheres containing our designed protein contrast agents could be formulated such that dissolution is timed to occur when microspheres have partitioned to tumors.

The goal of microsphere encapsulation of the contrast agents, 7E15 and 7E15-bombesin, is to provide a scaffold for tumor-specific drug delivery, while shielding from circulating protease activity. Although not discussed in this thesis, the possibility of vascular and pulmonary imaging, and the optimization of release kinetics, will be explored in the future.

The spray drying of albumin microspheres was performed by Neil J. Patel at Mercer University's Department of Pharmaceutical Science in Dr. Martin D'Souza's laboratory (see figure 4.2 for a diagram of a laboratory scale spray dryer).

4.1   Materials and Methods

4.1.1   Sample Preparation and Spray Drying

The BSA formula is patented by Dr. Martin J. D'Souza's group at Mercer University's Department of Pharmaceutical Science. To prepare a sample for spray

drying, protein contrast agents were combined with the BSA formula according to the desired drug/BSA ratio. The initial formulation is a liquid, with BSA at 5 mg/mL. 7E15-bombesin loading ranged from 1-10% by final composition of microspheres. The histidine tagged CD2.7E15 and CD2.7E15-bom could be concentrated to >200 μM using 0.1 % Polysorbate 20 in 50 mM TRIS, pH 7.4. A solution of 475 mg BSA was combined with 25 mg of CD2.7E15, CD2.7E15-bom or Gd-DTPA for 5 % loaded microspheres. For those microspheres containing stabilizing trehalose, a solution of 450 mg BSA, 25 mg trehalose, and 25 mg of CD2.7E15, CD2.7E15-bom or Gd-DTPA was used. The 2 % crosslinked microspheres were produced by reacting the BSA solution with glutaraldehyde and then stopping the crosslinking reaction before adding CD2.7E15, CD2.7E15-bom or Gd-DTPA.For those samples containing Gadolinium, the protein was incubated with 1:1 $GdCl_3$ (molar ratio) for >2 hrs before being combined with the BSA solution for spray drying. Before spray drying loaded microspheres, a blank sample was always prepared to check the machinery. Low yields would have required that adjustments be made until a suitable yield could be obtained using only BSA and the excipients (typically defined as >75 %).

All samples were spray-dried on Büchi B191 Laboratory Scale Spray Dryer in Mercer University's Department of Pharmaceutical Science. A homogenous mixture of MRI contrast agent**:** trehalose**:** BSA (1:1:18) was dissolved in citrate buffer, pH 6.0 so as to make a 5% solution was prepared for spray drying. Spray drying was performed using a laboratory scale spray dryer (Buchi B-191), which operates in co-current flow. This model uses co-current air flow so that the hottest air contacts the coolest liquid. A

pneumatic two-fluid pressure nozzle with a 0.7 mm diameter was used to atomize the homogenous solution. The nozzle was supported by a peristaltic pump rate of 5% and an in-house supply of compressed air at 700 NL/hr. The filtered air was aspirated at 75%. The inlet and outlet temperatures were 110°C and 63°C respectively. The solvent from the droplets of homogenous solution were evaporated by hot air during its descent within the spray cylinder, thereby forming solid microparticles. The solid microparticles were further processed by separation through a High Efficiency Performance Cyclone and ultimately settled and collected in a 30 dram glass vial. The vial was parafilmed upon completion of spray drying and stored at 4 °C.

4.1.2   Laser Particle Size Measurements

The size of the spray-dried microspheres was determined using a Spectrex IR Laser particle sizer, which measures the Rayleigh scattering of focused infrared light to determine particle sizes. Sizes greater than 10 micrometers or less than 1 micrometer cannot be discerned. Spray dried microspheres were simply dissolved in filtered sterile water and scanned (the exact concentration is not necessary). The Spectrex IR Laser particle sizer software averages all particle sizes together and provides a standard deviation. It will also give a particle count and categorize each particle according to micrometer size (using whole numbers up to 10). The values in Table 3.1 are the average of n=3 with standard deviations. The proteins marked "his-" were purified using the arginine solubilization or sucrose refolding procedures outlined in Chapter 1 of this thesis. The blank microspheres are microspheres consisting of albumin only. The protein that isn't marked "his-" was purified using the GST-fusion system.

4.1.3 Zeta Potential Determination

Equation 1

$$U_e = \frac{2 \cdot \varepsilon \cdot \zeta \cdot f(ka)}{3 \cdot \eta}$$

    U_e   =Electrophoretic mobility

    ε   =Dielectric constant

    Z   =Zeta potential

    f(ka) =Henry's function (1 or 1.5)

    η   =viscosity

Zeta potential measurements were done on a Malvern Zetasizer. The zeta potential is a measurement of the ion cloud surrounding a particle. Low zeta potentials indicate particles that need to be reformulated because they would tend to aggregate, preventing dissolution. This analysis is crucial for microspheres—particles with a low zeta potential should not be used in vivo because they would aggregate possibly causing a stroke or other ischemia.

To measure zeta potential, microspheres were dissolved in filtered 1 M KCl and the dissolved mixture was used to fill an electrophoretic cuvette provided by the manufacturer (Malvern) (approximately 1 mL is needed). An electrical field of known strength was applied, through which a laser is then passed. The electrophoretic mobility of the colloid dictates the velocity of the movement of charged particles. The zetasizer measures frequency shifts in an incident laser beam. Using the equation above, the zeta potential of the particles within the colloid can be calculated (see equation 1).

4.1.4 MALDI Linear Positive Mass Spectrometry

Mass spectrometry measurements were taken according to the same specifications given in section 2.2.3.

4.1.5 Measuring Protein Concentration

Please see section 2.1.8 for a detailed description.

4.2 Results & Discussion

The designed protein contrast agents were successfully spray-dried. The zeta potential measurements are shown in (Table 3.2). The zeta potential measures the relative stability of a colloid. The ion cloud surrounding a particle must be of a sufficient strength to counteract Van Der Waals force between particles. If it isn't large enough, the particles will aggregate. It is not possible to dictate an exact threshold of zeta potential that is ideal without knowing the magnitude of Van der Waals attraction between particles, but a zeta potential that is small in magnitude does suggest a particle with a tendency to aggregate. The particles with the lowest zeta potential were not the particles that were found to be the largest in the diameter measurements by Rayleigh scattering (Table 4.3), which suggests that perhaps the zeta potential is large enough in magnitude to prevent a significant aggregation of the particles.

There is a range of microsphere sizes produced by the methods described in this chapter. The optimal size range for passive targeting to tumor, pulmonary, or other vascular beds must be experimentally determined. The microsphere size is affected by

The initial sample volume and the spray nozzle diameter. Slight variations in sample

volume may have resulted in aberrations in particle size.

The mass spectrum of the blank microsphere shows that the blank microsphere

contains BSA only (represented by several m/z peaks in Fig 3.3.3). Any contaminants

significant enough to be detected by MALDI mass spectrometry could affect the outcome

of subsequent experiments. The CD2.7E15 microspheres contain only CD2.7E15 and

BSA (see Fig 4.3).

4.3   Conclusion

The microsphere preparation process produces microspheres of a range of sizes. At

this stage, the goal was merely to prepare albumin encapsulated formulations of the

designed protein contrast agents and determine whether or not spray drying had a

significant deleterious effect on the metal binding or relaxivity. The manipulations

necessary to produce particles of uniform size shall be done in the future when the

optimal size to suit our purpose is determined experimentally through in vivo studies.

The changes in formulation necessary to determine optimal size will likely be concurrent

with studies aimed toward determining the best crosslinking percentage to facilitate

passive targeting. Each new formulation will require new zeta potential measurements.

In summary, CD2.7E15 has been spray dried with and without equimolar

gadolinium, CD2.7E15-bom has been spray dried with gadolinium, Gd-DTPA has been

spray dried, and CD2.7E15 purified using the pGEX-2T expression and purification

system has been spray dried with and without gadolinium.
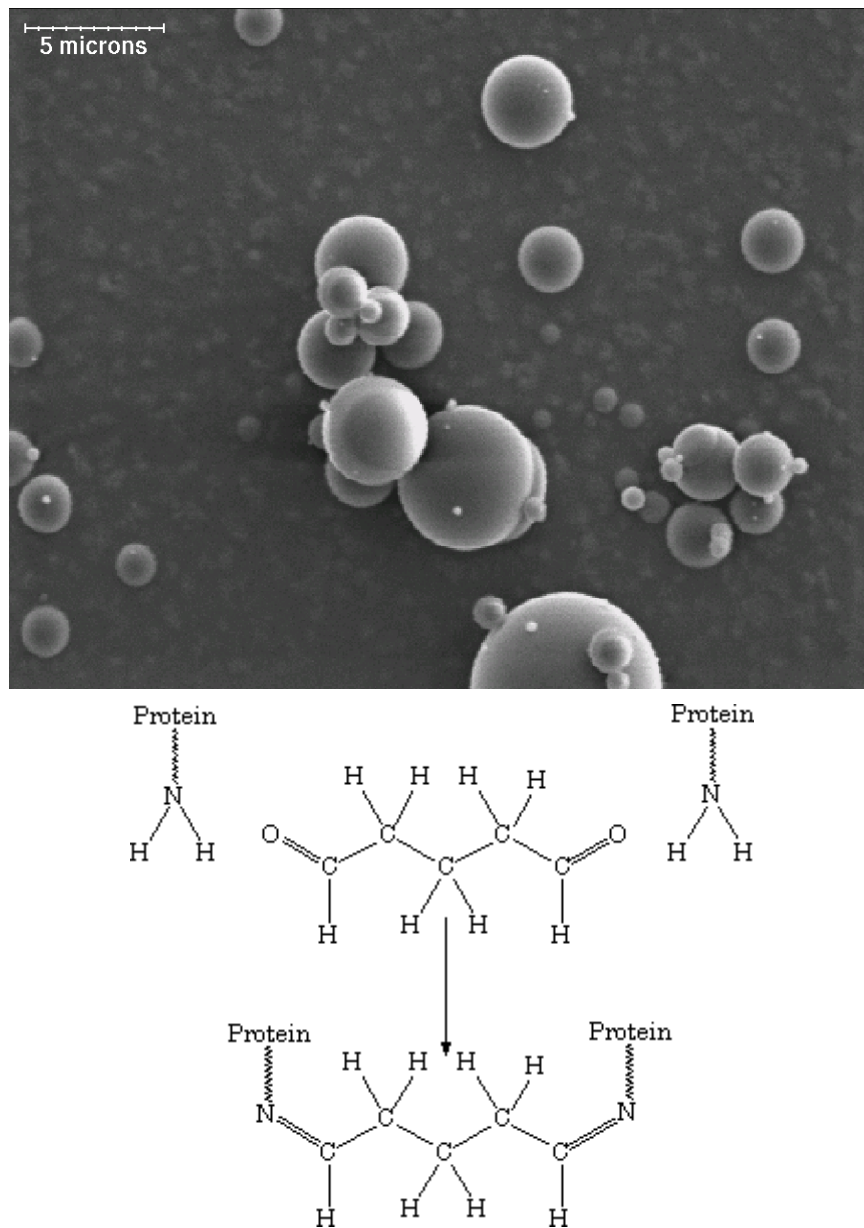
Figure 4.1 SEM of Albumin Microspheres and the Crosslinking Reaction
Top: Scanning electron micrograph of albumin microspheres. This micrograph is
of microspheres that do not contain any drugs (*http://www.alrise.de/images/great-
***microspheres.jpg*). Bottom: mechanism of glutaraldehyde crosslinking**
(*http://www.lsbu.ac.uk/biology/enzyme/images/practi11.gif*).
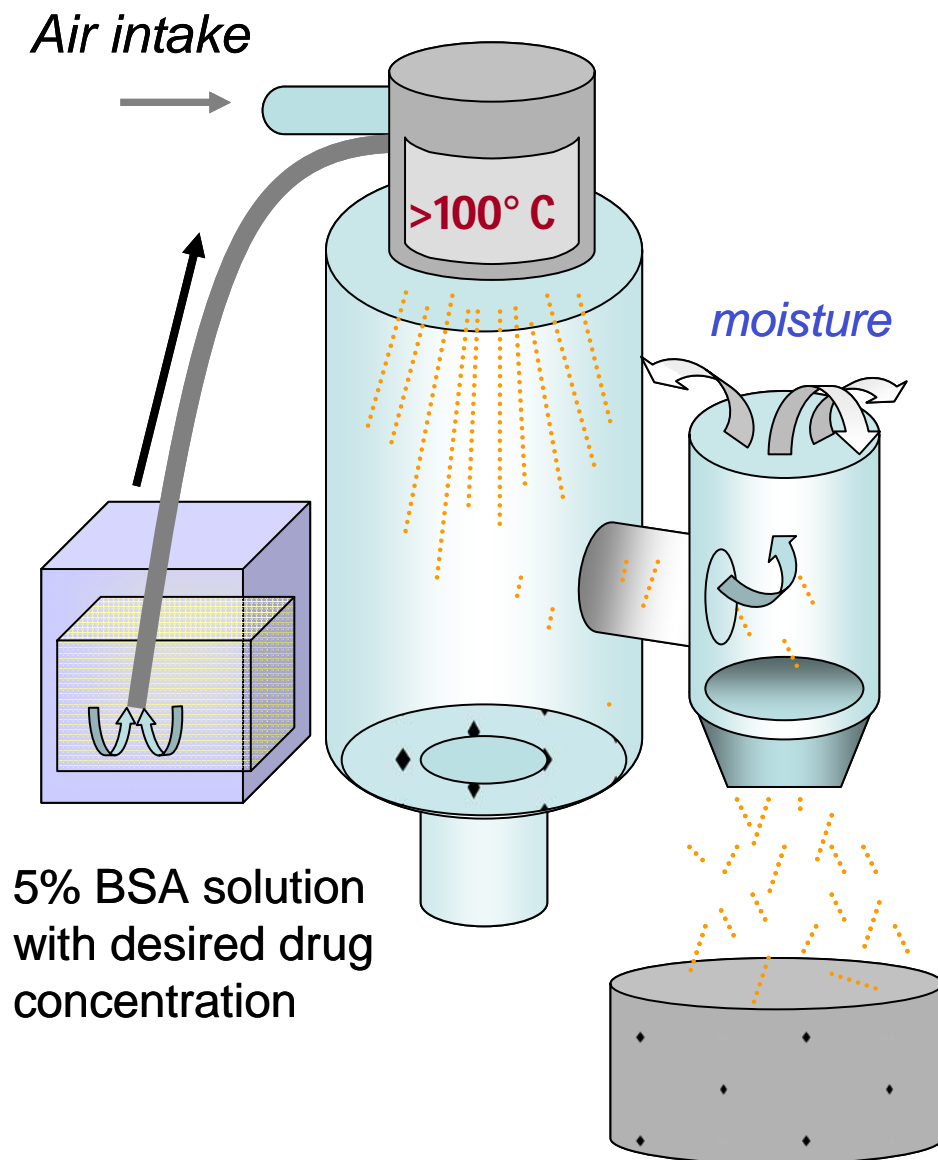
Figure 4.2 Diagram of a laboratory scale spray dryer.

Table 4.1 Size Distribution of Microspheres
Size distribution of microspheres measured by Spectrex Laser Particle Counter
(n=3). The proteins marked his- were purified using the solubilization protocol
developed in this thesis. The other was purified using the GST fusion system (see
chapter 1).

Contrast agent µsphere	Size (µm)
"empty" µsphere	4.93 ± 0.5 (4-6 µm range)
"empty" µsphere	5.72 ± 0.5 (5-7 µm range)
His-7E15+Gd	4.41 ± 0.6 (3-7 µm range)
His-7E15 no Gd	3.21 ± 0.5 (3-5 µm range)
His-7E15-bom+Gd	6.85 ± 0.8 (5-9 µm range)
7E15+Gd	3.17 ± 0.8 (3-4 µm range)

Table 4.2 Zeta Potential Measurements
Charge distribution of microspheres measured by a Malvern Zetasizer (n=3). The proteins marked his- were purified using the solubilization protocol developed in this thesis (chapter 2). The other was purified using the GST fusion system (see chapter 1).

Contrast agent μsphere	Charge (mV)
"empty" μsphere	-31.8 ± 0.8
"empty" μsphere	-11.6 ±0.9
His-7E15+Gd	-26.9 ±2.9
His-7E15 no Gd	-16.9 ±3.8
His-7E15-bom+Gd	-35.9 ±1.2
7E15+Gd	-27.6 ± 0.3
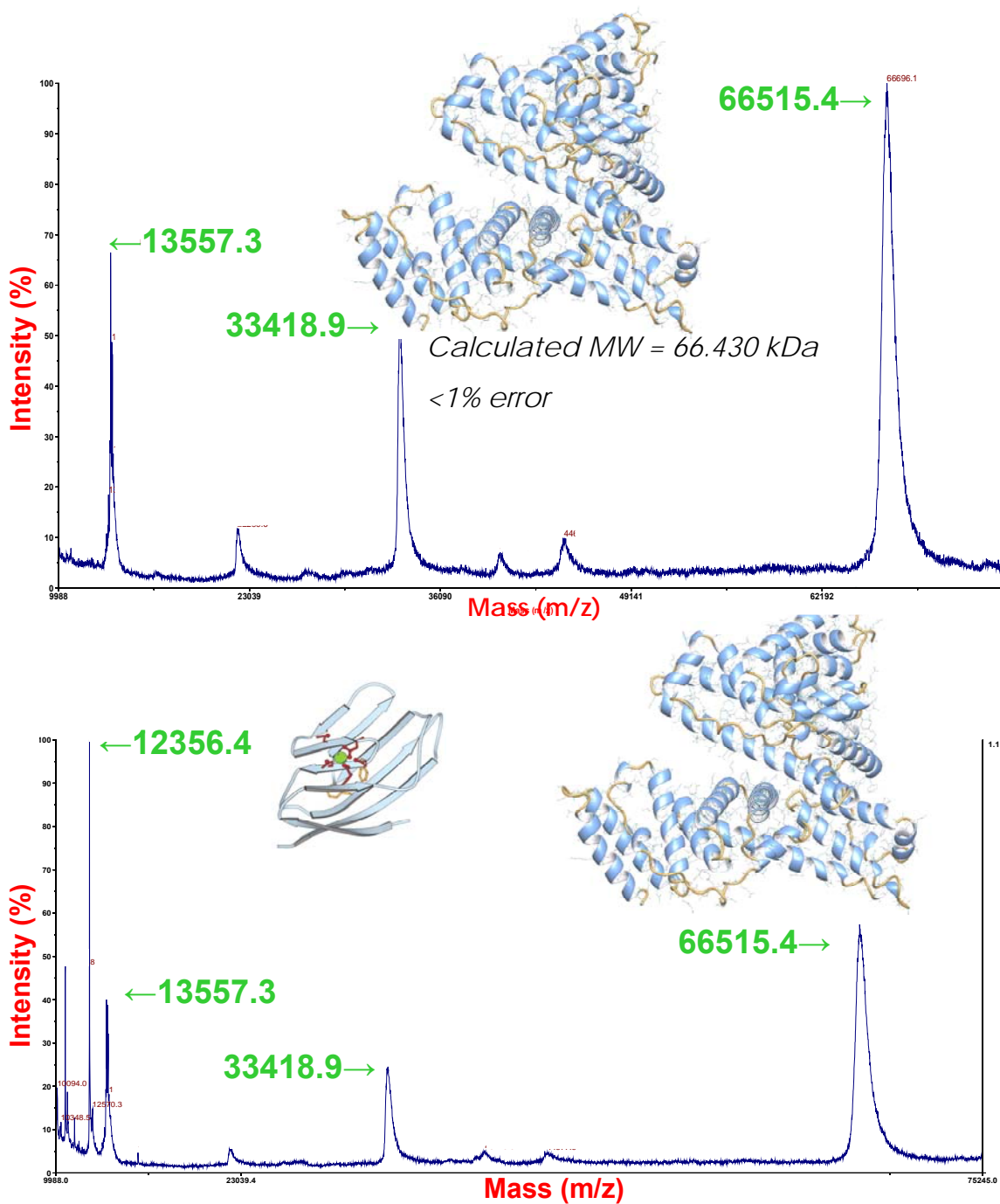
Figure 4.3 Linear positive MALDI mass spectra of blank microspheres (top) and CD2.7E15 microspheres loaded with Gd(III).
The tertiary structure of CD2.7E15 is a molscript construction based on wild-type CD2.D1. The tertiary structure of BSA is a crystal structure (*www.wikipedia.com*)

5 Biophysical characterization of contrast agents before & after encapsulation

5.1 Materials and Methods

5.1.1 Separation of his-7E15-bom from microspheres

The histidine tag was utilized to purify spray-dried protein. Microspheres dissolved in 50 mM Tris, pH 8.0 were decanted into a gravity-flow Ni-sepharose column to separate them. The microspheres were dissolved in 20 mM Imidazole, pH 8.0. Histidine-tagged protein was eluted with 500 mM Imidazole, pH 8.0. The resulting fractions were dialyzed against 10 mM Tris, 0.1% Tween 20, pH 8.0 to remove imidazole salt.

Alternatively, 25 mg spray dried albumin microspheres was dissolved in 11 mL 50 mM Tris, pH 8.0 for two hours to allow complete dissolution (this was done on uncrosslinked microspheres, which dissolve and release their contents very easily). After the required timeframe, 10 mL of the dissolved microsphere mixture was injected into a G200 Sephadex size exclusion column (G75 cannot be used; it does not resolve BSA) with the mobile phase as 10 mM Tris, pH 7.4.

5.1.2 Far Ultraviolet Circular Dichroism

Far UVCD was performed on a Jasco 810 Spectropolarimeter. In this section, protein concentrations were approximately 20 uM (0.2-0.25 mg/ml). A 50 nm/min scan speed was used with 6 or more accumulations per measurement. The response time was

2 seconds. The data pitch was 1 nm. All measurements were taken at room temperature (approximately 27 °C).

5.1.3   Trp Fluorescence

Trp fluorescence was used to determine the tertiary packing of the proteins before and after spray-drying. A 282 nm excitation was used and the emission of tryptophan was monitored from 300 to 400 nm. The relative fluorescence is given by finding the maximum emission and finding the minimum emission (in counts per second). The minimum is set at zero and the maximum is set at 1 by taking each point as x and using the following equation

Equation 2 Normalizing fluorescence data

(x −min emission)/(max emission −min emission)=normalized fluorescence

After normalization, a more accurate assessment of tertiary structural differences can be made because identical spectra will overlap regardless of concentration differences.

5.1.4   Tb-enhancement Resonance energy transfer

Trp residues were excited at 282 nm. The emission was monitored from 500 to 600nm. The baseline was normalized by deriving an exponential equation from the regions between 565-575 nm and 525-535 nm. The fluorescence enhancement was monitored at 545nm with a glass plate between the protein sample and the emission detector to prevent Raleigh scattering. The metal binding affinities were obtained by plotting the enhancement at 545 nm versus the total terbium concentration. The resulting

plot was fitted using the hill equation (equation 3; the data could not be fitted with a single site equation. The reasoning is discussed in the Discussion and the Conclusion).

Equation 3 Calculating Metal Binding Affinity (multiple sites)
$$(m1*m4*(m0\hat{}m6/(m5\hat{}m6+m0\hat{}m6)));$$
      m4= maximum enhancement at 545 nm
      m5= protein concentration (5 μM)
      m6= metal binding sites (2)

There were two different methods used to obtain a metal binding curve. The first used direct, stepwise addition of a high [Tb (III)] solution to a protein solution with 5-10 minutes between each addition. The second used separate samples for each [Tb (III)] with the metal added and incubated for 3 hours before a Tb(III) emission spectrum was taken.

5.1.5   Relaxivity measurements using NMR & MRI

To determine the potential for use of 7E15-bom purified using the protocol described in Chapter 1 as a protein contrast agent, its relaxivity was measured before and after the spray drying and encapsulation process. Relaxivity measurements were performed on 300 & 500 MHz NMR specrometers (GSU) and on 1.5, 3.0, and 9.4 Tesla MRI scanners (Emory U).

5.2   Results & Discussion

5.2.1   Far Ultraviolet Circular Dichroism

The contrast agent, his-7E15 was purified according to the Arginine solubilization procedure outlined in Chapter 1. 7E15 has a negative maximum of 216 nm in the

presence and absence of calcium or its lanthanide analogs and maintains its secondary structure over a wide range of pH values (from 3-10). His-7E15 was tested to determine if the new construct has lost any stability or secondary structure.

The far UVCD spectra of his-7E15 at pH 8.0 with and without metal are shown in figure 5.1. The protein maintains a similar secondary structure in both conditions, but this secondary deviates from that of CD2, 7E15 and the 7E15 variants (see Chapter 2). This is not unexpected, since the his-7E15 construct has an additional nine residues that most likely do not adopt the beta sheet arrangement.

The protein secondary structure does not change from pH 8 to pH 6 when metal is bound (figure 5.1B), but the protein precipitates at pH 4.5 causing a loss of total molar ellipticity and a change in the far UVCD spectrum (the precipitate here was visible during the experiment).

The spectral changes observed with changing pH in the absence of metal are less dramatic, but they do provide information on the solubility of the his-tagged CD2.7E15 protein. The far UVCD measurements are all taken with the same protein concentration, so changes in mdeg intensity (molar ellipticity) can indicate precipitation. The intensity with metal added is higher than the intensity without metal (figure 5.2.1 B and C), suggesting a loss of solubility. The spectra of his-7E15 with and without metal at pH 6.0 are highly similar, suggesting that the protein precipitates at this pH regardless of stabilization by metal binding. To determine whether or not a protein could be spray-dried and separated from the albumin matrix, an IgG was spray-dried according to the established protocol. The IgG was successfully separated from the albumin matrix using

size exclusion chromatography and subsequently analyzed using ELISA (done by collaborators at Mercer University) and far ultraviolet circular dichroism spectroscopy. The BSA maintains a mostly alpha helical conformation, as evidenced by the deep trough from 208 to 222nm (Fig 5.7). The IgG, however, has experienced some slight changes in secondary structure (Fig 5.7). The significance of these changes has yet to be investigated.

5.2.2 Trp Fluorescence

The tryptophan emission maximum of his-7E15 overlaps with the emission maximum of 7E15 and wild-type CD2, suggesting that they all maintain a highly similar tertiary packing. The tertiary packing does not change with the addition of 100 uM Tb(III). which is 20 times the protein concentration in these measurements. The large excess of Tb(III) should saturate the metal binding pockets. The fact that there is no tertiary structural change with the addition of metal suggests that the protein does not show a global conformational change when binding metal.

5.2.3 Tb (III)-enhancement Resonance energy transfer

The terbium fluorescence increases with increasing concentration, indicating a binding event (figure 4.2A). The Tb (III) binding constant could not be determined. There is only one designed metal binding site in his-7E15 (figure 5.2C). The fluorescence enhancement profile is consistent with two possibilities—either there is cooperative binding (often seen in proteins with 2 or more sites) or the metal binding causes a change in the structure of his-7E15. The large error seen in the average

observed enhancement seems to suggest an alternative explanation. Perhaps the binding

is so strong for other metals (e.g. calcium or magnesium) that Tb (III) must be at a high

concentration to compete with the other metals and cause displacement. This can be

alleviated by pretreating the buffers and protein samples with chelating reagents.

5.2.4 Relaxivity measurements using NMR & MRI

Table 5.1 Table Relaxivity measurements using 500 MHz NMR (approximately 11.7 T). All samples are measured in 10 mM TRIS buffer, pH 8.0.

Contrast agent	[CA-Gd] (μM)	T_1 (ms)	R_1 ($mM^{-1}s^{-1}$)	T_2 (ms)	R_2 ($mM^{-1}s^{-1}$)
his-7E15-Gd	100	1141	5.5	37	246.4
his-7E15-Gd	50	1902	4.0	85	187.6
his-7E15-Gd-µS	100	1259	4.7	135	50.2
his-7E15-Gd- µS	50	1881	4.1	204	50.3

- **Varian Inova 500 MHz NMR,** All samples in 10 mM Tris buffer, pH 8.0

The relaxivity measurements using 500 MHz NMR show that Gd-DTPA has a

R1relaxivity of 5.3 mM^{-1} s^{-1}, which closely correlates with the literature value of 5.0

mM^{-1} s^{-1} measured using clinical MRI scanners (*70*). This indicates that R1 relaxivity

measurements using a 500 MHz NMR may provide a good prediction of relaxivity

detected by a clinical MRI scanner. The most encouraging piece of information gleaned

from this experiment is that the R1 relaxivity of CD2.7E15 (referred to in the table as his-

7E15) does not change significantly after spray drying and encapsulation in albumin

microspheres (his-7E15-Gd-µS). The average R1 before spray drying is 4.75 ± 0.75 and

the average R1 after spray drying and encapsulation in albumin microspheres is 4.4 ± 0.3.

The two values are within error, suggesting little to no change in R1 relaxivity (see table

4.1).

Table 5.2 Relaxivity measurements using a 3 T clinical MRI scanner. Measurements provide by Dr. Hui Mao at Emory University Hospital

Table Relaxivity Measurements 3 T MRI scanner			
Microsphere Sample: buffer	[Gd(III)] (μM)	T_1 (*ms*)	R_1 (mM^{-1}s^{-1})
Gd-7E15-bom: Serum	100	252.2	31.3
Gd-7E15-bom: Serum	50	288.5	52.7
Gd-7E15-bom: Tris	100	377	18.2
Gd-7E15-bom: Tris	50	530.9	21.0
Gd-7E15-bom: PBS	100	343.2	20.8
Gd-7E15-bom: PBS	50	483.9	24.7
Gd-DTPA: PBS	100	452.5	13.8
Gd-DTPA: PBS	50	611.2	16.1
Gd-DTPA: Serum	100	366	19.0

The relaxivity of 7E15 does not exceed that of Gd-DTPA in this experiment.

One thing to consider is that this magnetic field strength is very high (roughly 11.4 T),

and R1 relaxivity is sensitive to changes in magnetic field strength. This magnetic field

strength is not FDA approved. 3 T, however has been approved, and measurements have

been taken at this magnetic field strength.

The results of relaxivity measurements on a 3 Tesla MRI at Emory University are

shown in table 4.2. The relaxivity measurements indicate that 7E15 generally has a

higher relaxivity than Gd-DTPA in serum and PBS buffer. Most importantly, Gd-7E15

microspheres in serum have a relaxivity that is more than twice as high as Gd-DTPA microspheres in serum.

5.3   Conclusion

According to the far UVCD data, the secondary structure of his-7E15 is different from that of 7E15. Moreover, the protein becomes less soluble in low pH buffer and is generally less soluble without metal. This may relate to the results of the initial metal binding titration, which seems to indicate a cooperative change (Fig. 4.3.2).

The titrations in Fig 5.2 show that no enhancement is seen in the lower Tb (III) concentrations. This could indicate a cooperative binding event, where the Tb (III) binding event must first cause a change in the CD2.7E15 structure before energy transfer from tryptophan residues is observed. A second possibility is that the metal binding is so strong that the protein has already accepted a metal from the buffer into its metal binding pocket, and that metal must be outcompeted by increasing Tb (III) concentrations before energy transfer can be seen.

Both CD2.7E15 and CD2.7E15-bom were found to bind Tb(III) and the estimated Tb(III) K_d for CD2.7E15 is 3.5 ± 0.5 μM in 20 mM PIPES, pH 6.8. This K_d was determined by preparing separate samples for each Tb (III) concentration and incubating them with the metal for three hours so that any residual metals that may have occupied the metal binding sites would be outcompeted by the Tb (III).   The energy transfer still shows little to know change in the lower Tb (III) concentrations, indicating that a more stringent means of metal removal should be employed for future titrations.

The 7E15 purified using the GST-fusion system and the CD2.7E15 purified using the system developed in this thesis have nearly identical maximum Tb (III) binding capabilities (Fig 5.4). The maximum energy transfer is not significantly reduced by the addition of 130 mM NaCl, indicating that a specific binding event is responsible for the vast majority of the energy transfer. Compared to CD2.7E15 purified using either GST-fusion or the arginine solubilization procedure, neither CD2.D1 nor Bovine serum albumin did not have a significant energy transfer with or without 130 mM NaCl.

Interestingly, there is a reduction in maximal enhancement between the 7E15 before spray drying and an equimolar solution of 7E15 in dissolved albumin microspheres, indicating that there may be some reduction in maximal metal binding. Nonetheless, the albumin encapsulated microspheres spray dried without gadolinium showed a very high FRET enhancement at 545 nm. In fact, the energy transfer increased when 130 mM NaCl was used in the buffer. This indicates that when nonspecific binding is minimized (e.g. that of BSA), the CD2.7E15 can bind more of the available 100 μM Tb (III) (Fig 5.4). If there was no BSA present in the solution, the enhancement would probably increase—even the "blank" microspheres (those containing no CD2.7E15 or any protein other than BSA) have a high enhancement at 545 nm. The spray-dried CD2.7E15 should be purified from the microspheres in the future so that this experiment can be repeated.

As described in chapter 3, a simple, high yield purification procedure has been developed for CD2.7E15. The protein shows a fully formed tertiary structure, but the secondary structure does not exactly overlap with that of 7E15 purified using the GST

fusion system. This should be explored by further attempts at optimizing folding of the

protein solubilized from inclusion bodies. One technique that should be explored is the

use of high pressure to facilitate folding, which, in combination with nondenaturing

concentrations of GdmHCl has been shown to facilitate solubilization and refolding of

growth hormone, lysozyme, and beta-lactamase (*71*). This procedure allows for high

concentrations to be refolded, abrogating the need for a concentrating step in the

purification. In chapter 4, the preparation of albumin encapsulated protein contrast

agents was described, showing that the protein can be successfully spray-dried into

micron sized particles of high quality. Chapter 5 shows that the spray-dried protein

contrast agents have a relaxivity that does not change significantly after spray drying.
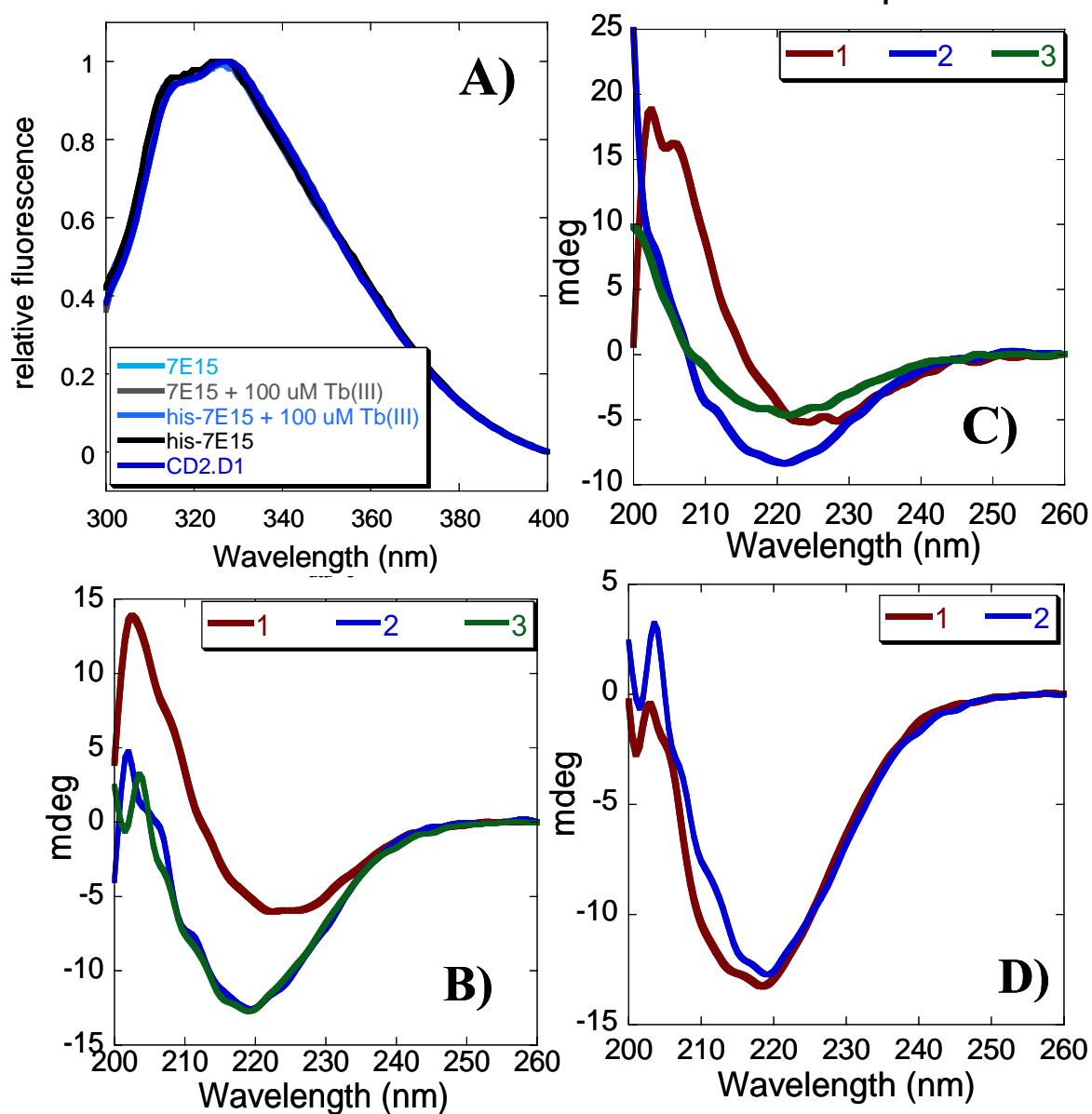
Figure 5.1 Conformational Analysis of his-tagged CD2.7E15 before Spray-drying A) the tryptophan fluorescence emission spectra of his-7E15, 7E15 and wild-type CD2 with and without metal in 20 mM PIPES, pH 6.8. B) The far UVCD spectra of his 7E15 in various buffers with 50 uM Gd(III) 1:50 mM NaAc, pH 4.5, 2: 50 mM PIPES, pH 6.8, 3: 20 mM Tris, pH 8.0. C) The far UVCD spectra of his-7E15 in various buffers treated with 1 mM EGTA 1:50 mM NaAc, pH 4.5, 2: 50 mM PIPES, pH 6.8, 3: 20 mM Tris, pH 8.0. D) The far UVCD spectra of his-7E15 with 100 uM Tb(III) (1) and with 1 mM EGTA (2).
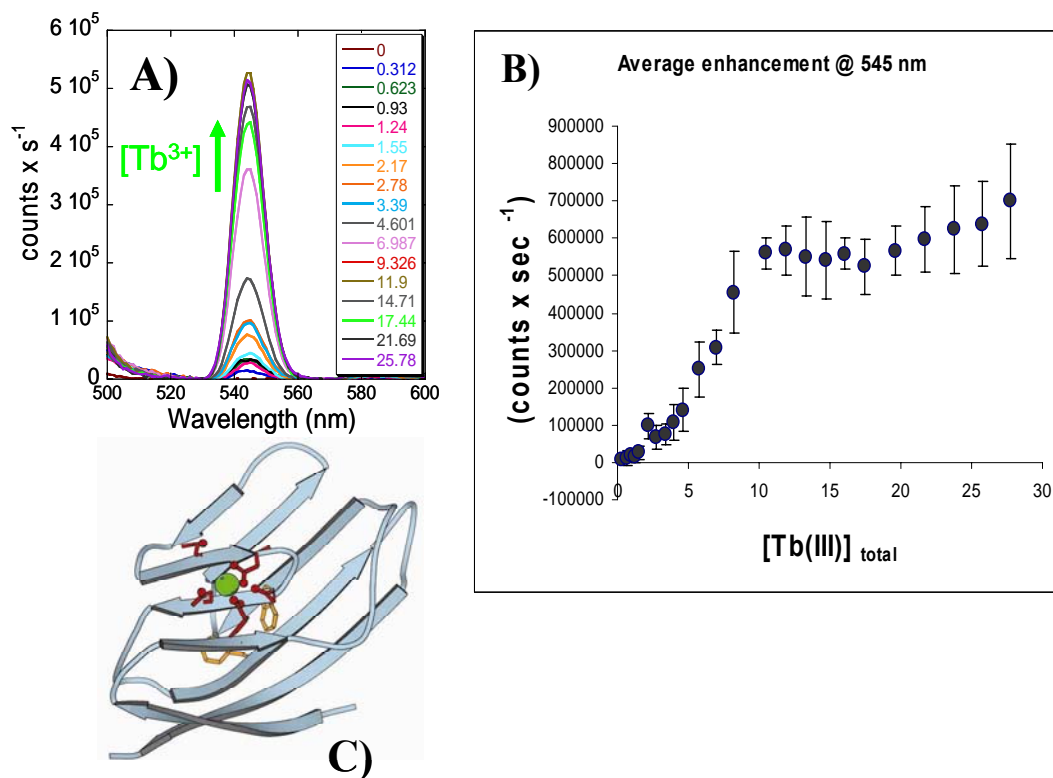
Figure 5.2 CD2.7E15 Metal binding studies
A) Tb(III) FRET with increasing concentrations of metal in uM (legend). B)
Average enhancement profile of his-7E15 in 20 mM PIPES, 50 mM KCl, 2 uM
protein. C) Rasmol model structure of 7E15. The potential metal residues are
shown in red and the tryptophan residues are shown in gold. The metal is colored
in green and is shown in the designed metal binding pocket.
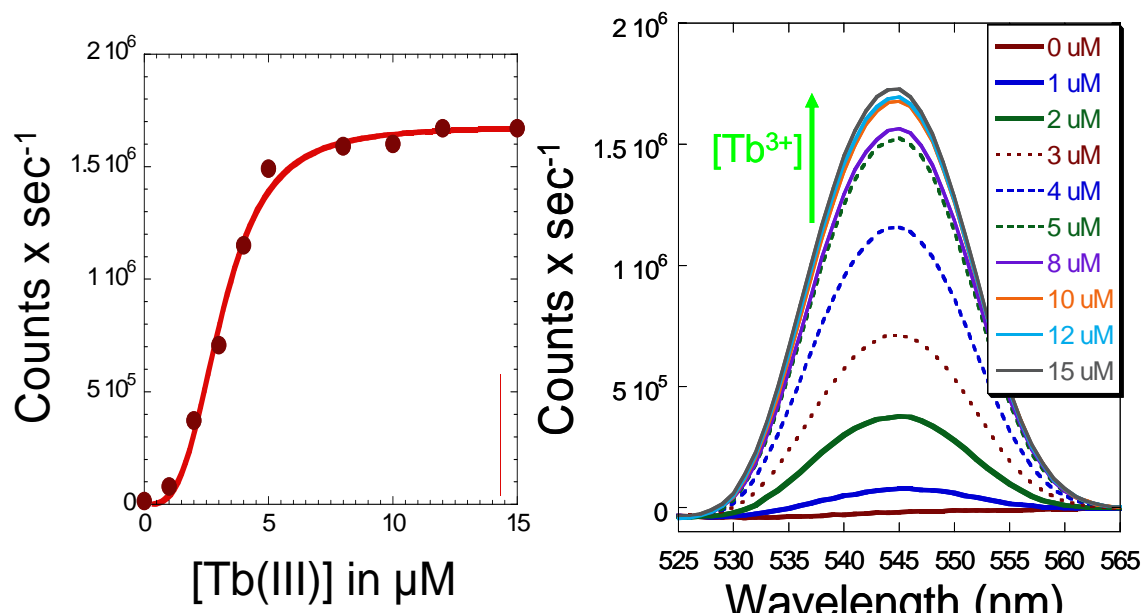
Figure 5.3 CD2.7E15 Metal Binding Studies II
Tb(III) titration using increasing Tb(III) concentrations. Rather than increasing
the Tb concentration in a single sample, separate samples were prepared for each
concentration and incubated for 3 hrs. to allow sufficient metal binding.   The
average of two measurements gives an estimated Tb(III) K_d for CD2.7E15 equaling
3.5 ± 0.5 uM
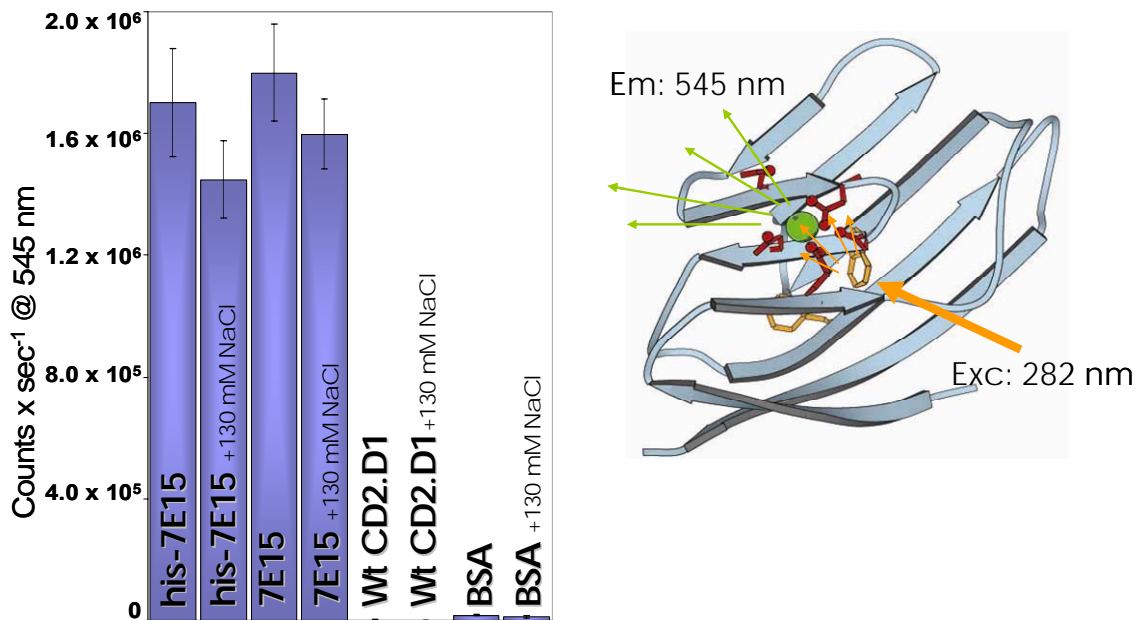
Figure 5.4 Total Enhancement Assay
Maximum energy transfer measured by enhancement at 545 nm in 20 mM PIPES,
100 μM Tb(III) with and without 130 mM NaCl.
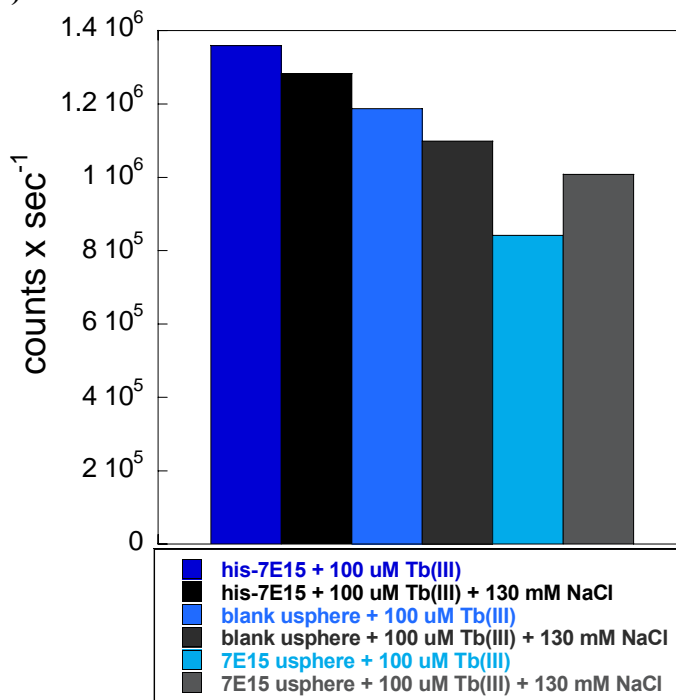
Figure 5.5 Total Enhancement Assay: Microspheres
Comparison between the total FRET enhancement at 545 nm (Tb(III) emission) 20
mM PIPES, pH 6.8 with and without 130 mM NaCl. His-7E15 is at 5 uM, the
microspheres are each 1mg/mL, roughly corresponding to a final concentration of 5
uM 7E15.
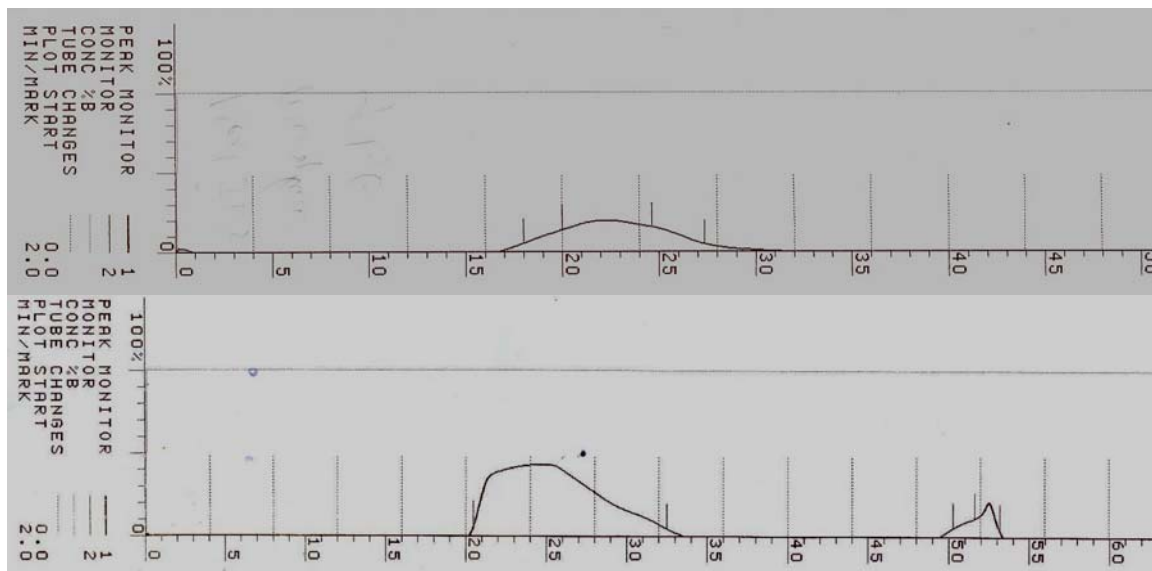
Figure 5.6 Size exclusion purification of spray-dried commercial IgG.
Top: G75 SEC Bottom: G200 SEC
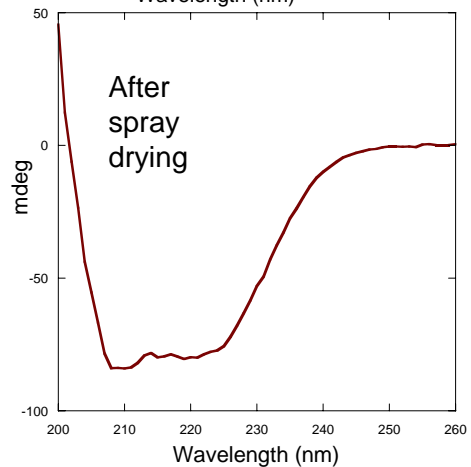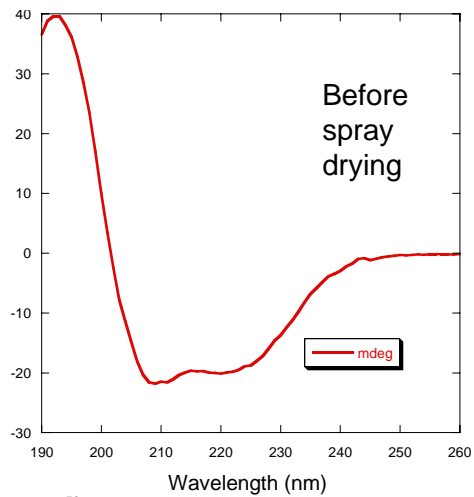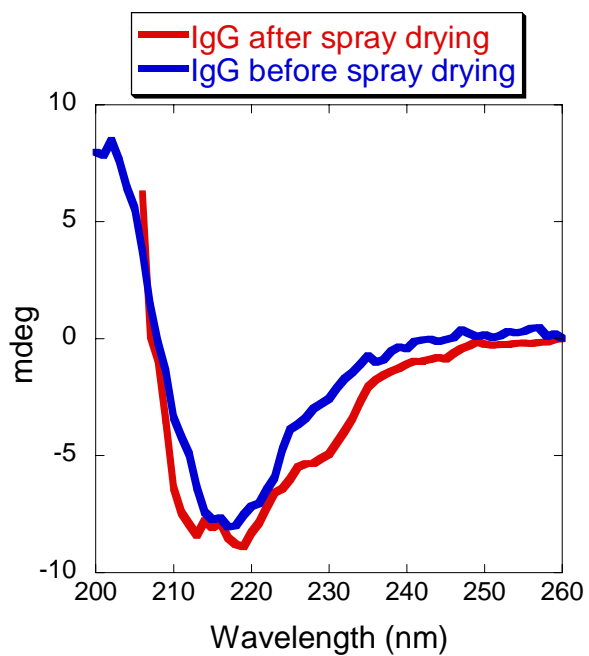
Figure 5.7 Spray-Dried IgG Far UVCD
Far UVCD spectra of an IgG (left)
and BSA(right) before and after spray-drying.

Table 5.3 Relaxivity Measurements on a 0.47 Tesla Relaxometer (Ga Tech)
The measurements are of microspheres prepared at Mercer University spray dried without gadolinium. Equimolar gadolinium was added after dissolution in 10 mM Tris, pH 8.0.

Sample	Protein (uM)	Gd (uM)	T1	T2	R1	R2
(10mM)Tris	0	0	2780	1407	x	x
Gd-DTPA	0	100	1817	899	1.9	4.0
His-7E15µsphere	50	0	2566	1212	x	x
His-7E15µs-Gd	50	50	1481	893	5.7	5.9
Blank µsphere	50	0	2673	1322	x	x
Blank µsphere-Gd	50	50	1417	868	6.6	7.9
7E15 µsphere-Gd	50	0	1342	829	x	x
7E15 µsphere-Gd	50	50	1350	824	7.3	9.1

6   Introduction to Part II: β2-microglobulin as a Prostate Cancer Biomarker for Signal Transduction Studies

Beta-2-microglobulin (β2m) is a structural constituent of the major histocompatibility complex I (MHC I), which is found on the surface of nearly all human somatic cells (*72*). It is thought to contribute to the selection of MHC I associated peptide fragments (*73, 74*). The structure of this 100 amino acid protein is similar to IgG light chains. In 2006, Huang, et al found that β2m stimulates the proliferation and osteomimicry of prostate cancer bone metastases (*75*). Use of an anti-β2m polyclonal antibody actually inhibited these effects, in some cases causing the bone metastases to atrophy (*75, 76*). Studies have shown that the most efficacious antibodies bind to the MHC I complex, are internalized and activate Lyn and PLC gamma 2 which in turn activates JNK and inhibits PI3K/Akt and ERK inducing apoptosis (in myeloma cells) (*76*). It has been suggested that the most potent antibodies have a higher affinity for MHC I-bound β2m. The third major objective of this thesis is to determine the nature of this anti-tumor effect. Since the antibody binding site is not known, our strategy involves identifying the epitope for the antibody that exhibited the inhibitory effects and producing a complementary peptide that can interfere with β2m signaling. Our collaborators will determine the manner of β2m signaling while our lab will focus on the protein chemistry, which involves expression and purification of β2m and the synthesis of β2m peptide fragments. Several epitope prediction algorithms were used to determine the regions of high antigenicity (*77-79*).

6.1 Expression and purification of rβ2microglobulin

A pGFP plasmid containing B2m was obtained from our collaborators at Emory U (*75, 80*). It was found that the expression level of this plasmid in BL21 was below the detection limit of SDS-PAGE, yielding a very poor purification (Fig 6.1). A second vector, called pET-Blue2, was obtained from Dr. Andrew Miranker (Yale U). This chapter details the expression and purification of protein obtained from this expression system.

Histag pulldown assays are often used to determine determine the putative binding partner(s) of known proteins. The known protein is expressed with a histidine tag so that when it binds to its partner(s) in vivo or in vitro, the entire complex can be precipitated using insoluble beads conjugated to a nickel atom chelated by a small organic molecule (e.g.: NTA).

The pETBlue2 plasmid obtained from Dr. Andrew Miranker was superior to the pGFP plasmid; however, the B2m was inserted in the cloning region of pETBlue2 such that there is no histag.

6.2 Materials & Methods

6.2.1 Transformation protocols: DH5- and BL21 (DE3) competent cells

The heat shock technique was used to transform all E. coli. To begin the procedure, a 1.5ml eppendorf tube containing approximately 100 uL desired competent cells (BL21 (DE3) for expression, DH5α for DNA purification) was obtained from a stock of competent kept at -80° C. The cells were placed on ice to thaw and aliquotted

into two 50 μL samples. One sample receives 0.5-1.0 μl of desired plasmid DNA while

the other did not receive DNA (this is the negative control). The thawed cells and DNA

were mixed by pipetting up and down or gently flicking the bottom of the tube. The cells

were left on ice for at least thirty minutes after the addition of DNA. The heat shock was

done by placing the cells in a 42 °C water bath for ninety seconds and then putting the

cells back on ice for two minutes. Then, 50 μL LB media was added and the media was

mixed with the cells by pipetting up and down or by gently flicking the bottom of the

eppendorf tube. The tubes were then incubated at 37 °C for 30 minutes. 50 μL of the

solution was added to desired agar plates (LB-Amp plates for expression) and streaked

onto the plates with a sterile triangle. The plates were then incubated at 37° C overnight.

The plates were wrapped in parafilm and placed upside-down in the refrigerator the

subsequent morning. No plates were kept longer than one month.

6.2.2   Transformation protocols:Tuner (DE3) pLacI competent cells

Tuner (DE3) pLacI competent cells were obtained from Novagen and transformed

as follows. The desired quantity of cells (20 uL per transformation) was thawed on ice

and mixed gently to ensure that cells were evenly suspended. 100-200ng DNA was

directly pipetted into the thawed cells followed by trituration to ensure all DNA was

released into the suspension. Then the tubes were inverted to allow further mixing. The

cells were placed back on ice for 5 minutes before heat shocking for 30 seconds in a 42

°C water bath. Afterwards, the cells were placed back on ice for 2 minutes. Finally, 80

uL of room temperature SOC medium was added to each tube and the entire mixture was plated onto LB-Ampicillin agar plates.

6.2.3 Expression

Lauria-Bertani broth was prepared using a single colony from a transformed plate with the plasmid of the desired protein was inoculated into at least 100-500 ml of LB broth with an ampicillin concentration of 100 μg/ml for overnight growth at 37° C and 200-220rpm agitation. The following morning, 30-100 ml of the overnight growth was transferred to 1L of fresh LB broth with an ampicillin concentration of 100 μg/ml. If kanamycin was used as the selective antibiotic, as in pET30a expression, the final concentration used was 30 mg/L. The flask was then incubated at the desired temperature and 200-220 rpm agitation. The growth of the cells was monitored by measuring the optical density at 600 nm with fresh LB as a reference. The cells were induced with 1 mM IPTG when the desired optical density was reached (0.8-1.0). The cells were allowed to grow 4 hours after induction. The cells were harvested by centrifugation in 500 ml bottles at 7 krpm for 15-20 minutes using a GS3 rotor. The cell pellets were collected using a spatula and less than 5 ml PBS buffer and placed in a 50 ml falcon tube and stored at -20 °C for purification at a later date. The supernatant was discarded.

6.2.4 Purification scheme

6.2.4.1 Solubilization in Arg

See section 3.1.3 for a detailed protocol. The only difference was that 2 M Arginine was used for beta-2-microglobulin solubilization according to Umetsu, et al (*60*).

6.2.4.2 Size exclusion chromatography

Size exclusion chromatography was performed on 10 mL solubilized beta-2-microglobulin inclusion bodies. The protocol was identical to the protocol used in section 3.1 of this thesis.

6.2.4.3 Cation exchange chromatography

Cation exchange chromatography was performed on the SEC fractions containing beta-2-microglobulin. The protocol for cation exchange chromatography was identical to the protocol followed in section 1.1 of this thesis. The concentration of the fractions obtained after cation exchange chromatography was calculated using a theoretical extinction coefficient from Expasyweb.com ($19300 \text{ M}^{-1} \text{ cm}^{-1}$) and the calculated molecular weight

6.2.5 Primer design

The pGFP plasmid was obtained from Dr. Wen Chin Huang and Dr. Leland Chung at Emory University's Winship Cancer Institute. The restriction enzymes were

obtained from New England Biolabs and the KOD Hotstart Polymerase kits were

obtained from

The forward primer was designed to match the C terminal of the beta-2-

microglobulin sequence (obtained using a pET-Blue2 primer, sequenced at the Georgia

State University Biology DNA Core Facility). The forward primer has the following

sequence:

CAT CAT CAT CAT CAT CAT TAA AAG CTT GCG GCC GCA CAG

The reverse primer was designed complimentary to the pET-Blue2 vector sequence

immediately following the beta-2-microglobulin stop codon. The reverse primer has the

following sequence:

CAT GTC TCG ATC CCA CTT AAC

The stock solution of both the forward and reverse primers was 50 micromolar.

6.3 Transformation of DH5-α , JM109, BL21, and Tuner(DE3) Competent Cells after PCR

The competent cells were all transformed according to the protocol given in

section 2.1.2 and section 8.1.2 of this thesis.

6.4 Results & Discussion

6.4.1 pGFP- rβ2microglobulin

The pGFP vector and BL21 (DE3) E.coli were unsuitable for expression and

purification of recombinant beta-2-microglobulin using a range of IPTG concentrations

(Fig 6.1). This prompted the search for various other vectors. The first expression system attempted was pET-Blue2 vector and Tuner (DE3) pLacI cells.

6.4.2   pET-Blue2: Tuner DE3 system

The Tuner (DE3) E. coli and pET-Blue2 vector produced a substantial expression band visible on SDS-PAGE (Fig 6.2). The protein was completely insoluble after sonication and centrifugation, so the protein was purified using arginine resolubilization (see section 3.2 for a detailed protocol). The beta-2-microglobulin has been successfully expressed and purified. The resulting purification yields were 24 ± 2 mg per purification procedure. Since each purification procedure uses only about ½ of a liter of cell culture, the yield is about 50 mg per liter of cell culture using this purification procedure. Unfortunately, our collaborators wish to use the purified protein for a histidine-tag pull down assay, so this purified protein cannot be used. The protein must have a histidine tag, so PCR was attempted to insert a histidine tag at the C terminal of beta-2-microglobulin in the pET-Blue2 vector.

6.4.3   Cloning

PCR products were successfully obtained using Green Master Mix reaction system. The result of the KOD Hotstart Polymerase system shows a much lower yield than the Green Master Mix system. In fact, the band on the Agarose gel may be simply template DNA (Figs 6.4 and 6.5). Additionally, the lower forward and reverse primer concentrations resulted in a higher produce yield.

The PCR consistently showed a good yield, but the transformation step proved problematic. The transformation step after the PCR failed using the DH5-α , JM109, BL21, and Tuner(DE3) competent cells.

6.5   Conclusions and Future Work

The beta-2-microglobulin construct within the pGFP vector cannot be expressed in BL21. Successful expression and purification requires the pETBlue2 vector and Tuner (DE3) pLacI E.coli competent cells. Unfortunately, this protein cannot be used for the proposed work using a his-tag pulldown assay. An alternative approach would be to use an immunoprecipitation employing an anti-beta-2-microglobulin antibody.

The cloning results suggest that the final ligation step is faulty, as this would result in a linear plasmid that may not confer antibiotic resistance, causing the transformation using selective media to fail.

[IPTG] mM   0   0.25* 0.50 0.75 1.00,   β2M (0.25 μg)

Anti-β2M Ab

12 kDa →
(β2M-His)

Anti-His Ab

12 kDa →
(β2M-His)
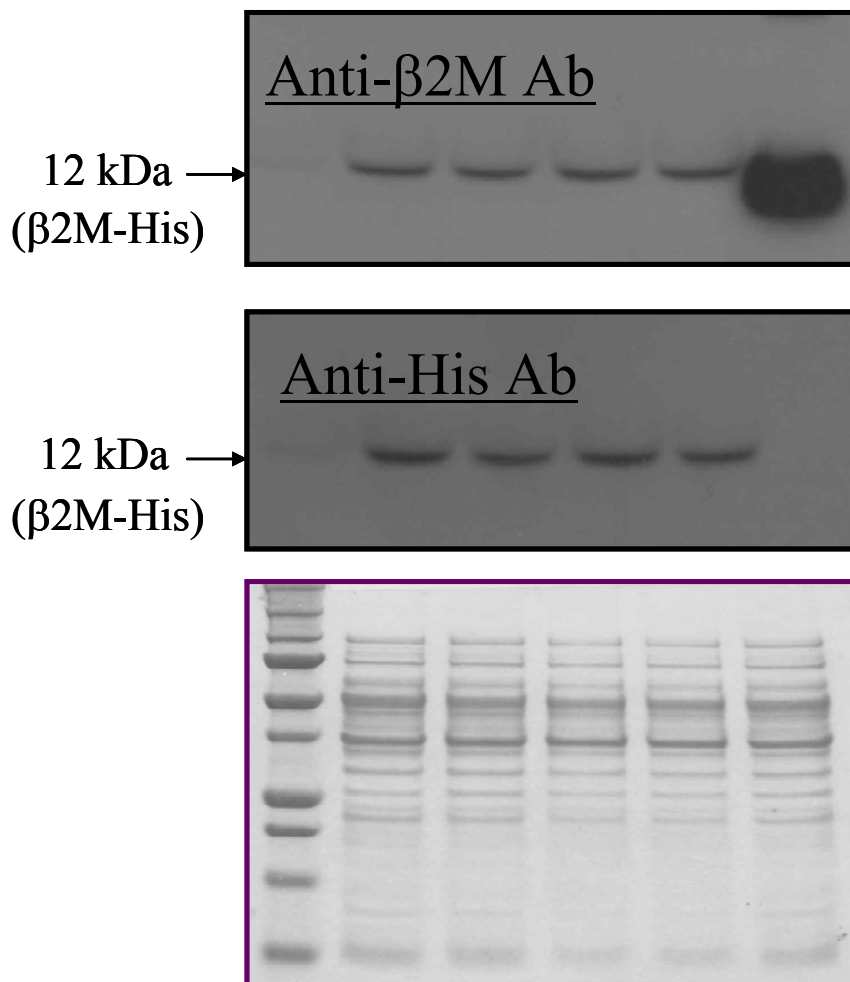
Figure 6.1 Beta-2-microglobulin pGFP vector SDS-PAGE analysis
SDS-PAGE analysis of beta-2-microglobulin expression in pGFP vector (bottom).
Western blots were performed using anti beta-2-microglobulin antibody (top) and
an anti-histidine tag antibody (center)[performed by Wen Chin Huang at Emory
University Winship Cancer Ins.]
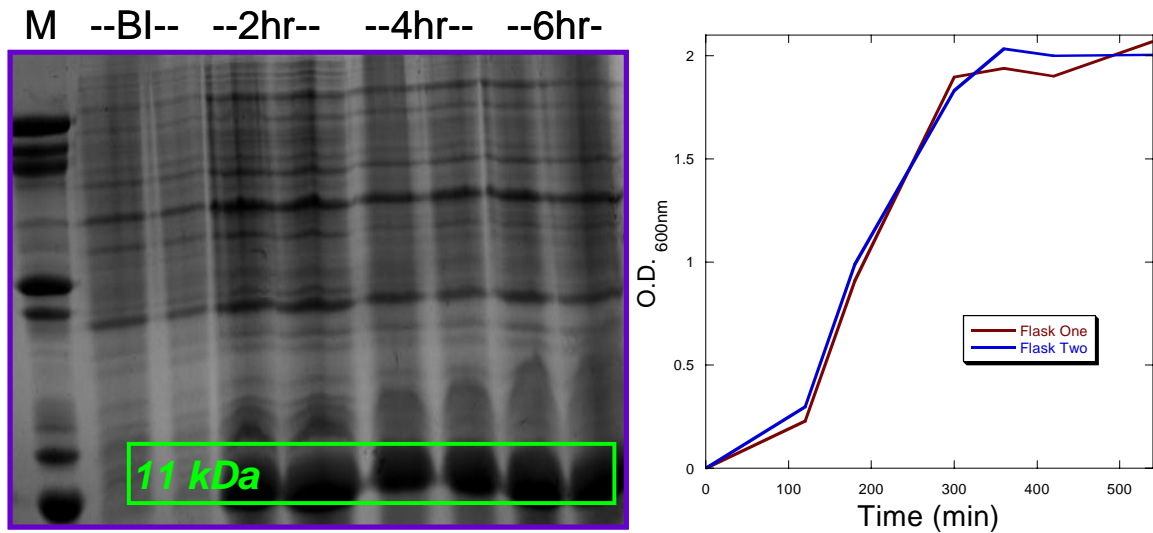
Figure 6.2 Beta-2-microglobulin pET-Blue2 Growth Curve and SDS-PAGE
Successful expression of beta-2-microglobulin in pETBlue2 vector and Tuner (DE3) pLacI BL21 cells. Theleft shows SDS-PAGE of expression. The right is the optical density measurements of cell culture monitored at 600 nm.
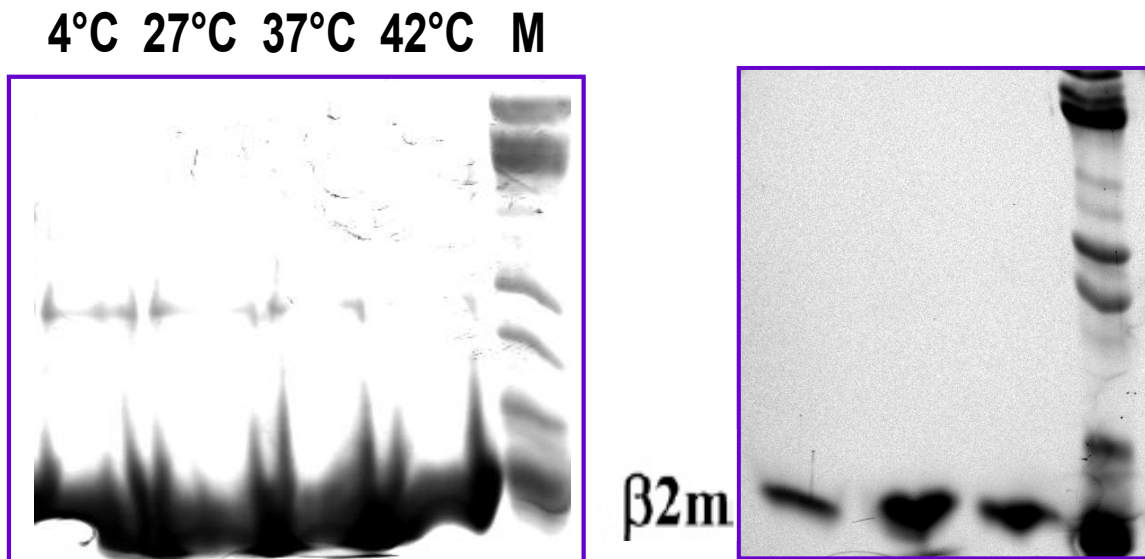
Figure 6.3 Beta-2-microglobulin Purification
Left: SDS-PAGE analysis of beta-2-microglobulin solubilized in 2M Arginine, 200 mM NaCl, 50 mM TRIS, pH 8.0 at 4, 27, 37, and 42 °C. Right: SDS-PAGE analysis of beta-2-microglobulin purified by cation exchange chromatography.
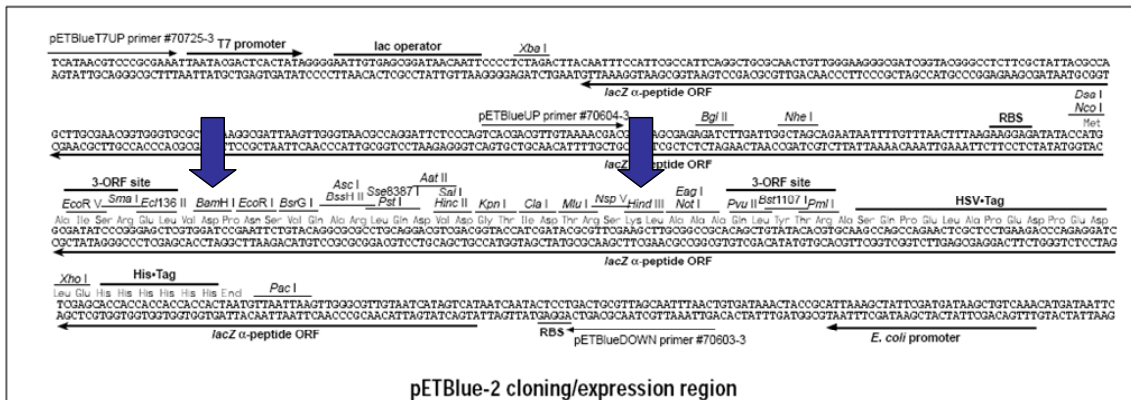
Figure 6.4 pEt-Blue 2 Vector Map
The beta-2-microglobulin was found to be inserted between the BamH1 and the HindIII enzyme cleavage sites.
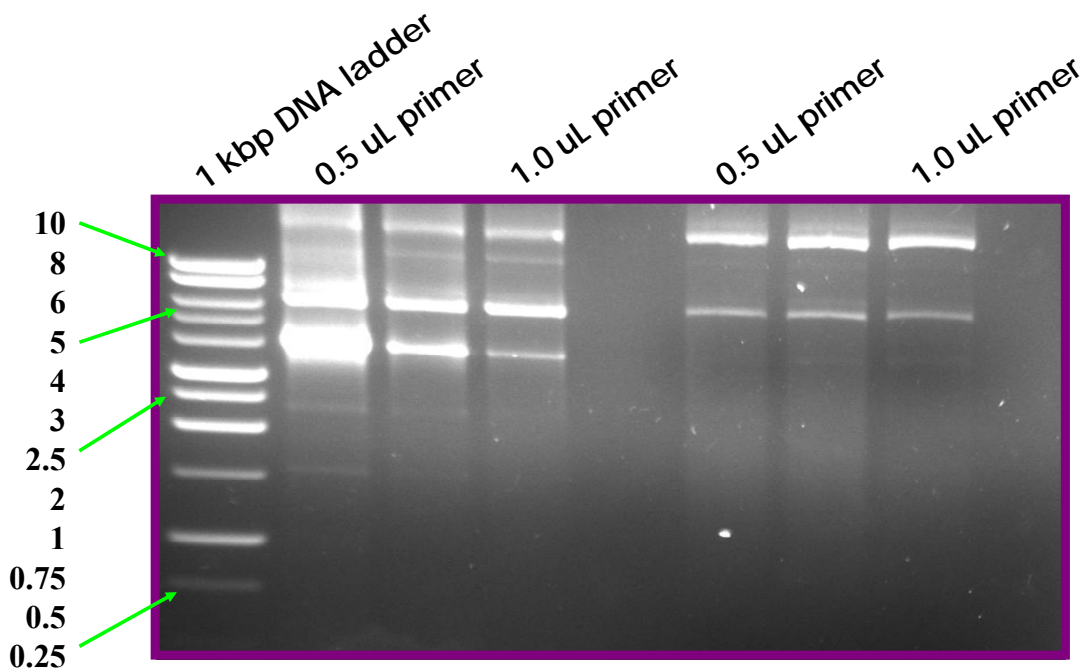
Figure 6.5 Agarose Gel of PCR Result using KOD Hotstart Polymerase kit.
The Green Master Mix system was used in the three left lanes, and the KOD Hotstart Polymerase system was used in the three right lanes.

7   Appendix I: Expression of a Single Chain anti-HER-2 antibody

The HER-2 receptor is a member of the human epidermal growth factor receptor family. This protein is also known as the avian erythroblastosis oncogene 2 (ErbB2), and the neuroglioblastoma (Neu) receptor.   Overexpression of this receptor is associated with decreased survival and increased recurrence (*81-87*). Unfortunately, HER-2 is overexpressed in 20-40% of mammary carcinomas (*72, 84, 86, 88, 89*).

Dimerization is required for activation of all human epidermal growth factor receptors (HERs) and all human HER isoforms are activated by binding to epidermal growth factor (EGF), which changes the conformation of the receptor to the dimerization-competent form (*85*). HER-2 overexpression is dangerous because all HER isoforms seem to prefer HER-2 as their dimerizion partner and the HER is permanently locked in the peptide-bound, dimerization-competent conformation. Additionally, HER-2 activation requires only that the HER-2 concentration be sufficiently high (*90*). Finally, HER-2 overexpression correlates with resistance to tamoxifen, which is one of the most popular anti-breast cancer therapeutics today (*85*).

There are many monoclonal antibodies directed against this receptor, the most well-known of these is trastuzumab (Hercpetin), which is used to inhibit the function of this receptor. We have obtained a single chain antibody (ScFv), which is much smaller than an actual antibody (27 kDa vs >100 kDa). Our goal is to conjugate this anti-HER-2 ScFv to our protein contrast agent, 7E15, to use MRI to detect HER-2 overexpressing

tumors and metastases. Efforts toward the expression and purification of the anti-HER-2-ScFv will be outlined in this chapter.

7.1   Materials & Methods

7.1.1   Transformation

The anti-HER-2 construct was contained within pCYN-B vector (T7 promoter). This vector codes for the beta-lactamase gene for selective plating on Ampicillin or carbenicillin plates.

The heat shock technique and elecrtroshock techniques were not necessary when using TG1 cells (ZYMO research). To transform these cells, only 100 ng DNA was incubated with 50 uL cells on ice for 2 to 5 minutes. Then, the entire mixture was spread onto a pre-warmed LB-agar plate (according to manufacturer's instructions).

When using BL21 or DH5-alpha competent cells, heat shock technique was needed. To begin the procedure, a 1.5ml eppendorf tube containing approximately 100 uL desired competent cells (BL21 (DE3) for expression, DH5α for DNA purification) was obtained from a stock of competent kept at -80° C. The cells were placed on ice to thaw and aliquotted into two 50 μL samples. One sample receives 0.5-1.0 μl of desired plasmid DNA while the other did not receive DNA (this is the negative control). The thawed cells and DNA were mixed by pipetting up and down or gently flicking the bottom of the tube. The cells were left on ice for at least thirty minutes after the addition of DNA. The heat shock was done by placing the cells in a 42 °C water bath for ninety seconds and then putting the cells back on ice for two minutes. Then, 50 μL LB media was added and

the media was mixed with the cells by pipetting up and down or by gently flicking the bottom of the eppendorf tube. The tubes were then incubated at 37 °C for 30 minutes. 50 μL of the solution was added to desired agar plates (LB-Amp plates for expression) and streaked onto the plates with a sterile triangle. The plates were then incubated at 37° C overnight. The following morning, the plates were wrapped in parafilm and placed upside-down in the refrigerator to retard drying of the agar gel. No plates were kept longer than one month.

7.1.2   Expression

A single colony was inoculated into 500 mL LB media containing 100 mg/L ampicillin. The colony was allowed to grow overnight at 37 °C and 180 to 220 rpm agitation. 50 to 100 mL overnight culture was inoculated into 1 L fresh LB medium (100 mg/L ampicillin). Expression at 37 C was monitored by measuring the light scattering of the media (O.D.$_{600nm}$). When the O.D.$_{600nm}$= 0.8 to 1.0, 1 mL of 1 M IPTG solution was added to the growth to induce protein expression. After three to five hours of expression, the cells were harvested by in 500 ml bottles at 7 krpm for 15-20 minutes using a GS3 rotor. The cell pellets were collected using a spatula and less than 5 ml PBS buffer and placed in a 50 ml falcon tube and stored at -20 °C for purification at a later date. The supernatant was discarded.

7.1.3   Purification

The desired cell pellet was thawed out on ice or in cold water. 50 ml 1X PBS, 0.1 % Sarcosine, 1 mM EDTA buffer per 2L culture pellet was added to re-suspend the cell

pellet from expression. First, the suspended cell pellet was homogenized in a commercial blender by blending 2-3 times for 30 seconds. This solution was sonicated 6 times for 90 seconds using a Branson 450 Sonifier with the duty cycle set on 90 with 5-10 minutes between sonications. The solutions were kept on ice during sonications. The solutions were centrifuged in 50 ml tubes at 17 krpm for 20 minutes using the S34 rotor after sonications. The supernatant was purified using Ni-NTA Affinity Column Purification

Ni-NTA Affinity Column Purification (FPLC)

The Ni-NTA affinity column purification was performed identically to the manner described in section

7.1.3.1   Gravity Flow Ni-Sepharose Affinity column purification

7.2   Results & Discussion

Transformation of BL21 (DE3) and DH5-α could yield sparse colonies after transformation. TG1 cells grew much stronger. In both BL21 (DE3) and TG1 cells, expression of the anti-HER-2 ScFv was not detectable by SDS-PAGE (Fig 10.1). Not surprisingly, the purification did not yield an appreciable amount of protein.

7.3   Conclusion

The anti-HER-2 ScFv was not successfully expressed. This may be due to a codon bias or the presence of disulfide bonds in the ScFv.
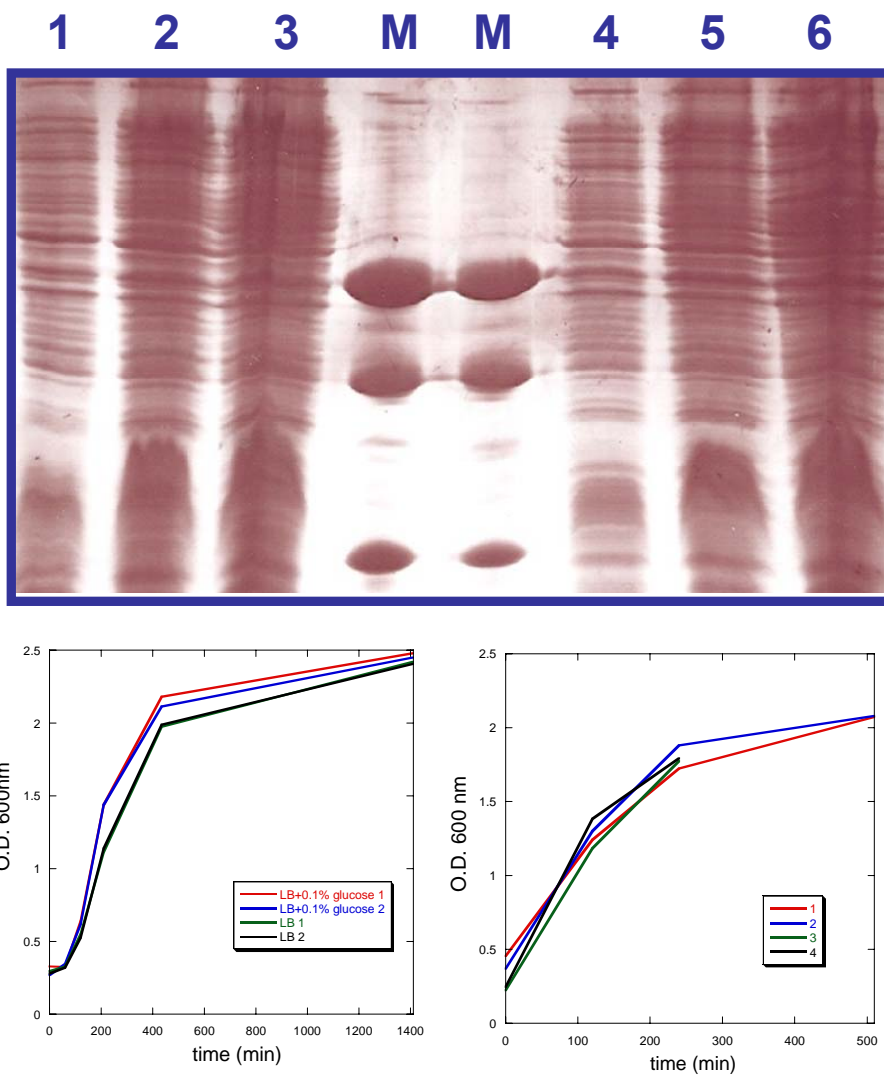
Figure 7.1

8   Appendix II: The Biodistribution of Protein Drugs

8.1   Introduction

Therapeutic use of proteins first gained popularity in the early 1900s when researchers first began to isolate purified peptide hormones from animals. Bovine growth hormone was purified from the pituitary gland of beef cattle for the treatment of dwarfism (*91*). While bovine growth hormone was found to be inactive in humans, other hormones proved clinically effective. For example, calcitonin purified from salmon (and teleosts in general) is more active in humans than the human calcitonin (*92*). The most successful early protein pharmaceutical was probably insulin purified from canine and porcine pancreatic homogenates (*93*). The Novo Insulinlaboratorium (now Novo Nordisk, inc.) and Eli Lilly were major players in the initial stages of protein pharmaceutical development. Both companies invested heavily in the isolation of insulin from canine and bovine pancreatic islets.

For decades the production and discovery of protein pharmaceuticals was limited to proteins that occur naturally. Today's most powerful protein pharmaceuticals, antibodies, were useless in the clinical arena until relatively recent years. Antibodies from nonhuman species are certain to elicit an immune response upon prolonged or repeated exposure. It is difficult to purify antibodies from human blood and unethical to purposefully expose humans to antigens for the sake of antibody production. The current expansion in the number of protein and peptide pharmaceuticals is due to the genomics revolution which began with the discovery of restriction enzymes in 1978 (*94, 95*) (*96*)

(*97*). Antibodies and other peptides can now be humanized to avoid an adverse immune response. Also, classical peptide pharmaceuticals such as insulin, human growth hormone, and luteinizing hormone releasing hormone can be mutated to manipulate circulation time or receptor affinity. Finally, and perhaps most importantly, current technology allows various overexpression systems to simplify the production and purification of these recombinant proteins.

In describing the in vivo behavior of a pharmaceutical, "biodistribution" is the terminology commonly favored by non-clinical research scientists. This word usually describes the ultimate fate of an agent in a multicellular organism.   "Pharmacokinetics" is a much more descriptive word favored by clinicians and clinical researchers. Pharmacology deals with the absorption, distribution, metabolism, and excretion of drugs. Each of these issues will be detailed in this review Drugs are designed to have an effect on the body and pharmacokinetics/Biodistribution describes what the body does to the drug. .

The distribution of any drug is based on the specific and nonspecific interactions at the molecular level. Protein-protein interactions are dictated by size, charge, functional groups, and hydrophobic constraints. In order for a protein drug to interact with another molecule, it must obviously come into close proximity. The fate of a protein drug is first dictated by circulation and tissue penetration constraints, and ultimately by molecular interactions. Thus, the principles of tissue perfusion provide the outline for this review.

Many protein drugs must retain a specific tertiary structure to remain biologically active. Oral administration would inevitably lead to denaturation by the rapid pH changes associated with the digestive system and proteolysis by gastric pepsin or pancreatic enzymes. Hence, protein drugs are largely limited to intravenous and intramuscular injections (blood or interstitium). A few exceptions are on the horizon, such as inhalable recombinant growth hormone, calcitonin, and monoclonal antibodies (*98, 99*), but a detailed discussion of these topics is beyond the scope of this review. This review will focus more on the pharmacokinetics of protein pharmaceuticals as a result of molecular characteristics rather than routes of administration, formulation, or packaging.

8.2   Circulation and tissue penetration

Table 8.1: **Tissue Perfusion and O_2 Consumption**

Organ	Blood Flow Rate ml/min/100 g	O_2 Consumption/ O_2 Delivery (%)
Brain	*54*	*34*
Heart	*87*	*65*
Skel. Musc.	*2.7*	*34*
Liver	*58*	*18*
Kidney	*420*	*8*

The majority of drugs are intended for ingestion and absorption across the intestinal or stomach wall. Generally, this route of administration is not feasible for protein and peptide pharmaceuticals. Proteins typically rely on tertiary structure to maintain their ability to specifically interact with a target molecule. Ingestion of proteins

would probably lead to unfolding in the low pH environment of the stomach. The digestive enzymes of the stomach (pepsin) and duodenum (pancreatic enzymes and brush border carboxy- and aminopeptidases) would undoubtedly cleave most peptides. Nearly all protein therapeutic agents are intended to be injected intramuscularly or intravenously. Intramuscular injections simply provide a reservoir for proteins to slowly enter the bloodstream; therefore, the circulation is the major determinant for the distribution component of pharmacokinetics. The brain, liver, heart, and kidney are the most well perfused organs (see Table 10.1). In addition to circulation to these organs, diffuse and ordered lymphatic tissues are likely to encounter protein drugs.

8.3   The Brain

Due to the blood brain barrier (BBB), the brain is highly unlikely to receive a significant amount of an intravenously administered protein drug. The blood brain barrier refers to a combination of several barriers rather than one contiguous structure. Capillary endothelial cells that perfuse the brain possess exceptionally tight occluding junctions and phagocytic astrocytes surround these capillaries. The ependymal cells that line the junction between the central nervous tissue and the cerebrospinal fluid also possess tight junctions. Therefore, should an agent leave the capillaries in the brain, it must first pass between the endothelial cells (which is nearly impossible), diffuse through the endothelial cells (hydrophobic small molecules only), or enter and exit the endothelial cells through receptor mediated endocytosis. The endothelial cells in the blood brain barrier present an additional hurdle—several plasma membrane proteins that reject drugs (MRP1 and MRP2), proteins, and other disruptive molecules. The effective molecular

weight cutoff of the combined elements of the blood-brain barrier is about 500 Daltons.

In terms of protein and peptide pharmaceuticals, that amounts to 4-6 amino acids. Most

protein drugs are at least ten times larger than this.

Some proteins can enter the brain through receptor mediated endocytosis,

including insulin, transferrin, high-density lipoprotein (HDL) and diphtheria toxin (*100*).

Some researchers have developed single domain antibodies and other tags that can

successfully traverse the blood-brain barrier carrying conjugated, therapeutically active

proteins along with them (*101, 102*). There are some areas of neurons that lay outside of

the blood-brain barrier. These areas are called circumventricular organs. Researchers

seeking to target these areas of the CNS may have less difficulty. The choroid plexus,

pineal gland, subfornical organ (thirst center), area postrema (vomiting center), median

eminence, subcommissural organ, and posterior pituitary gland are all outside of the

blood-brain barrier.

The layers of connective tissue surrounding the central nervous system prevent

diffusion of nearly all molecules from the surrounding interstitium to the nervous tissue

and cerebrospinal fluid. From superficial to deep, the layers are known as the dura mater,

arachnoid mater, and pia mater.

8.4   The Liver

The liver is the largest internal organ, receiving roughly 25% of cardiac output in

normal individuals (Table 10.1). The liver is a critical component of drug metabolism,

responsible for the destruction and chemical modification of most drugs. Protein drugs

seem to be no exception; many protein drugs are found to accumulate in the liver (*29, 30*)

(*103*). This accumulation of proteins is likely due to the phagocytic Kupffer cells of the liver, which are responsible for the nonspecific phagocytosis of circulating cellular debris and pathogens.

It is highly likely that non-antigenic peptides and proteins are subject to chemical modification in the liver (*104*). Supporting evidence can be observed in the elimination of large monoclonal antibody fragments, such as the Fab_2 studied by Kobayashi et al (*30*). These antibodies are larger than the exclusion limit in the glomerular charge barrier and probably must be cleaved into smaller fragments in order to reach the urinary space of the nephrons in the timeframe observed

8.5   The Kidney

The human kidney filters the entire blood volume thirty times in one day (assuming 6 L blood volume, 180 L filtered blood). Since most protein drugs are intended for injection, the concentration of the protein pharmaceutical in the bloodstream reaches its zenith almost immediately after injection (intraperitoneal and intramuscular injections are slower, but still fast in terms of pharmacokinetics). Until relatively recently, it was believed that the kidney was very efficient at preventing proteins from entering the urinary space (*105*). The distribution of albumin, a 70 kDa molecule accounting for approximately half of the circulating plasma protein, gives insight to the mechanism of renal protein metabolism and excretion. The concentration of albumin in the urine is less than 100 mg/dL; however, the concentration of albumin in the ultrafiltrate is 220-320 mg/dL, which is highly suggestive a proteolytic or endocytotic mechanism for albumin reabsorption in the nephron (*105*). This mechanism was recently found to be a result of

the activity of two proteins present on the brush border of epithelial cells lining the nephron: megalin and cubulin (*105*). These two proteins were later found to be capable of binding many proteins of varying structure (see Fig 1). In fact, there is evidence that the body actually relies on the kidney to destroy certain circulating proteins; patients with chronic renal failure develop excessive serum beta-2-microglobulin (*106*).

The proteolysis of proteins in the kidney in itself is not a point of contention. There are two main issues with renal metabolism/excretion of protein drugs. First, after renal proteolysis, proteins accumulate in the kidney (most likely in the epithelial cells as small peptide and amino acid fragments) without being excreted in a timely manner. This can be extremely dangerous—many therapeutic proteins under development are labeled with radioactive isotopes or other adducts that may be harmful if allowed to accumulate in kidney cells.

8.6 Lymphatic Cells and Tissues

Obviously the cells responsible for protection against foreign molecules are expected to play a role in the fate of exogenous proteins and peptides. In addition to destroying non-self proteins, the lymph nodes, spleen, tonsils, liver and several types of loose connective tissues (sub-epithelial layers of hollow organs, tunica adventitia of blood vessels, etc.) contain cells that can easily ingest proteins and large particles that are not necessarily immunogenic (Fig.11.2).

The spleen is very well perfused and is the largest collection of lymphoid tissue in the body, so it is not surprising that many researchers have found their protein to accumulate in the spleen (*30, 31*). The spleen exists to activate B and T lymphocytes,

remove senescent, damaged and abnormal erythrocytes and platelets, store erythrocytes (in some species, but not in humans), and--most relevant to this review—remove macromolecules from the blood. The high perfusion rate of the spleen is coupled with a unique sinusoidal circulation large enough to allow the cells to move freely. The large fenestrations are likely a major contributing factor to the high tissue penetration of protein drugs in the spleen while the promiscuous phagocytic cells are responsible for the accumulation of protein drugs here.

There are several ways to reduce recognition and opsonization by the diffuse and ordered lymphatic tissues. If at all possible, most of the protein should be humanized. Most antibody therapeutics approved by the FDA are chimeric antibodies or humanized antibodies. Before chimeric and humanized antibodies were available, monoclonal antibodies generated in nonhuman species were used. Of course, these provoked a strong immune response in patients, greatly diminishing their usefulness.

Chimeric antibodies are mostly human IgG except for the variable domains. Humanized antibodies are advertised as more than 90% human in terms of their peptide sequence; only the region responsible for recognition (CDR-complementarity determining region) is generated from a non-human species or other means. This is slightly flawed reasoning, as there is a high degree of homology between mouse and human antibodies to begin with, so a 100% mouse antibody is quite "human" in most regions (*107*). Nonetheless, humanization is the optimal means of reducing immunogenicity and reducing rapid degradation and accumulation in the lymphatic tissues.

Some researchers may wish to target the immune system. For example, anti IL1-B and anti TNF- antibodies have been used to curb allograft rejection in murine models (*108*). To specifically target the immune system, the IgGs were encapsulated in 1 μm albumin-glutaraldehyde microspheres, which are rapidly ingested by cells of the reticuloendothelial system (*108, 109*).
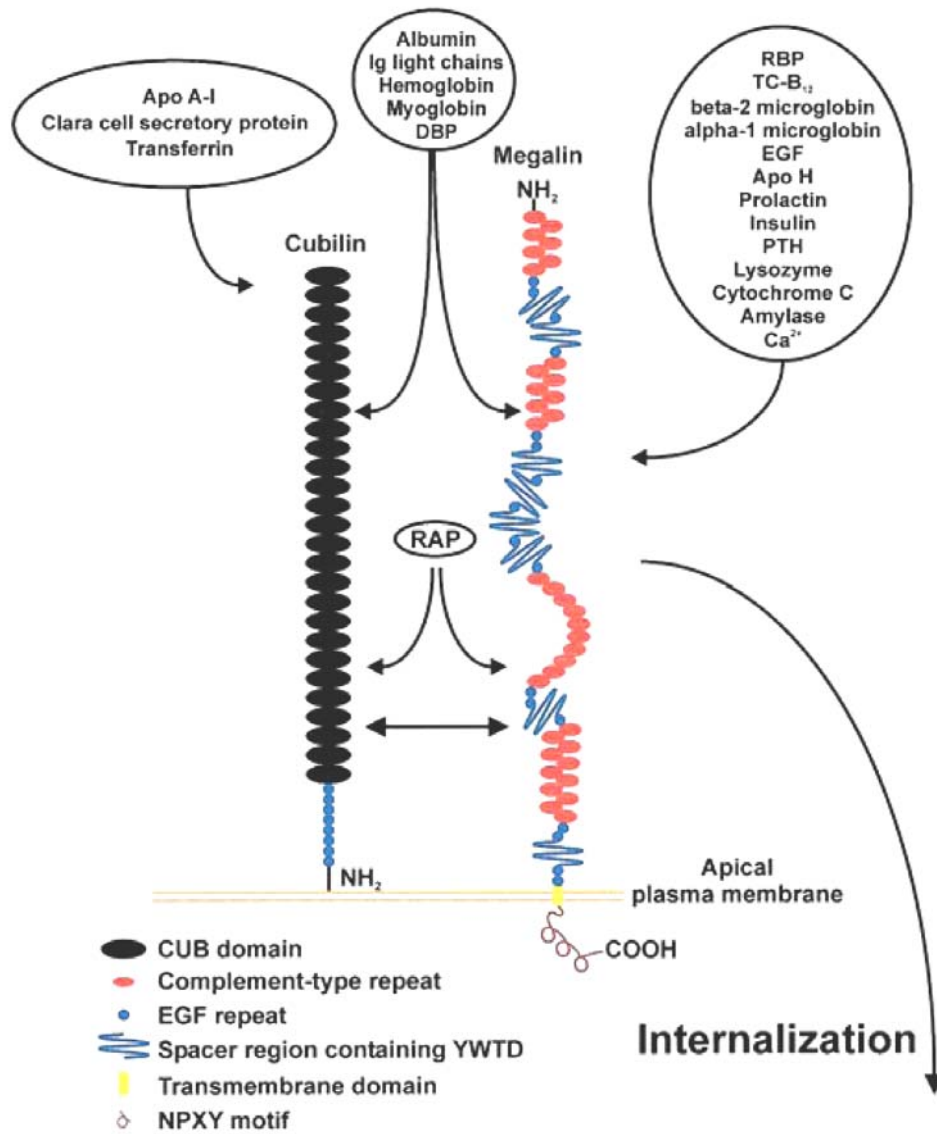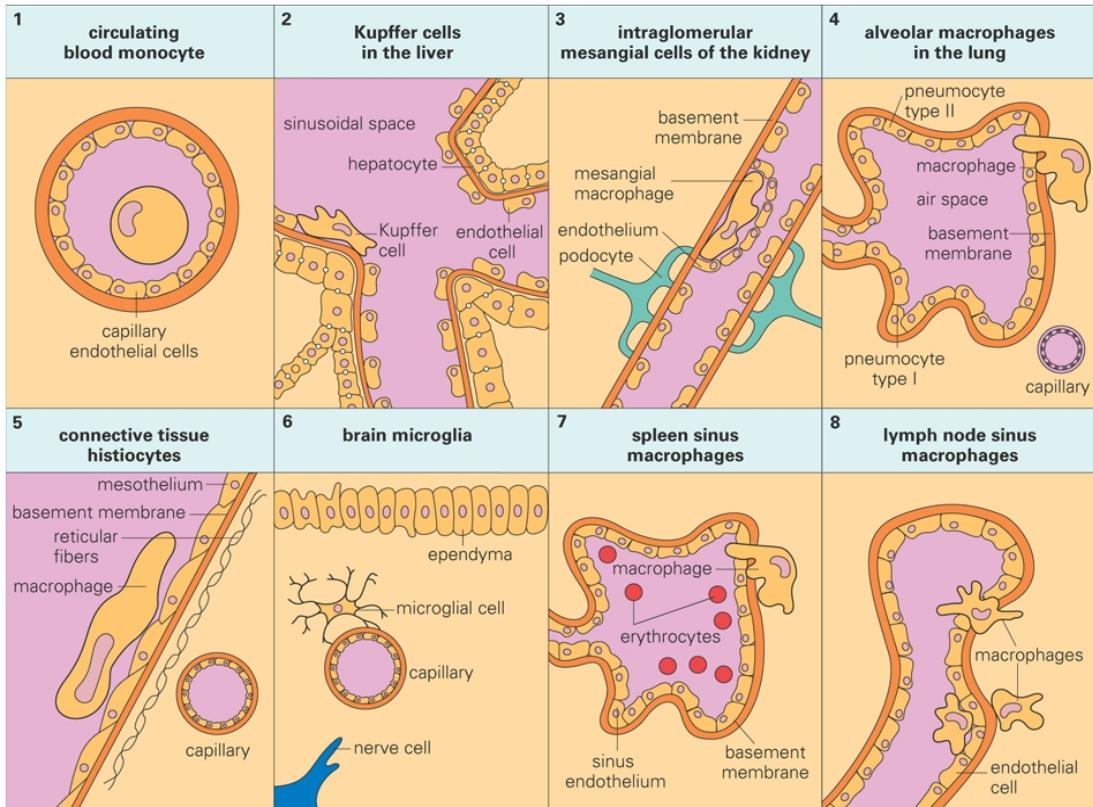
Figure 8.1 Megalin and cubulin.
Taken from Christensen et al 2003 Pediatric Nephrology

Figure 8.2 Some of the phagocytic cells of the body

9 References

(1) Wilkins, A. L., Yang, W., and Yang, J. J. (2003) Structural biology of the cell adhesion protein CD2: from molecular recognition to protein folding and design. *Curr Protein Pept Sci 4*, 367-73.

(2) Yang, W., Jones, L. M., Isley, L., Ye, Y., Lee, H. W., Wilkins, A., Liu, Z. R., Hellinga, H. W., Malchow, R., Ghazi, M., and Yang, J. J. (2003) Rational design of a calcium-binding protein. *J Am Chem Soc 125*, 6165-71.

(3) Yang, W., Wilkins, A. L., Ye, Y., Liu, Z. R., Li, S. Y., Urbauer, J. L., Hellinga, H. W., Kearney, A., van der Merwe, P. A., and Yang, J. J. (2005) Design of a calcium-binding protein with desired structure in a cell adhesion molecule. *J Am Chem Soc 127*, 2085-93.

(4) Martin, R. B., and Richardson, F. S. (1979) Lanthanides as probes for calcium in biological systems. *Q Rev Biophys 12*, 181-209.

(5) Maniccia AW, Y. W., Li SY, Johnson JA, Yang JJ. (2006) Using protein design to dissect the effect of charged residues on metal binding and protein stability. *Biochemistry 9*, 5848-5856.

(6) Meade, T. J., Taylor, A. K., and Bull, S. R. (2003) New magnetic resonance contrast agents as biochemical reporters. *Curr Opin Neurobiol 13*, 597-602.

(7) Artemov, D. (2003) Molecular magnetic resonance imaging with targeted contrast agents. *J Cell Biochem 90*, 518-24.

(8) Cheng, L. L., Chang, I. W., Louis, D. N., and Gonzalez, R. G. (1998) Correlation of high-resolution magic angle spinning proton magnetic resonance spectroscopy with histopathology of intact human brain tumor specimens. *Cancer Res 58*, 1825-32.

(9) Zhao, M., Beauregard, D. A., Loizou, L., Davletov, B., and Brindle, K. M. (2001) Non-invasive detection of apoptosis using magnetic resonance imaging and a targeted contrast agent. *Nat Med 7*, 1241-4.

(10) Bogdanov, A. A., Lewin, M., and Weissleder, R. (1999) Approaches and agents for imaging the vascular system. *Adv Drug Deliv Rev 37*, 279-293.

(11) Battey, J. F., Way, J. M., Corjay, M. H., Shapira, H., Kusano, K., Harkins, R., Wu, J. M., Slattery, T., Mann, E., and Feldman, R. I. (1991) Molecular cloning of the bombesin/gastrin-releasing peptide receptor from Swiss 3T3 cells. *Proc Natl Acad Sci U S A 88*, 395-9.

(12) Ferris, H. A., Carroll, R. E., Lorimer, D. L., and Benya, R. V. (1997) Location and characterization of the human GRP receptor expressed by gastrointestinal epithelial cells. *Peptides 18*, 663-72.

(13) Gugger, M., and Reubi, J. C. (1999) Gastrin-releasing peptide receptors in non-neoplastic and neoplastic human breast. *Am J Pathol 155*, 2067-76.

(14) Markwalder, R., and Reubi, J. C. (1999) Gastrin-releasing peptide receptors in the human prostate: relation to neoplastic transformation. *Cancer Res 59*, 1152-9.

(15) Ferris, H. A., Carroll, R. E., Rasenick, M. M., and Benya, R. V. (1997) Constitutive activation of the gastrin-releasing peptide receptor expressed by the

nonmalignant human colon epithelial cell line NCM460. *J Clin Invest 100*, 2530-7.

(16)   Chave, H. S., Gough, A. C., Palmer, K., Preston, S. R., and Primrose, J. N. (2000) Bombesin family receptor and ligand gene expression in human colorectal cancer and normal mucosa. *Br J Cancer 82*, 124-30.

(17)   Corjay, M. H., Dobrzanski, D. J., Way, J. M., Viallet, J., Shapira, H., Worland, P., Sausville, E. A., and Battey, J. F. (1991) Two distinct bombesin receptor subtypes are expressed and functional in human lung carcinoma cells. *J Biol Chem 266*, 18771-9.

(18)   Sun, B., Schally, A. V., and Halmos, G. (2000) The presence of receptors for bombesin/GRP and mRNA for three receptor subtypes in human ovarian epithelial cancers. *Regul Pept 90*, 77-84.

(19)   Reubi, J. C., Wenger, S., Schmuckli-Maurer, J., Schaer, J. C., and Gugger, M. (2002) Bombesin receptor subtypes in human cancers: detection with the universal radioligand (125)I-[D-TYR(6), beta-ALA(11), PHE(13), NLE(14)] bombesin(6-14). *Clin Cancer Res 8*, 1139-46.

(20)   Kim, C. W., Han, K. S., Ryu, K. S., Kim, B. H., Kim, K. H., Choi, S. I., and Seong, B. L. (2007) N-terminal domains of native multidomain proteins have the potential to assist de novo folding of their downstream domains in vivo by acting as solubility enhancers. *Protein Sci 16*, 635-43.

(21)   Carroll, A., Yang, W., Ye, Y., Simmons, R., and Yang, J. J. (2006) Amyloid fibril formation by a domain of rat cell adhesion molecule. *Cell Biochem Biophys 44*, 241-9.

(22)   Chang, J. Y. (1985) Thrombin specificity. Requirement for apolar amino acids adjacent to the thrombin cleavage site of polypeptide substrate. *Eur J Biochem 151*, 217-24.

(23)   Chang, J. Y., Alkan, S. S., Hilschmann, N., and Braun, D. G. (1985) Thrombin specificity. Selective cleavage of antibody light chains at the joints of variable with joining regions and joining with constant regions. *Eur J Biochem 151*, 225-30.

(24)   Lichty, J. J., Malecki, J. L., Agnew, H. D., Michelson-Horowitz, D. J., and Tan, S. (2005) Comparison of affinity tags for protein purification. *Protein Expr Purif 41*, 98-105.

(25)   Carson, M., Johnson, D. H., McDonald, H., Brouillette, C., and Delucas, L. J. (2007) His-tag impact on structure. *Acta Crystallogr D Biol Crystallogr 63*, 295-301.

(26)   Hutchinson, M. H., and Chase, H. A. (2006) Adsorptive refolding of histidine-tagged glutathione S-transferase using metal affinity chromatography. *J Chromatogr A 1128*, 125-32.

(27)   Christensen, E. I., and Gburek, J. (2004) Protein reabsorption in renal proximal tubule-function and dysfunction in kidney pathophysiology. *Pediatr Nephrol 19*, 714-21.

(28)   Christensen, E. I., and Verroust, P. J. (2002) Megalin and cubilin, role in proximal tubule function and during development. *Pediatr Nephrol 17*, 993-9.

(29)   de Jong, M., Barone, R., Krenning, E., Bernard, B., Melis, M., Visser, T., Gekle, M., Willnow, T. E., Walrand, S., Jamar, F., and Pauwels, S. (2005) Megalin is essential for renal proximal tubule reabsorption of (111)In-DTPA-octreotide. *J Nucl Med 46*, 1696-700.

(30)   Kobayashi, H., Le, N., Kim, I. S., Kim, M. K., Pie, J. E., Drumm, D., Paik, D. S., Waldmann, T. A., Paik, C. H., and Carrasquillo, J. A. (1999) The pharmacokinetic characteristics of glycolated humanized anti-Tac Fabs are determined by their isoelectric points. *Cancer Res 59*, 422-30.

(31)   Shankar, S., Vaidyanathan, G., Kuan, C. T., Bigner, D. D., and Zalutsky, M. R. (2006) Antiepidermal growth factor variant III scFv fragment: effect of radioiodination method on tumor targeting and normal tissue clearance. *Nucl Med Biol 33*, 101-10.

(32)   Kramer, P. A. (1974) Letter: Albumin microspheres as vehicles for achieving specificity in drug delivery. *J Pharm Sci 63*, 1646-7.

(33)   Tomilson E, B. J. (1987) Monolithic albumin particles as drug carriers. *Polymers in Controlled Drug delivery*, 25-48.

(34)   Matsumura, Y., and Maeda, H. (1986) A new concept for macromolecular therapeutics in cancer chemotherapy: mechanism of tumoritropic accumulation of proteins and the antitumor agent smancs. *Cancer Res 46*, 6387-92.

(35)   O'Mullane, J. E., Artursson, P., and Tomlinson, E. (1987) Biopharmaceutics of microparticulate drug carriers. *Ann N Y Acad Sci 507*, 120-40.

(36)   Thakkar, H., Sharma, R. K., Mishra, A. K., Chuttani, K., and Murthy, R. R. (2005) Albumin microspheres as carriers for the antiarthritic drug celecoxib. *AAPS PharmSciTech 6*, E65-73.

(37)   Takakura, Y., Fujita, T., Hashida, M., and Sezaki, H. (1990) Disposition characteristics of macromolecules in tumor-bearing mice. *Pharm Res 7*, 339-46.

(38)   Bernard NG, S. S., Kessler WV, Landolt RR, Peck GE, Dockerty GH. (1980) Distribution and degradation of I-125 albumin microspheres and technetium 99m sulphur colloid. *J Pharm Sci*, 30-34.

(39)   Schafer, V., von Briesen, H., Rubsamen-Waigmann, H., Steffan, A. M., Royer, C., and Kreuter, J. (1994) Phagocytosis and degradation of human serum albumin microspheres and nanoparticles in human macrophages. *J Microencapsul 11*, 261-9.

(40)   Muller, B. G., Leuenberger, H., and Kissel, T. (1996) Albumin nanospheres as carriers for passive drug targeting: an optimized manufacturing technique. *Pharm Res 13*, 32-7.

(41)   F Kratz, I. F., U Beyer, P Schumacher, T Roth, HH Fiebig, C Unger. (1997) Antitumor activity of acid labile transferring and albumin doxorubicin conjugates in in vitro and in vivo human tumor xenograft models. *Eur J Cancer*, S175.

(42)   Lee, M. H., Ducheyne, P., Lynch, L., Boettiger, D., and Composto, R. J. (2006) Effect of biomaterial surface properties on fibronectin-alpha5beta1 integrin interaction and cellular attachment. *Biomaterials 27*, 1907-16.

(43)   Shah, A. U., and D'Souza, M. J. (1999) Sustained-release interleukin-12 microspheres in the treatment of cancer. *Drug Dev Ind Pharm 25*, 995-1004.

(44)   Elkordy, A. A., Forbes, R. T., and Barry, B. W. (2004) Stability of crystallised and spray-dried lysozyme. *Int J Pharm 278*, 209-19.

(45)   Patel, N., Craddock, B. L., Staniforth, J. N., Tobyn, M. J., and Welham, M. J. (2001) Spray-dried insulin particles retain biological activity in rapid in-vitro assay. *J Pharm Pharmacol 53*, 1415-8.

(46)   Millqvist-Fureby, A., Malmsten, M., and Bergenstahl, B. (1999) Surface characterisation of freeze-dried protein/carbohydrate mixtures. *Int J Pharm 191*, 103-14.

(47)   Millqvist-Fureby, A., Malmsten, M., and Bergenstahl, B. (1999) Spray-drying of trypsin - surface characterisation and activity preservation. *Int J Pharm 188*, 243-53.

(48)   Honig, B., and Nicholls, A. (1995) Classical electrostatics in biology and chemistry. *Science 268*, 1144-9.

(49)   Rocchia, W., Alexov, E., and Honig, B. (2001) Extending the applicability of the nonlinear Poisson-Boltzmann equation: Multiple dielectric constants and multivalent ions. *Journal of Physical Chemistry B 105*, 6507-6514.

(50)   Rocchia, W., Sridharan, S., Nicholls, A., Alexov, E., Chiabrera, A., and Honig, B. (2002) Rapid grid-based construction of the molecular surface and the use of induced surface charge to calculate reaction field energies: applications to the molecular systems and geometric objects. *J Comput Chem 23*, 128-37.

(51)   Yang, J. J., Yang, H., Ye, Y., Hopkins, H., Jr., and Hastings, G. (2002) Temperature-induced formation of a non-native intermediate state of the all beta-sheet protein CD2. *Cell Biochem Biophys 36*, 1-18.

(52)   Strickler, S. S., Gribenko, A. V., Gribenko, A. V., Keiffer, T. R., Tomlinson, J., Reihle, T., Loladze, V. V., and Makhatadze, G. I. (2006) Protein stability and surface electrostatics: a charged relationship. *Biochemistry 45*, 2761-6.

(53)   Permyakov, S. E., Khokhlova, T. I., Nazipova, A. A., Zhadan, A. P., Morozova-Roche, L. A., and Permyakov, E. A. (2006) Calcium-binding and temperature induced transitions in equine lysozyme: new insights from the pCa-temperature "phase diagrams". *Proteins 65*, 984-98.

(54)   Prasad, A., and Pedigo, S. (2005) Calcium-dependent stability studies of domains 1 and 2 of epithelial cadherin. *Biochemistry 44*, 13692-701.

(55)   D'Auria, S., Ausili, A., Marabotti, A., Varriale, A., Scognamiglio, V., Staiano, M., Bertoli, E., Rossi, M., and Tanfani, F. (2006) Binding of glucose to the D-galactose/D-glucose-binding protein from Escherichia coli restores the native protein secondary structure and thermostability that are lost upon calcium depletion. *J Biochem (Tokyo) 139*, 213-21.

(56)   Chen, H. A., Pfuhl, M., McAlister, M. S., and Driscoll, P. C. (2000) Determination of pK(a) values of carboxyl groups in the N-terminal domain of rat CD2: anomalous pK(a) of a glutamate on the ligand-binding surface. *Biochemistry 39*, 6814-24.

(57)   Chen, H. A., Pfuhl, M., and Driscoll, P. C. (2002) The pH dependence of CD2 domain 1 self-association and 15N chemical exchange broadening is correlated with the anomalous pKa of Glu41. *Biochemistry 41*, 14680-8.

(58)   Jayaraman, S., Gantz, D. L., and Gursky, O. (2006) Effects of salt on the thermal stability of human plasma high-density lipoprotein. *Biochemistry 45*, 4620-8.

(59)   Schueler-Furman, O., Wang, C., Bradley, P., Misura, K., and Baker, D. (2005) Progress in modeling of protein structures and interactions. *Science 310*, 638-42.

(60)   Umetsu, M., Tsumoto, K., Nitta, S., Adschiri, T., Ejima, D., Arakawa, T., and Kumagai, I. (2005) Nondenaturing solubilization of beta2 microglobulin from inclusion bodies by L-arginine. *Biochem Biophys Res Commun 328*, 189-97.

(61)   Lee, J. C., and Timasheff, S. N. (1981) The stabilization of proteins by sucrose. *J Biol Chem 256*, 7193-201.

(62)   Lin, T. Y., and Timasheff, S. N. (1996) On the role of surface tension in the stabilization of globular proteins. *Protein Sci 5*, 372-81.

(63)   Timasheff, S. N. (1993) The control of protein stability and association by weak interactions with water: how do solvents affect these processes? *Annu Rev Biophys Biomol Struct 22*, 67-97.

(64)   Timasheff, S. N. (1992) Water as ligand: preferential binding and exclusion of denaturants in protein unfolding. *Biochemistry 31*, 9857-64.

(65)   Moelbert, S., Normand, B., and De Los Rios, P. (2004) Kosmotropes and chaotropes: modelling preferential exclusion, binding and aggregate stability. *Biophys Chem 112*, 45-57.

(66)   Haswani, D. K., Nettey, H., D'Souza, M. J., and Oettinger, C. W. (2007) In vitro evaluation and targeting of E. coli internalized by endothelial cells using albumin microspheres loaded with gentamicin. *Drug Dev Ind Pharm 33*, 181-90.

(67)   Nettey, H., Haswani, D., D'Souza, M., and Oettinger, C. (2007) In vitro antimicrobial effect of encapsulated vancomycin on internalized Staphylococcus aureus within endothelial cells. *Drug Dev Ind Pharm 33*, 133-9.

(68)   Tomilson, E. B. J. (1987) *Monolithic albumin particles as drug carriers.*

(69)   Kratz, I. F., Beyer, U., Schumacher, P., Roth, T., Fiebig, H.H., Unger, C. ((1997) Antitumor activity of acid labile transferring and albumin doxorubicin conjugates in in vitro and in vivo human tumor xenograft models. *Eur J Cancer*, S175.

(70)   Donahue, K. M., Burstein, D., Manning, W. J., and Gray, M. L. (1994) Studies of Gd-DTPA relaxivity and proton exchange rates in tissue. *Magn Reson Med 32*, 66-76.

(71)   St John, R. J., Carpenter, J. F., and Randolph, T. W. (1999) High pressure fosters protein refolding from aggregates at high concentrations. *Proc Natl Acad Sci U S A 96*, 13029-33.

(72)   Becker, J. W., and Reeke, G. N., Jr. (1985) Three-dimensional structure of beta 2-microglobulin. *Proc Natl Acad Sci U S A 82*, 4225-9.

(73)   Perarnau, B., Siegrist, C. A., Gillet, A., Vincent, C., Kimura, S., and Lemonnier, F. A. (1990) Beta 2-microglobulin restriction of antigen presentation. *Nature 346*, 751-4.

(74)   Tarleton, R. L., Koller, B. H., Latour, A., and Postan, M. (1992) Susceptibility of beta 2-microglobulin-deficient mice to Trypanosoma cruzi infection. *Nature 356*, 338-40.

(75) Huang, W. C., Wu, D., Xie, Z., Zhau, H. E., Nomura, T., Zayzafoon, M., Pohl, J., Hsieh, C. L., Weitzmann, M. N., Farach-Carson, M. C., and Chung, L. W. (2006) beta2-microglobulin is a signaling and growth-promoting factor for human prostate cancer bone metastasis. *Cancer Res 66*, 9108-16.

(76) Yang, J., Qian, J., Wezeman, M., Wang, S., Lin, P., Wang, M., Yaccoby, S., Kwak, L. W., Barlogie, B., and Yi, Q. (2006) Targeting beta2-microglobulin for induction of tumor apoptosis in human hematological malignancies. *Cancer Cell 10*, 295-307.

(77) Saha, S. a. R. (2004) GPS BcePRed: Prediction of Continuous B-Cell Epitopes in Antigenic Sequences Using Physico-Chemical Properties. *IN G Nicosia, V Cutello, PJ Bently and J Timis (Eds.) LNCS 3239*, 197-204.

(78) Saha, S., and Raghava, G. P. (2006) Prediction of continuous B-cell epitopes in an antigen using recurrent neural network. *Proteins 65*, 40-8.

(79) Kulkarni-Kale, U., Bhosle, S., and Kolaskar, A. S. (2005) CEP: a conformational epitope prediction server. *Nucleic Acids Res 33*, W168-71.

(80) Huang, W. C., Xie, Z., Konaka, H., Sodek, J., Zhau, H. E., and Chung, L. W. (2005) Human osteocalcin and bone sialoprotein mediating osteomimicry of prostate cancer cells: role of cAMP-dependent protein kinase A signaling pathway. *Cancer Res 65*, 2303-13.

(81) Stark AT, C. S., Kapke A, Lu M, Linden M, Griggs J. (2006) Race modifies the association between breast carcinoma pathologic prognostic indicators and positive status for HER-2/neu. *Cancer 104*, 2189-2196.

(82) Sidoni A, F. I., Cavaliere A, Bellezza G, Scheibel M, Bucciarelli E. Detection of HER-2/neu (c-erbB-2) overexpression and amplification in breast carcinoma with ambiguous immunohistochemical results: a further contribution to defining the role of fluorescent in situ hybridizations. *Anticancer Res 26*, 2333-2337.

(83) Sawaki, M., Ito, Y., Akiyama, F., Tokudome, N., Horii, R., Mizunuma, N., Takahashi, S., Horikoshi, N., Imai, T., Nakao, A., Kasumi, F., Sakamoto, G., and Hatake, K. (2006) High prevalence of HER-2/neu and p53 overexpression in inflammatory breast cancer. *Breast Cancer 13*, 172-8.

(84) Elledge RM, C. G., Chamness GC, Osborne CK. (1994) Tumor biologic factors and breast cancer prognosis among white, Hispanic, and black women in the United States. *J Natl Cancer Inst*, 705-712.

(85) Casalini, P., Iorio, M. V., Galmozzi, E., and Menard, S. (2004) Role of HER receptors family in development and differentiation. *J Cell Physiol 200*, 343-50.

(86) Bernstein JL, L.-C. L., Wang L. (1999) The epidemiology of Her-2/neu and p53 in breast cancer. *Salud Publica Mex 41*, S114-S123.

(87) Al-Abbadi MA, W. T., Saleh HA, Tekyi-Mensah SE, Lucas DR. Differential expression of HER-2/neu receptor of invasive mammary carcinoma between Caucasion and African American patients in the Detroit metropolitan area. *Breast Cancer Res and Treat*.

(88) Ravdin PM, C. G. (1995) The c-erb-2 proto-oncogene as a prognostic and predictive marker in breast cancer: a paradigm for the development of other macromolecular markers--a review. *Gene*, 19-27.

(89)   Kaptain, S., Tan, LK, Chen B. (2001) Her-2/neu and breast cancer. *Diagn Mol Pathol 10*, 139-152.

(90)   Zhang, X., Gureasko, J., Shen, K., Cole, P. A., and Kuriyan, J. (2006) An allosteric mechanism for activation of the kinase domain of epidermal growth factor receptor. *Cell 125*, 1137-49.

(91)   Dellacha, J. M., and Sonenberg, M. (1964) Purification Of Bovine Growth Hormone. *J Biol Chem 239*, 1515-20.

(92)   Gorn, A. H., Lin, H. Y., Yamin, M., Auron, P. E., Flannery, M. R., Tapp, D. R., Manning, C. A., Lodish, H. F., Krane, S. M., and Goldring, S. R. (1992) Cloning, characterization, and expression of a human calcitonin receptor from an ovarian carcinoma cell line. *J Clin Invest 90*, 1726-35.

(93)   Dudley, H. W. (1923) The Purification of Insulin and some of its Properties. *Biochem J 17*, 376-90.

(94)   van Noordwijk, J. (1988) Quality assurance of products manufactured by recombinant DNA technology. Introduction and elements of a philosophy. *Arzneimittelforschung 38*, 943-7.

(95)   Hess, P. N. (1987) Biotechnology in bulk drug production. Objectives and strategies of process development. *Arzneimittelforschung 37*, 1210-5.

(96)   Bachmayer, H. (1988) Quality control of protein drugs. *Arzneimittelforschung 38*, 590-1.

(97)   Kroon, A. M. (1979) [The Nobel Prize for Medicine and Physiology in 1978 (Werner Arber, Daniel Nathans, Hamilton Smith)]. *Ned Tijdschr Geneeskd 123*, 153-6.

(98)   Daugherty, A. L., and Mrsny, R. J. (2006) Formulation and delivery issues for monoclonal antibody therapeutics. *Adv Drug Deliv Rev 58*, 686-706.

(99)   Deftos, L. J., Nolan, J. J., Seely, B. L., Clopton, P. L., Cote, G. J., Whitham, C. L., Florek, L. J., Christensen, T. A., and Hill, M. R. (1997) Intrapulmonary drug delivery of salmon calcitonin. *Calcif Tissue Int 61*, 345-7.

(100) Gaillard, P. J., Visser, C. C., and de Boer, A. G. (2005) Targeted delivery across the blood-brain barrier. *Expert Opin Drug Deliv 2*, 299-309.

(101) Abulrob, A., Sprong, H., Van Bergen en Henegouwen, P., and Stanimirovic, D. (2005) The blood-brain barrier transmigrating single domain antibody: mechanisms of transport and antigenic epitopes in human brain endothelial cells. *J Neurochem 95*, 1201-14.

(102) Riikonen, R. (2006) Insulin-like growth factor delivery across the blood-brain barrier. Potential use of IGF-1 as a drug in child neurology. *Chemotherapy 52*, 279-81.

(103) Behr, T. M., Goldenberg, D. M., and Becker, W. (1998) Reducing the renal uptake of radiolabeled antibody fragments and peptides for diagnosis and therapy: present status, future prospects and limitations. *Eur J Nucl Med 25*, 201-12.

(104) Racanelli, V., and Rehermann, B. (2006) The liver as an immunological organ. *Hepatology 43*, S54-62.

(105) Gekle, M. (2005) Renal tubule albumin transport. *Annu Rev Physiol 67*, 573-94.

(106) Dobson, C. M. (2006) An accidental breach of a protein's natural defenses. *Nat Struct Mol Biol 13*, 295-7.
(107) Bolt, S., Routledge, E., Lloyd, I., Chatenoud, L., Pope, H., Gorman, S. D., Clark, M., and Waldmann, H. (1993) The generation of a humanized, non-mitogenic CD3 monoclonal antibody which retains in vitro immunosuppressive properties. *Eur J Immunol 23*, 403-11.
(108) Gerber, D. A., Oettinger, C. W., D'Souza, M., Milton, G. V., Larsen, C. P., and Pearson, T. C. (1995) Prolongation of murine cardiac allograft survival by microspheres containing TNF alpha and IL1-beta neutralizing antibodies. *J Drug Target 3*, 311-5.
(109) Zolle, I., Rhodes, B. A., and Wagner, H. N., Jr. (1970) Preparation of metabolizable radioactive human serum albumin microspheres for studies of the circulation. *Int J Appl Radiat Isot 21*, 155-67.